

DISSERTATION

Physical Modeling of Electron Transport in Strained Silicon and Silicon-Germanium

ausgeführt zum Zwecke der Erlangung des akademischen Grades
eines Doktors der technischen Wissenschaften

unter der Betreuung von
Ao.Univ.Prof. Dipl.-Ing. Dr.techn. Hans Kosina
und
O.Univ.Prof. Dipl.-Ing. Dr.techn. Siegfried Selberherr

eingereicht an der Technischen Universität Wien,
Fakultät für Elektrotechnik und Informationstechnik, von

SERGEY SMIRNOV

Jubilejny Proezd 12/100
141420 Skhodnya, Russland

Matr. Nr. 0127158
geboren am 6. März 1976 in Skhodnya, Russland

Wien, im Dezember 2003

Kurzfassung

Die Skalierung von Si Bauelementen führte zu einer stetigen Leistungssteigerung von integrierten Schaltungen. Mit jeder neuen Technologiegeneration wird jedoch die Skalierung zu einer immer komplexeren und kostenintensiveren Aufgabe. Eine zusätzliche Möglichkeit zur Leistungssteigerung besteht in der Verbesserung des Ladungsträgertransports durch Veränderung des Materials. Eine vielversprechende Option ist verspanntes Si, welches deutlich verbesserte Transporteigenschaften aufweist.

Diese Arbeit beschäftigt sich mit den elektronischen Eigenschaften von $\text{Si}_{1-x}\text{Ge}_x$ Schichten auf $\text{Si}_{1-y}\text{Ge}_y$ Substraten. Im entwickelten Modell kann der Ge Anteil beider Schichten im gesamten Bereich variiert werden. Durch mechanische Verspannung wird die Entartung von Leitungsbandzuständen mit unterschiedlichem Quasiimpuls aufgehoben. Diese Entartungsreduktion hängt von der relativen Orientierung des Quasiimpulses der Bandminima und der auf die Schicht einwirkenden Kräfte ab. Die Aufspaltung der Bandminima hängt über den Verzerrungstensor von den Legierungszusammensetzungen der epitaktischen Schicht und des Substrats ab. Die Aufspaltung und die mittlere Verschiebung der X- und L-Täler werden mit Hilfe der Deformationspotentialtheorie berechnet. Die Form des Verzerrungstensors wird von der Orientierung des Substrats bestimmt und ist im allgemeinen Fall nicht diagonal. Der Einfluss des Verzerrungstensors auf die verschiedenen Leitungsbandminima führt zu veränderten elektronischen Eigenschaften des Halbleitermaterials.

Um die Kinetik der Ladungsträger in verspannten SiGe Schichten zu untersuchen, wird die semiklassische Boltzmann Transportgleichung verwendet. Diese ermöglicht es, die gegenseitigen Abhängigkeiten von Streuprozessen, Bandstruktureffekten und Verspannungseffekten in sehr allgemeiner Weise zu berücksichtigen.

In dieser Arbeit wird ein analytisches Leitungsbandmodell verwendet, welches Anisotropie und Nichtparabolizität berücksichtigt. Dadurch können die Streuraten sowie der Einfluss der Verspannung auf die Streuraten analytisch angegeben werden. Es werden folgende Streumechanismen berücksichtigt: akustische Innertal-Phononstreuung, welche elastisch angenommen wird, Zwischenband-Streuung durch optische und akustischen Phononen, bei höheren Elektronenkonzentrationen Elektron-Plasmon-Streuung, Legierungsstreuung, sowie die Streuung an ionisierten Störstellen. Im letzteren Modell werden Effekte wie die Paar-Streuung, impulsabhängige Ab-

schirmung und eine Korrektur für die zweite Born'sche Näherung berücksichtigt. Durch die Verspannung werden sämtliche Streuraten verändert, etwa durch die geänderte kinetische Energie im Endtal und die Anzahl der verfügbaren Endtälern. Die Störstellenstreuung wird durch die geänderten Abschirmungsparameter beeinflusst.

Die Boltzmann-Gleichung wird mit Hilfe der Monte Carlo Methode gelöst. Diese Methode erlaubt eine Lösung des semiklassischen Transportproblems, ohne zusätzliche physikalische Näherungen treffen zu müssen. Um den Beweglichkeitstensor bei niedrigen elektrischen Feldstärken zu berechnen, wird ein spezieller Monte Carlo Algorithmus für verschwindendes Feld angewendet. Da bei hohen Elektronenkonzentrationen das Pauli-Verbot an Einfluss gewinnt, wurde dieser Algorithmus für entartete Halbleiter erweitert. Ebenso wurde ein bestehender Monte Carlo Algorithmus zur Berechnung der Kleinsignal-Beweglichkeit für entartete Halbleiter erweitert.

Es wurden unterschiedliche Transportberechnungen in verspannten SiGe Schichten durchgeführt. Als Parameter werden die Dotierungskonzentration, die Legierungszusammensetzungen der epitaktischen Schicht und des Substrats, sowie die kristallografische Orientierung des Substrats variiert. Um das komplexe Verhalten der Niederfeldbeweglichkeit zu erklären, kann die Besetzung der Täler als Funktion der Dotierung und der Legierungszusammensetzungen herangezogen werden. Für Substrate, deren Orientierung nicht mit den Hochsymmetrie-Richtungen $\langle 100 \rangle$ und $\langle 111 \rangle$ zusammenfallen, wird die Elektronenbeweglichkeit in der Schicht anisotrop. Für MOS-Transistoren ist insbesondere die Beweglichkeitskomponente parallel zur Grenzfläche von Bedeutung. Der höchste Wert für die Parallelskomponente konnte in verspanntem Si auf einem $\langle 100 \rangle$ SiGe Substrat beobachtet werden. Ab einem Ge Anteil von 0.2 sättigt die Erhöhung der Gitterbeweglichkeit bei etwa 55% im Vergleich zu unverspanntem Si. Im Fall von Heterostruktur-Bipolartransistoren ist die Normalkomponente der Elektronenbeweglichkeit in der verspannten SiGe Basis maßgeblich. Für diese Komponente kann keine Verbesserung erzielt werden, da der positive Effekt durch die Aufspaltung der Bandminima durch die starke Legierungsstreuung kompensiert wird.

Im Weiteren wird das Zusammenspiel von Verspannungseffekten und dem Effekt durch das Pauli-Verbot gezeigt. Der Anstieg des Fermi-Niveaus kann in bestimmten Fällen dem positiven Effekt durch die Bandaufspaltung entgegenwirken. Es wurde die Kleinsignal-Beweglichkeit für verspannte und unverspannte Si Schichten berechnet, sowie der Einfluss des Pauli-Verbots untersucht.

Abstract

Geometric scaling of Si devices has provided a continual performance improvement of integrated circuits. However, with each new technology generation geometric scaling has become an increasingly complex and expensive task. An additional way to improve device performance is to enhance the carrier transport by changing the material properties. A promising candidate is strained Si which shows significantly improved carrier transport properties.

This work deals with electron transport in strained $\text{Si}_{1-x}\text{Ge}_x$ layers grown on $\text{Si}_{1-y}\text{Ge}_y$ substrates. The Ge compositions of both layers and substrates can vary in the whole range. Due to the strain the degeneracy of the conduction band states with different quasi-momentum is reduced. This degeneracy reduction depends on the relative orientation of the quasi-momentum of a band minimum and the forces applied to the layer. The strength of the minima splitting also depends on the Ge composition of both the layer and the substrate. Deformation-potential theory is applied to calculate the splitting of the conduction band extrema and the mean energy shift of both X and L valleys. Within this theory the strain tensor is used which depends on the substrate orientation. It can be diagonal and non-diagonal which strongly changes the influence of the conduction band minima of different types and leads to new kinetic properties of the material.

To investigate the kinetics in strained SiGe layers the formalism based on the semiclassical Boltzmann transport equation is used. This allows incorporation of scattering processes and band structure effects including the strain effects in a rather complete and comprehensive manner. In this work an analytical conduction band structure which considers the anisotropy and non-parabolicity is employed. In this case the scattering rates of different scattering mechanisms can be analytically obtained and modified so as to include strain effects.

The scattering mechanisms are intravalley acoustic phonon scattering treated as an elastic process, intervalley phonon scattering, which can be both of acoustic and optic type and which are considered inelastic, elastic alloy scattering originating from the alloy lattice disorder, inelastic electron-plasmon scattering coming into play at higher electron densities, elastic scattering on ionized impurities which includes effects such as two-ion scattering, momentum dependent screening and the second Born correction. The presence of strain modifies the scattering rates. Strain affects the phonon scattering rates through the final energy of scattered electrons and

ABSTRACT

the number of available valleys. The ionized impurity scattering rate is modified through the screening parameters.

The Boltzmann kinetic equation is solved using the Monte Carlo method. By this approach semiclassical transport is exactly modeled without any additional physical approximations. To find the low field electron mobility tensor a zero field Monte Carlo algorithm is applied. Since at high electron concentrations the quantum mechanical Pauli exclusion principle becomes important, a new zero field Monte Carlo algorithm accounting for degeneracy effects is developed and applied to find the low field mobility tensor in strained doped SiGe. To perform a small signal analysis of highly degenerate SiGe layers for both low and high electric fields a new small signal Monte Carlo method is developed which takes the Pauli exclusion principle into consideration.

Finally, results obtained for strained SiGe layers are given. Both doped and undoped layers are considered for different Ge compositions x and y of the layer and the substrate, respectively. The substrate orientation dependence is also investigated. To explain the behavior of the low field electron mobility the valley population is analyzed as a function of the Ge compositions x and y and impurity concentration. The in-plane component of the electron mobility is found to be dependent on the in-plane angle for a general substrate orientation. The in-plane mobility, a key parameter for MOSFET performance, is highest for strained Si on [001] SiGe substrates. For Ge compositions above 0.2, the enhancement of the pure lattice mobility saturates at 55% as compared to unstrained Si. In the case of HBT the perpendicular component of the electron mobility in the strained SiGe base increases due to the band minima splitting, but strong alloy scattering suppresses this gain. The interplay between strain effects and effects caused by the Pauli exclusion principle at high electron density is shown. The small signal response of strained Si layers is modeled and compared with the relaxed case. To understand the behavior of the response functions the energy distribution functions are analyzed for two carrier ensembles. It is shown that for the case of high degeneracy these distribution functions are nearly the same at the very beginning and strongly shifted to the high energy domain due to the Pauli exclusion principle.

Acknowledgment

I thank Prof. Selberherr and Prof. Langer for providing me with the support I could enjoy during the work on this thesis. The weekly seminars of Prof. Selberherr always stimulated to find new ways of solving non-trivial problems.

I thank Prof. Kosina for his help since the very beginning. He is a great scientist and great teacher. I am grateful to him for teaching me a lot of tricks on Monte Carlo methods. The same must be said about Mihail Nadjalkov. Together they created a real school with its own style and scientific language on Monte Carlo modeling of transport in semiconductors and I am proud to be trained in this school by these outstanding experts. The knowledge I got from Prof. Kosina and Prof. Nadjalkov is a real treasure which is beyond any price.

I thank Andreas Gehring for his great help not only in the Institute but also in general in my life in Vienna. He was so kind to be my translator from German so many times and never refused to help with filling in numerous documents since the very beginning till the very end. Visa, bank account, shops, library are only a few examples where his help was so invaluable. But most of all I was impressed by his strong knowledge of device simulation especially of tunneling. I was lucky to work all this time together with him in the same room.

Markus Gritsch was my second room colleague at the beginning. And I was lucky again. He was always so kind to answer all my questions about LaTeX and Linux in general. His deep knowledge always impressed me and helped a lot.

Soon after Markus left the Institute, Stefan Holzer came into my room and I learnt a lot from him about modern hardware and software. He is a real expert in this area.

Tesfaye Ayalew told me a lot of interesting things about modern semiconductor devices and his questions to me were always useful for myself.

Interesting and fruitful discussions I shared with other colleagues among whom Jong Mun Park, Robert Klima, Robert Kosik, Robert Entner, Stephan Enzo Ungersböck, Klaus-Tibor Grassner and many others too numerous to mention here.

I would like to thank Intel Corporation, Santa Clara, USA and Semiconductor Research Corporation, USA for supporting this thesis.

CONTENTS

Kurzfassung	i
Abstract	iii
Acknowledgment	v
Contents	vi
Physical Quantities	xi
Constants	xii
List of Figures	xiii
List of Tables	xvi
1 Introduction	1
2 The Semiclassical Transport Model	4
2.1 Equations of Motion	6
2.1.1 Real Space Equation of Motion	6
2.1.1.1 Equation of Motion	6
2.1.1.2 Velocity-Band Structure Relationship	7
2.1.2 Time Evolution of the Quasi-Momentum	7
2.1.2.1 Equation of Motion	8

CONTENTS

2.1.2.2	Force Expression	8
2.1.3	General Properties of Semiclassical Dynamics	9
2.1.3.1	Phase Space Domain Evolution.	9
2.1.3.2	Constant External Electric Field	9
2.2	Distribution Function	9
2.2.1	Equilibrium Distribution	10
2.2.1.1	Statistical Distribution	11
2.2.1.2	Distribution of Fermions	12
2.2.1.3	Distribution of Bosons	13
2.2.2	Non-Equilibrium Distribution	14
2.2.2.1	Non-Equilibrium State	14
2.2.2.2	Interpretation Within the Relaxation Time Approximation . . .	15
2.3	Boltzmann's Transport Equation	16
2.3.1	Liouville's Theorem	16
2.3.2	Collision Integral	17
2.3.2.1	Scattering Probability	18
2.3.2.2	Pauli Exclusion Principle	18
2.3.2.3	Out-Scattering and In-Scattering Terms	19
2.3.3	Principle of Detailed Balance	21
2.4	Band Structure	21
2.4.1	Electron in a Periodic Potential	21
2.4.1.1	Bloch's Theorem	22
2.4.1.2	Energy Bands	22
2.4.1.3	Band Structure Periodicity	23
2.4.2	Analytical Band Structure	23
2.4.2.1	Effective Mass Tensor	23
2.4.2.2	Nonparabolic Band Structures	24
2.4.2.3	Analytical Band Structures of Si and Ge	24
2.4.2.4	Herring-Vogt Transformation	25
2.5	Scattering Mechanisms	27
2.5.1	Perturbation Theory	27

CONTENTS

2.5.1.1	First Order Perturbation	27
2.5.1.2	Fermi's Golden Rule	29
2.5.2	Scattering on Phonons	29
2.5.2.1	Phonon Concept	29
2.5.2.2	Intravalley Scattering by Acoustic Phonons	31
2.5.2.3	Intravalley Scattering by Optical Phonons	32
2.5.2.4	Intervalley Phonon Scattering	32
2.5.3	Plasmon Scattering	35
2.5.3.1	Plasmon Concept	35
2.5.3.2	Scattering Rate	36
2.5.4	Alloy Scattering	37
2.5.5	Ionized Impurity Scattering	37
2.5.5.1	Brooks-Herring Model	37
2.5.5.2	Two-Ion Scattering	38
2.5.5.3	Screening Theory	38
2.5.5.4	Second Born Correction	40
2.5.5.5	Ridley's Model	41
3	Strain Effects in $\text{Si}_{1-x}\text{Ge}_x$ Grown on a $\text{Si}_{1-y}\text{Ge}_y$ Substrate	42
3.1	SiGe Strained Layers	42
3.1.1	Critical Thickness and Dislocations	42
3.1.2	Applications of Strain	45
3.1.3	Strained Layers in Semiconductor Devices	45
3.1.3.1	Modulation-Doped FET	46
3.1.3.2	Strained MOSFET	46
3.2	Linear Deformation-Potential Theory	47
3.2.1	General Description of the Conduction Band Splitting in Strained SiGe	47
3.2.2	Strain Tensor	47
3.2.3	Stress Tensor	50
3.2.4	Energy Shift	52
3.2.4.1	Shift of Conduction Band Minima	52
3.2.4.2	Shift of the Mean Energy	53

CONTENTS

3.3	Substrate Orientation and Strain Tensor	53
3.3.1	Strain Tensor in the Interface Coordinate System	53
3.3.2	Coordinate System Transformation	55
3.3.2.1	Euler's Angles	55
3.3.2.2	Transformation Operator	55
3.3.2.3	Tensor Transformations	56
3.3.3	Strain Tensor Elements in the Principle Coordinate System	56
3.4	Band Structure of Strained SiGe layers	57
3.4.1	Hydrostatic Strain	57
3.4.2	Uniaxial Strain	57
3.4.2.1	Splitting of the X Valleys	58
3.4.2.2	Splitting of the L Valleys	58
3.4.3	Effective Masses in Strained SiGe	58
3.5	Scattering Mechanisms in Strained SiGe	59
3.5.1	Electron-Phonon Scattering	59
3.5.2	Ionized Impurity Scattering	59
3.5.3	Plasmon Scattering	60
4	Monte Carlo Methods for the Solution of the Boltzmann Equation	61
4.1	Perturbation Approach to the Boltzmann Equation Including the Pauli Principle	62
4.1.1	The Zeroth Order Equation	63
4.1.2	The First Order Equation	64
4.2	Integral Form of the First Order Equation	64
4.2.1	New Differential and Total Scattering Rates	64
4.2.2	Integral Form for the Distribution Function Perturbation	65
4.2.3	Free Term and Initial Distribution	66
4.2.4	The Resolvent Series	66
4.2.5	The Second Iteration of the Forward Resolvent Series	68
4.3	Zero Field Monte Carlo Algorithm Including the Pauli Principle	71
4.3.1	Low Field Carrier Mobility and Monte Carlo Techniques	72

CONTENTS

4.3.2	Specific of the Equilibrium Distribution	72
4.3.3	Total Scattering Rate	73
4.3.4	Expression for the Initial Distribution	74
4.3.5	Monte Carlo Algorithm for the Mobility Tensor	75
4.4	The High Field Small Signal Monte Carlo Algorithm	77
4.4.1	Solution of the Zeroth Order Equation	77
4.4.1.1	Initial Distributions of the Two Ensembles	78
4.4.1.2	Normalization of the Stationary Distribution Function	78
4.4.1.3	Integral Form of the Nonlinear Boltzmann Equation	79
4.4.2	Solution of the First Order Equation	81
4.4.3	Monte Carlo Algorithm for the Impulse Response	82
5	Modeling of Strained $\text{Si}_{1-x}\text{Ge}_x$ on $\text{Si}_{1-y}\text{Ge}_y$ Substrates	85
5.1	Low Field Electron Mobility in Undoped Layers	85
5.1.1	Si layers on $\text{Si}_{1-y}\text{Ge}_y$ substrates	85
5.1.1.1	Ge Composition Dependence of Perpendicular and In-plane Components	85
5.1.1.2	Substrate Orientation Dependence	89
5.1.2	$\text{Si}_{1-x}\text{Ge}_x$ layers on $\text{Si}_{1-y}\text{Ge}_y$ substrates	95
5.2	Low Field Electron Mobility in Doped Layers	99
5.3	Small Signal Response	104
6	Summary	107
A	Second Quantization	109
A.1	Many-Body Operators	109
A.2	Creation and Annihilation Operators	110
B	Random Phase Approximation and Plasmons	112
	Bibliography	114
	Own Publications	120
	Curriculum Vitae	122

List of Symbols

Physical Quantities

Ψ	...	time-dependent wave function
ψ	...	time-independent wave function
\mathbf{v}_n	...	electron velocity in band n
u_n	...	Bloch's envelope wave function
\mathbf{P}	...	momentum
\mathbf{p}	...	quasi-momentum
ε	...	dielectric function
$\boldsymbol{\varepsilon}$...	strain tensor
m^{-1}	...	inverse effective mass tensor
β_s	...	inverse screening length
β	...	the second Euler angle
α	...	the first Euler angle, nonparabolicity parameter
γ	...	the third Euler angle, band-form function
f	...	phase space distribution function
$\mathbf{K}(t)$...	phase space trajectory
$S(\mathbf{k}', \mathbf{k}, \mathbf{r}, t)$...	differential scattering rate from \mathbf{k}' to \mathbf{k}
$\lambda(\mathbf{k})$...	total scattering rate
Ξ	...	deformation potentials
E_f	...	Fermi energy
E_s	...	static electric field
E_1	...	perturbation of the electric field
f_s	...	static distribution
f_1	...	perturbation of the electronic distribution
Q	...	scattering term
$\epsilon(\mathbf{k})$...	dispersion law
\hat{H}	...	Hamiltonian operator
\mathcal{H}	...	Hamiltonian function

LIST OF SYMBOLS

\mathbf{H}	...	external magnetic field
\mathbf{A}	...	vector potential
\mathbf{E}	...	external electric field
\mathbf{F}	...	total external force
σ_{ik}	...	stress tensor components
Ω	...	thermodynamic potential
μ	...	chemical potential, mobility
$\omega(\mathbf{k})$...	dispersion law for phonons
τ	...	relaxation time
f_{eq}	...	equilibrium distribution
L	...	Lagrangian function
\mathbf{u}	...	atomic displacement
$a_{\mathbf{q}}$...	annihilation operator for a phonon with wave vector \mathbf{q}
$a_{\mathbf{q}}^+$...	creation operator for a phonon with wave vector \mathbf{q}
$c_{\mathbf{k}}$...	annihilation operator for an electron with wave vector \mathbf{k}
$c_{\mathbf{k}}^+$...	creation operator for an electron with wave vector \mathbf{k}
I_{ov}	...	overlap integral
u_s	...	sound velocity
D_A	...	acoustic deformation potential
D_o	...	optical deformation potential
ω_o	...	optical phonon energy
T_L	...	lattice temperature
ω_{pl}	...	plasmon frequency
\mathbf{q}_c	...	cut-off wave vector
\mathcal{F}	...	Fermi integrals
G	...	screening function
\mathbf{b}	...	Burger's vector

Constants

h	...	PLANCK's constant,	$6.6260755 \times 10^{-34} \text{ J s}$
\hbar	...	reduced PLANCK's constant,	$\hbar/(2\pi)$
k_B	...	BOLTZMANN's constant,	$1.380662 \times 10^{-23} \text{ J/K}$
q	...	elementary charge,	$1.6021892 \times 10^{-19} \text{ C}$
m_0	...	electron rest mass,	$9.1093897 \times 10^{-31} \text{ kg}$

LIST OF FIGURES

2.1	Momentum and quasi-momentum differ by the vector $\mathbf{D} = \frac{i\hbar}{m_0} \int u_{n\mathbf{k}}^*(\mathbf{r}) \nabla u_{n\mathbf{k}}(\mathbf{r}) d\mathbf{r}$.	7
2.2	Momentum and quasi-momentum for different shapes of the surface of constant energy.	8
2.3	Evolution of a domain in the (\mathbf{r}, \mathbf{k}) space. The domain changes its form but its volume is the same during the semiclassical evolution process.	10
2.4	The Fermi-Dirac distribution at zero and finite temperatures.	14
2.5	The Pauli exclusion principle forbids transitions to the states which are already occupied by electrons.	19
2.6	The surfaces of constant energy for Si and Ge.	25
2.7	Angles α and β with respect to the coordinate system which diagonalizes m^{-1} . .	26
3.1	Edge dislocation.	43
3.2	Screw dislocation.	44
3.3	S-MODFET structure.	46
3.4	Full degeneracy reduction due to the applied stress for a hypothetical band structure. For a general orientation of applied forces $\varepsilon_1 \neq \varepsilon_2 \neq \varepsilon_3 \neq \varepsilon_4$	48
3.5	Partial degeneracy reduction due to the applied stress for a hypothetical band structure. For applied forces oriented along high symmetry axes $\varepsilon_1 \neq \varepsilon_2 = \varepsilon_3 \neq \varepsilon_4$. 49	
3.6	The stress tensor components in terms of the applied forces.	51
3.7	Repopulation effect between X and L valleys in strained material.	54
4.1	Graphical representation of the first iteration term.	68

LIST OF FIGURES

4.2	Graphical representation of the second iteration term.	69
4.3	The same integration area can be covered either vertically a) or horizontally b). .	71
4.4	Schematic illustration of the scattering processes at high degeneracy.	73
4.5	Schematic representation of the zero field Monte Carlo algorithm. Here \mathbf{k}_b and \mathbf{k}_a denote before- and after-scattering states, respectively.	75
4.6	Zero field Monte Carlo flow chart.	76
4.7	Schematic representation of the small-signal algorithm.	83
4.8	Flow chart of the small-signal algorithm.	84
5.1	The perpendicular component of the low field electron mobility μ_{\perp}	86
5.2	The in-plane component of the low field electron mobility μ_{\parallel}	86
5.3	The valley population for the substrate orientation [001].	87
5.4	The valley population for the substrate orientation [111].	87
5.5	The band edges in strained Si grown on the substrate with the orientation [111].	88
5.6	μ_{\perp} as a function of α for $\beta = 40^\circ, 60^\circ$, and 80° in Si/Si _{0.5} Ge _{0.5}	90
5.7	μ_{\parallel} as a function of α for $\beta = 40^\circ, 60^\circ$, and 80° in Si/Si _{0.5} Ge _{0.5}	90
5.8	μ_{\perp} as a function of α for $\beta = 40^\circ, 60^\circ$, and 80° in Si/Si _{0.1} Ge _{0.9}	91
5.9	μ_{\parallel} as a function of α for $\beta = 40^\circ, 60^\circ$, and 80° in Si/Si _{0.1} Ge _{0.9}	91
5.10	The valley populations as functions of α for $\beta = 40^\circ$ in Si/Si _{0.5} Ge _{0.5}	92
5.11	The valley populations as functions of α for $\beta = 40^\circ$ in Si/Si _{0.1} Ge _{0.9}	92
5.12	The in-plane electron mobility μ_{\parallel} (cm ² /V·s) as a function of γ in Si grown on [110] Si _{1-y} Ge _y	93
5.13	The in-plane electron mobility μ_{\parallel} (cm ² /V·s) as a function of γ in Si grown on [412] Si _{1-y} Ge _y	93
5.14	The in-plane electron mobility μ_{\parallel} (cm ² /V·s) as a function of γ in Si grown on [123] Si _{1-y} Ge _y	94
5.15	The electron mobility μ_{\perp} and μ_{\parallel} in relaxed and strained Si _{1-x} Ge _x on the Si substrate with the orientation [001].	96
5.16	μ_{\perp} in Si _{1-x} Ge _x on Si _{0.7} Ge _{0.3} for several substrate orientations.	96
5.17	μ_{\parallel} in Si _{1-x} Ge _x on Si _{0.7} Ge _{0.3} for several substrate orientations.	97
5.18	μ_{\perp} in Si _{1-x} Ge _x on Si _{0.1} Ge _{0.9} for several substrate orientations.	97
5.19	μ_{\parallel} in Si _{1-x} Ge _x on Si _{0.1} Ge _{0.9} for several substrate orientations.	98
5.20	The valley populations as functions of the active layer composition for the Si _{0.1} Ge _{0.9} substrate with the orientation [221].	98

LIST OF FIGURES

5.21	The majority electron mobility in relaxed Si.	100
5.22	The doping dependence of μ_{\perp} in Si on $\text{Si}_{0.7}\text{Ge}_{0.3}$	100
5.23	The doping dependence of μ_{\parallel} in Si on $\text{Si}_{0.7}\text{Ge}_{0.3}$	101
5.24	The doping dependence of μ_{\perp} in Si on $\text{Si}_{0.1}\text{Ge}_{0.9}$	101
5.25	The doping dependence of μ_{\parallel} in Si on $\text{Si}_{0.1}\text{Ge}_{0.9}$	102
5.26	The valley population in strained Si grown on the $\text{Si}_{0.1}\text{Ge}_{0.9}$ substrate oriented along [111].	102
5.27	The composition dependence of μ_{\perp} in $\text{Si}_{1-x}\text{Ge}_x$ on [001] Si at several doping levels.103	
5.28	The composition dependence of μ_{\parallel} in $\text{Si}_{1-x}\text{Ge}_x$ on [001] Si at several doping levels.103	
5.29	The differential velocity in non-degenerate and degenerate ($n=10^{21} \text{ cm}^{-3}$) relaxed Si for a stationary electric field $E_s = 5\text{kV/cm}$	104
5.30	Energy distribution functions for the two carrier ensembles in non-degenerate relaxed Si.	105
5.31	Energy distribution functions for the two carrier ensembles in degenerate relaxed Si.	105
5.32	The differential velocity in non-degenerate relaxed and strained Si for $E_s = 5\text{kV/cm}$.106	
B.1	Feynman diagram for a single link.	112

LIST OF TABLES

2.1	Analytical conduction band structure parameters for Si and Ge.	25
2.2	Numerical values for the acoustic phonon scattering rate.	32
2.3	Numerical values for the intravalley L-L optical deformation potential scattering rate.	33
2.4	Numerical values for the intervalley X-X scattering rate.	33
2.5	Numerical values for the intervalley L-L scattering rate.	34
2.6	Numerical values for the non-equivalent intervalley scattering rate.	35
1	Publication Statistics	121

Chapter 1

Introduction

The application of strained layers in semiconductor devices took on another point of view when it was recognized that strained-layer structures might display new electronic and optical properties not seen in the unstrained-constituent materials. Before this conceptually new point of view, strained-layer growth was considered a compromise between a desire to produce semiconductor heterostructures and simultaneously to avoid misfit dislocations in these structures. This was changed later by noting that strain could be a tool for modifying the band structure of semiconductors in a useful and predictable fashion. As the bigger part of modern technology is silicon based, much research interest on strained layers is devoted to this material. Before silicon became dominant in semiconductor industry, germanium was the main material, and its properties are also well developed. As there is a difference in the lattice constants of these two materials, it is quite natural to strain silicon based devices by introducing germanium or its alloy with silicon into both active layers and substrates.

First data on SiGe were published in 1955 based on measurements of magneto-resistance [1]. Later in 1975 first $\text{Si}_{1-x}\text{Ge}_x$ layers with $x \leq 0.15$ were grown on Si substrates using ultra high vacuum epitaxy [2]. As the lattice constants of Si and Ge differ by 4.2%, the epitaxial layers were strained when sufficiently thin. At the beginning the strain was essentially considered a drawback which destroys the perfect crystal structure and cannot be avoided. But later in 1982 it was realized that this provided an additional option for band structure engineering [3]. Soon after that the strained-layer modulation-doped field effect transistor was fabricated [4]. Two years later the hetero-junction bipolar transistor was reimplemented using strained-layer $\text{Si}_{1-x}\text{Ge}_x/\text{Si}$ heterostructures [5–8]. In the early 1990s short-period SiGe superlattices became popular as promising results were obtained in this field. The most important results were enhanced optical absorption at the bandgap of short-period superlattice structures [9] and band to band photoluminescence and electroluminescence [10, 11]. At the end of the 1990s the idea of cascade lasers based on Si and SiGe heterostructures was discussed [12]. This idea turned into a large modern research area. Another present-day topic concerns quantum computing using SiGe heterostructures [13]. The idea is based on the difference of g factors in Si and Ge and the possibility to shift the electron wave function into layers with different Ge composition. This

INTRODUCTION

changes the spin Zeeman energy and in this way produces single-qubit operations.

This short historical review demonstrates undiminished interest in electronic devices based on strained SiGe and that this area is quite large and diversified. Thus the investigation of SiGe properties and their changes under strain conditions plays an important role for future applications of strained SiGe layers in electronic devices. However, the complicated physics of SiGe systems gets even more sophisticated when strain comes into play. This leads to the need for physical modeling of strained SiGe layers.

In particular, the necessity of physical modeling stems from the fact that the kinetic processes in semiconductors have a complex behavior which cannot be described analytically. The strain makes the situation even worse as it affects the kinetic properties of the material. One of the main tasks for the modeling of strained SiGe layers is thus to examine the modifications introduced by strain into the kinetic properties of the semiconductor.

One possible way to describe the kinetic properties of the material is based on the kinetic Boltzmann equation. This is an integral-differential equation which can be nonlinear when the quantum mechanical Pauli exclusion principle is taken into account. There are very many approaches for the solution of the kinetic equation, both analytical and numerical ones. However, only the Monte Carlo approach allows a comprehensive physical model to be included without further approximations. Additionally, strain effects can be included in a natural way in the formalism provided by the Boltzmann equation.

In this thesis electron transport in strained $\text{Si}_{1-x}\text{Ge}_x$ layers is studied using an analytical anisotropic and nonparabolic band structure model. The influence of strain on low field as well as high field kinetics including the small signal response is studied using Monte Carlo methods. Undoped and doped layers are considered and the quantum mechanical Pauli exclusion principle is taken into account. New Monte Carlo methods which are equally applicable to any level of degeneracy are developed.

The thesis is organized as follows:

Chapter 2 provides the description of the semiclassical transport model used in this work. The equations of motion, the distribution function, the Boltzmann equation and its validity, band structure and scattering mechanisms are discussed.

Chapter 3 treats the strain effects in SiGe within the deformation-potential theory. The stress and the strain tensor are introduced. Their transformations is then given and applied to obtain the elements of the strain tensor in the principle axes using Hooke's law. Finally, the influence of the strain on the band structure and the scattering mechanisms is considered.

Chapter 4 develops the zero field Monte Carlo algorithm used to obtain the low field electron mobility tensor in strained SiGe. The Pauli exclusion principle is included into the scattering operator. The Monte Carlo algorithm is then derived using an integral representation of the Boltzmann equation. The role of the Pauli exclusion principle on the scattering processes is explained and reversing of the inelastic processes is found at high degeneracy. Finally, a small signal Monte Carlo algorithm accounting for the Pauli exclusion principle is developed.

In **Chapter 5** applications are presented. The dependence of the low field mobility on the transport direction, Ge compositions of the substrate and the layer, substrate orientation and the doping level is investigated. To explain the mobility behavior the valley populations and the

INTRODUCTION

role of repopulation effects is studied. The small signal response including degeneracy effects is also explained.

Finally, **Chapter 6** presents a summary of the thesis.

Chapter 2

The Semiclassical Transport Model

The semiclassical transport model represents a generalization of the theory of free electrons in the case of a spatially-periodic potential. In the free electron theory electrons move between two collisions according to the classical equations of motion. From the quantum mechanical point of view these equations of motion actually describe the behavior of wave packets constructed using energy levels of a free electron. This can be generalized for the case of electrons in an arbitrary periodic potential where plane waves are replaced by Bloch's waves. The proof of this generalization is a difficult mathematical task. However it removes various contradictions of the free electron theory. In particular, in the semiclassical model electron collisions with motionless periodic ions do not influence the resistivity of a solid because now the electron interaction with fixed periodic lattice has been taken into account in the original Schrödinger's equation which Bloch's wave is obtained from. In other words, within Bloch's theory the classical point of view about scattering on fixed periodic ions is not valid any longer. From the quantum mechanical point of view this means that in a periodic structure of scattering centers a wave can move without any damping [14].

The semiclassical model based on the concept of Bloch's wave packets correctly works only when the electron position is measured with an accuracy of the wave packet width. The fact that the wave packet width must be less than the size of the Brillouin zone can be used to estimate the size of Bloch's wave packets and the limitations of the semiclassical model. Similar to the theory of free electrons, the wave packet is constructed using energy levels of an electron. But now an electron is represented by Bloch's wave:

$$\Psi_n(\mathbf{r}, t) = \sum_{\mathbf{k}'} A_{\mathbf{k}'} \psi_{n\mathbf{k}'}(\mathbf{r}) \exp\left(-\frac{i}{\hbar} E_n(\mathbf{k}') t\right), \quad (2.1)$$

where n numerates bands and $A_{\mathbf{k}'} \approx 0$ for $|\mathbf{k}' - \mathbf{k}| > \Delta k$. Changing the position of an electron from \mathbf{r} to $\mathbf{r} + \mathbf{R}$, where \mathbf{R} is a Bravais lattice vector, gives:

$$\Psi_n(\mathbf{r} + \mathbf{R}, t) = \sum_{\mathbf{k}'} A_{\mathbf{k}'} \psi_{n\mathbf{k}'}(\mathbf{r}) \exp\left(i\mathbf{k}' \cdot \mathbf{R} - \frac{i E_n(\mathbf{k}') t}{\hbar}\right). \quad (2.2)$$

THE SEMICLASSICAL TRANSPORT MODEL

As a function of \mathbf{R} this expression is just a superposition of plane waves with another weight. Thus the wave packet must be localized in a domain with a characteristic size $\Delta R \approx 1/\Delta k$. The characteristic size Δk is less than the size of the Brillouin zone which is of the order of $1/a$, where a is the lattice constant. This gives the condition $\Delta R > a$, that is, the wave packet built from Bloch energy levels and which has a wave vector correctly determined in a domain smaller than the size of the Brillouin zone is smeared over a large number of elementary crystal cells in the coordinate space. Therefore the conclusion is that the semiclassical model describes the electron response to external electric and magnetic fields which slowly change within the wave packet's width and thus more slowly within an elementary cell. In this model such fields are responsible for the creation of classical forces which determine the evolution of the wave packet's coordinate and its wave vector.

It should be noted that the semiclassical model is more complex than the classical limit of free electrons. This difference comes from the fact that the characteristic length at which the lattice periodic potential considerably changes is smaller than the wave packet's width and thus this potential cannot be treated classically. Consequently, the semiclassical model represents only in part the classical limit as the external fields are only considered classically while the ion periodic field is treated quantum mechanically.

An additional element of the quantum mechanical nature of the semiclassical model is that the electron wave vector is only accurate to the vector \mathbf{k}_b of the reciprocal lattice. Thus two sets of variables $(n, \mathbf{r}, \mathbf{k})$ and $(n, \mathbf{r}, \mathbf{k} + \mathbf{k}_b)$ specify the same electron state. This means that all physically distinguishable wave vectors within the same band are located within the elementary cell of the reciprocal lattice.

The fact that in the semiclassical model the band number represents an integral of motion allows to formulate some restrictions on the external fields. For the amplitude of the electric field E the condition reads:

$$qEa \ll \frac{\Delta\epsilon(\mathbf{k})^2}{\epsilon_f}, \quad (2.3)$$

and for the amplitude of the magnetic field H the condition has a similar form:

$$\frac{\hbar q H}{mc} \ll \frac{\Delta\epsilon(\mathbf{k})^2}{\epsilon_f}, \quad (2.4)$$

where $\Delta\epsilon(\mathbf{k}) = \epsilon_n(\mathbf{k}) - \epsilon_{n'}(\mathbf{k})$ and ϵ_f is the Fermi energy. The frequency of the external electromagnetic field must satisfy the following condition:

$$\hbar\omega \ll \Delta\epsilon(\mathbf{k}), \quad (2.5)$$

which prevents that a photon with a high enough energy causes an interband transition. For the wave length of the external electromagnetic field the condition

$$\lambda \gg a \quad (2.6)$$

is necessary to make the concept of wave packets meaningful.

2.1 Equations of Motion

The semiclassical model predicts how the electron's position and wave vector change with time between two collisions under external fields. This description is possible from the knowledge of the band structure given by the functions $\epsilon_n(\mathbf{k})$. In the semiclassical model the functions $\epsilon_n(\mathbf{k})$ are known and the main goal is to relate the band structure to the kinetic properties.

2.1.1 Real Space Equation of Motion

In the semiclassical transport model the real space equation of motion relates the change of the electron position to the band structure of a solid.

2.1.1.1 Equation of Motion

The motion in real space is described by the following equation:

$$\frac{d\mathbf{r}}{dt} = \mathbf{v}_n(\mathbf{k}), \quad (2.7)$$

where $\mathbf{v}_n(\mathbf{k})$ is the quantum mechanical average of the velocity operator over an electron state represented as a Bloch wave packet for band index n :

$$\begin{aligned} \mathbf{v}_n(\mathbf{k}) &= \int \psi_{n\mathbf{k}}^*(\mathbf{r}) \hat{\mathbf{v}} \psi_{n\mathbf{k}}(\mathbf{r}) d\mathbf{r}, \\ \hat{\mathbf{v}} &= -i \frac{\hbar}{m_0} \nabla_{\mathbf{r}}. \end{aligned} \quad (2.8)$$

Using Bloch's wave function with the periodic amplitude $u_{n\mathbf{k}}(\mathbf{r})$ and the ortho-normality condition, equation (2.8) gives:

$$\mathbf{v}_n(\mathbf{k}) = \frac{\hbar \mathbf{k}}{m_0} - \frac{i\hbar}{m_0} \int u_{n\mathbf{k}}^*(\mathbf{r}) \nabla u_{n\mathbf{k}}(\mathbf{r}) d\mathbf{r}. \quad (2.9)$$

The important difference of this expression from that of the free electron theory consists in the second term which is in general not equal to zero. Thus $\mathbf{v}_n(\mathbf{k}) \neq \frac{\hbar \mathbf{k}}{m_0}$ and the directions of the quantum mechanical average of the velocity and quasi-momentum do not coincide in general as it is shown in Fig. 2.1. In the limiting case of free electrons the amplitude $u_{n\mathbf{k}}$ does not depend on position and thus the second term in (2.9) vanishes. In this case $\mathbf{v}_n(\mathbf{k}) = \frac{\hbar \mathbf{k}}{m_0}$ as in the theory of free electrons. This is another consequence of the quantum mechanical aspect of the semiclassical model, which uses the concept of quasi-momentum.

Note that the quasi-momentum does not coincide with the momentum of a Bloch electron. The point is that the momentum $\mathbf{P}_n(\mathbf{k}) = m_0 \mathbf{v}_n(\mathbf{k})$ of an electron changes under the action of the total force which also includes the periodic potential. The quasi-momentum $\mathbf{p} = \hbar \mathbf{k}$ of an electron only changes under the action of external fields and the periodic field of a crystal does not change the quasi-momentum of an electron.

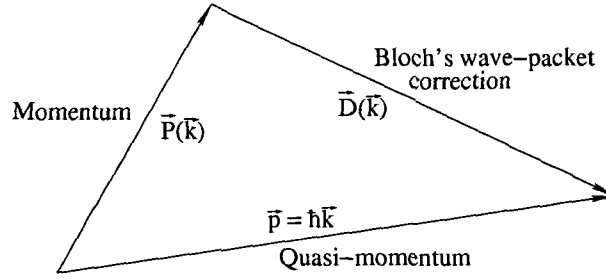


Figure 2.1: Momentum and quasi-momentum differ by the vector $\vec{D} = \frac{i\hbar}{m_0} \int u_{n\mathbf{k}}^*(\mathbf{r}) \nabla u_{n\mathbf{k}}(\mathbf{r}) d\mathbf{r}$.

2.1.1.2 Velocity-Band Structure Relationship

The relation of the average electron velocity to the band structure is established by the Schrödinger equation for the amplitude of a Bloch wave:

$$-\frac{\hbar^2}{2m_0} \nabla^2 u_{n\mathbf{k}}(\mathbf{r}) - \frac{i\hbar}{m_0} \mathbf{p} \cdot \nabla u_{n\mathbf{k}}(\mathbf{r}) + U(\mathbf{r}) u_{n\mathbf{k}}(\mathbf{r}) = \left(\epsilon_n(\mathbf{k}) - \frac{\mathbf{p}^2}{2m_0} \right) u_{n\mathbf{k}}(\mathbf{r}). \quad (2.10)$$

Using periodic boundary conditions and the Gauss theorem one obtains from (2.10):

$$-\frac{i\hbar}{m_0} (\mathbf{p} - \mathbf{p}') \cdot \int u_{n'\mathbf{k}'}^*(\mathbf{r}) \nabla u_{n\mathbf{k}}(\mathbf{r}) d\mathbf{r} = [\epsilon_n(\mathbf{k}) - \epsilon_{n'}(\mathbf{k}') - \frac{\mathbf{p}^2 - \mathbf{p}'^2}{2m_0}] \int u_{n'\mathbf{k}'}^*(\mathbf{r}) u_{n\mathbf{k}}(\mathbf{r}) d\mathbf{r}. \quad (2.11)$$

If $n = n'$ and $\mathbf{p}' \rightarrow \mathbf{p}$, so that $\epsilon_n(\mathbf{k}) - \epsilon_{n'}(\mathbf{k}') \approx (\mathbf{p} - \mathbf{p}') \cdot \frac{\nabla_{\mathbf{k}} \epsilon_n(\mathbf{k})}{\hbar}$, $\mathbf{p}^2 - \mathbf{p}'^2 \approx 2\mathbf{p} \cdot (\mathbf{p} - \mathbf{p}')$, it follows from (2.11):

$$-\frac{i\hbar}{m_0} \int u_{n\mathbf{k}}^*(\mathbf{r}) \nabla u_{n\mathbf{k}}(\mathbf{r}) d\mathbf{r} = \frac{1}{\hbar} \nabla_{\mathbf{k}} \epsilon_n(\mathbf{k}) - \frac{\mathbf{p}}{m_0}. \quad (2.12)$$

This equation together with (2.9) gives for the average electron velocity in band n with wave vector \mathbf{k} :

$$\mathbf{v}_n(\mathbf{k}) = \frac{1}{\hbar} \nabla_{\mathbf{k}} \epsilon_n(\mathbf{k}). \quad (2.13)$$

This relationship means that the average electron velocity in the band n is the gradient of the energy branch $\epsilon_n(\mathbf{k})$ in quasi-momentum space and is thus perpendicular to the surface of constant energy $\epsilon_n(\mathbf{k}) = \text{const}$. This also emphasizes the difference between momentum and quasi-momentum which are not parallel in general. For example, in the vicinity of a non-degenerate band extremum the surface of constant energy can be either a sphere or an ellipsoid. In the former case momentum and quasi-momentum are parallel and in the latter they are not parallel as it is shown in Fig. 2.2(a) and (b), respectively.

2.1.2 Time Evolution of the Quasi-Momentum

The equation of motion in quasi-momentum space describes how an electron quasi-momentum changes under applied external forces.

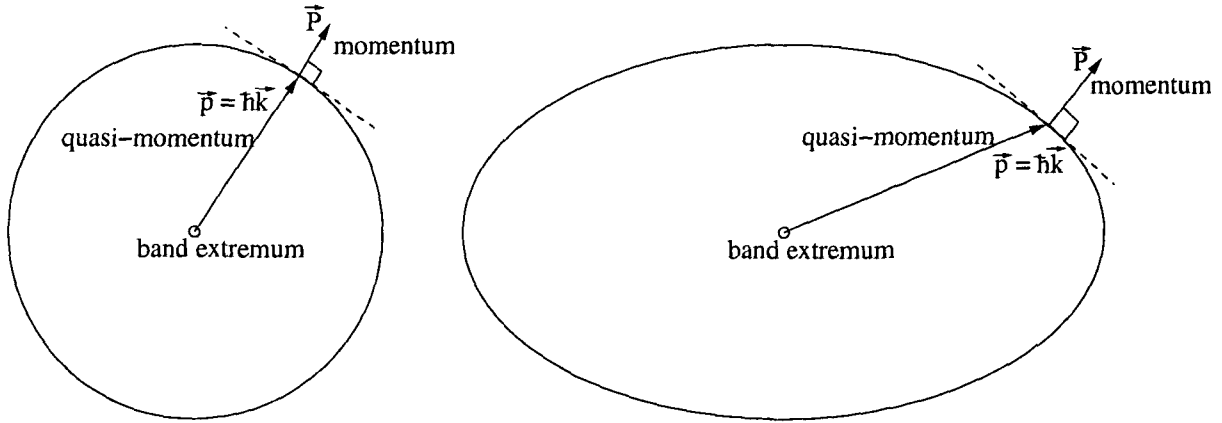


Figure 2.2: Momentum and quasi-momentum for different shapes of the surface of constant energy.

2.1.2.1 Equation of Motion

The evolution of the quasi-momentum governed by the equation:

$$\frac{d\mathbf{k}}{dt} = \frac{1}{\hbar} \mathbf{F}(\mathbf{r}, \mathbf{k}, t), \quad (2.14)$$

where $\mathbf{F}(\mathbf{r}, \mathbf{k}, t)$ is an external force which has a spatial and a time dependence. This equation looks like Newton's law but the sense is quite different because now only external fields are considered.

2.1.2.2 Force Expression

The external force in (2.14) includes both electric and magnetic forces. It represents their vector sum:

$$\mathbf{F}(\mathbf{r}, \mathbf{k}, t) = q \left(\mathbf{E}(\mathbf{r}, t) + \mathbf{v}_n(\mathbf{k}) \times \mathbf{B}(\mathbf{r}, t) \right), \quad (2.15)$$

where q is the particle charge. In the case of a time-independent electric field such an expression for the external force can be justified by the energy conservation law. If the electric field is fixed and $\phi(\mathbf{r})$ is the electrostatic potential then the Bloch wave packets travel in such a way that $\epsilon_n(\mathbf{k}(t)) + q\phi(\mathbf{r}(t)) = \text{const}$. The time derivative of this expression vanishes and taking (2.13) into account results in

$$\mathbf{v}_n(\mathbf{k}) \cdot (\hbar \dot{\mathbf{k}} + q \nabla \phi(\mathbf{r})) = 0. \quad (2.16)$$

This is the equation of motion in quasi-momentum space with the electric force according to (2.15). However, (2.16) is not a unique expression for the energy conservation as the expression $\hbar \dot{\mathbf{k}} + q \nabla \phi(\mathbf{r}) + \mathbf{f}$, where \mathbf{f} is a vector perpendicular to the average electron velocity \mathbf{v}_n , can also fulfill this requirement. It is possible to show that the only possible additional term is $\mathbf{f} = \mathbf{v}_n(\mathbf{k}) \times \mathbf{B}$, the Lorentz force, and that (2.15) is valid for time dependent external fields [15].

2.1.3 General Properties of Semiclassical Dynamics

The semiclassical equations of motion (2.7) and (2.14) with the band structure relation (2.13) and the force expression (2.15) have several important properties.

2.1.3.1 Phase Space Domain Evolution.

The equations of motion can be rewritten in a canonical form using the Hamiltonian for electrons in band n :

$$\mathcal{H}(\mathbf{r}, \mathbf{p}_c) = \epsilon_n \left(\frac{1}{\hbar} \{ \mathbf{p}_c - q\mathbf{A}(\mathbf{r}, t) \} \right) + q\phi(\mathbf{r}, t), \quad (2.17)$$

where \mathbf{p}_c stands for the quasi-momentum canonical conjugate to the electron coordinate \mathbf{r} and $\mathbf{A}(\mathbf{r}, t)$ is the vector potential. This canonical conjugate quasi-momentum differs from the quasi-momentum:

$$\mathbf{p} = \mathbf{p}_c - q\mathbf{A}(\mathbf{r}, t). \quad (2.18)$$

Therefore the semiclassical evolution process conserves volume of a domain moving in the $(\mathbf{r}, \mathbf{p}_c)$ space. Since the difference between quasi-momentum and conjugate quasi-momentum is a vector independent of \mathbf{p}_c , the domain volumes are also conserved in (\mathbf{r}, \mathbf{k}) space if the evolution process is described by the semiclassical equations of motion. This statement is schematically depicted in the Fig. 2.3. From this volume conservation law it follows that bands which are fully occupied do not contribute to the electrical conductivity and thus conduction is only possible for materials with partially filled bands.

2.1.3.2 Constant External Electric Field

For a uniform time-independent electric field the equation of motion in the quasi-momentum space (2.14) has the general solution

$$\mathbf{k}(t) = \mathbf{k}(0) + \frac{q\mathbf{E}}{\hbar}t. \quad (2.19)$$

This means that for a given time all wave vectors are shifted by the same vector. If an electron could travel in the quasi-momentum space between two collisions for distances longer than the size of the Brillouin zone, the static electric field would cause a time dependent current due to the periodicity of the average electron velocity in the quasi-momentum space. The fact that a static electric field can cause a time dependent electrical current cannot be explained from the classical point of view and represents the quantum mechanical property of the semiclassical model.

2.2 Distribution Function

Electrons in solids are described statistically by the distribution function in the phase space. This is a function of some coordinates and corresponding quasi-momenta. Additionally, in a non-equilibrium state the distribution function can depend also on time.

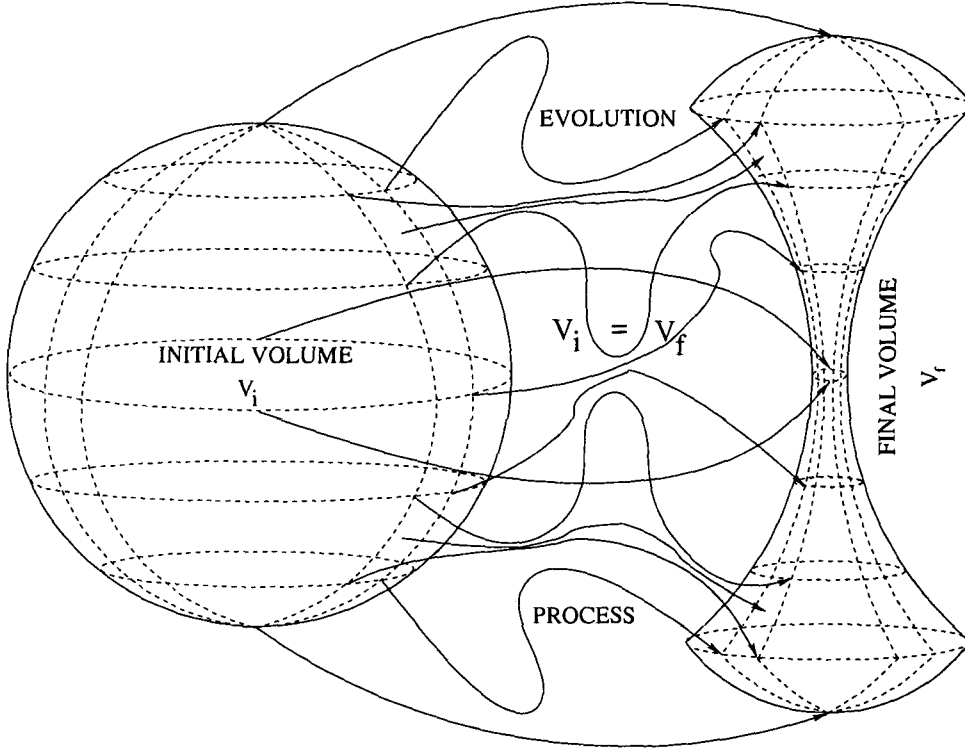


Figure 2.3: Evolution of a domain in the (\mathbf{r}, \mathbf{k}) space. The domain changes its form but its volume is the same during the semiclassical evolution process.

2.2.1 Equilibrium Distribution

Using the equations of motion described in Section 2.1 it is in principle possible to obtain the complete information about the motion of particles in a solid. However, in practice it would be necessary to solve a huge number of ordinary differential equations, which is not possible from a computational point of view. Due to the large number of degrees of freedom particle trajectories are on the one hand very quickly mixed in a complex way such that there is no possibility to find some regularity in physical properties but on the other hand new properties come into play at large number of degrees of freedom. These properties allow the system to be described by a statistical approach. This approach has nothing to do with mechanical regularity of a system and does not make any sense for systems with a small number of particles.

The statistical approach considers a closed system. From this system a subsystem¹ is separated, which is not closed and interacts with other subsystems of the system. Because of the large number of degrees of freedom of the system the interactions have a very complex character. Thus the state of the subsystem changes in a complex way. By this very nature the subsystem passes many times all its states during a rather long time interval T . A small domain² $\Delta\mathbf{r}\Delta\mathbf{k}$ of the subsystem will be visited many times. If Δt is the total time the subsystem spends in

¹In particular, this subsystem may be represented by one particle.

²Here \mathbf{r} and $\mathbf{p} = \hbar\mathbf{k}$ denote all coordinates and quasi-momenta of the subsystem. For an electron they are just (x, y, z) and (p_x, p_y, p_z) (in Cartesian coordinates).

$\Delta\mathbf{r}\Delta\mathbf{k}$, the quantity

$$w = \lim_{T \rightarrow \infty} \frac{\Delta t}{T} \quad (2.20)$$

can be treated as the probability of finding the subsystem in a state within the phase space domain $\Delta\mathbf{r}\Delta\mathbf{k}$ around (\mathbf{r}, \mathbf{k}) .

2.2.1.1 Statistical Distribution

Considering an infinitesimal element of the phase space $d\mathbf{r}d\mathbf{k}$ the probability dw that coordinates and quasi-momenta have values within intervals $[\mathbf{r}, \mathbf{r} + d\mathbf{r}]$ and $[\mathbf{k}, \mathbf{k} + d\mathbf{k}]$ is introduced through the expression:

$$dw = f(\mathbf{r}, \mathbf{k}) d\mathbf{r}d\mathbf{k}, \quad (2.21)$$

where $f(\mathbf{r}, \mathbf{k})$ is called a phase space distribution function³. The distribution function must satisfy the normalization condition

$$\int f(\mathbf{r}, \mathbf{k}) d\mathbf{r}d\mathbf{k} = 1, \quad (2.22)$$

which means that the sum of probabilities for all possible states must be equal to unity. The important property of the distribution function of a subsystem is that it does not depend on the initial state of another subsystem as its influence dies out by other subsystems. It does not depend on its own initial state either because the subsystem passes all its states during a long time interval and each of these states can be chosen as an initial one.

Using the distribution function it is possible to calculate the average of a function $g(\mathbf{r}, \mathbf{k})$ which depends on the coordinates and quasi-momenta of a subsystem

$$\langle g \rangle = \int g(\mathbf{r}, \mathbf{k}) f(\mathbf{r}, \mathbf{k}) d\mathbf{r}d\mathbf{k}. \quad (2.23)$$

This statistical average removes the necessity to follow $g(\mathbf{r}, \mathbf{k})$ in time in order to make an average. It is completely equivalent to the time average

$$\langle g \rangle = \lim_{T \rightarrow \infty} \frac{1}{T} \int g(t) dt. \quad (2.24)$$

If the closed system is in a state in which all its parts have their physical values close to their statistical averages, the system is in the statistical or thermodynamic equilibrium. It is clear that a closed system spends the most of its time in the thermodynamic equilibrium. If at some moment it is not in the thermodynamic equilibrium then it will relax to the equilibrium state. The time interval of the transition to the equilibrium state is called a relaxation time.

³Note that due to the fact that $\frac{\partial(\mathbf{r}, \mathbf{k})}{\partial(\mathbf{r}, \mathbf{k}_c)} = 1$ we can consider the phase space distribution as a function of the variables $(\mathbf{r}, \mathbf{k}_c)$ in the phase space of the variables which are canonically conjugated through the Hamiltonian (2.17). This will be assumed in the following.

The fact that different subsystems do not interact with each other⁴ leads to the possibility to consider them independent in a statistical sense. The statistical independence implies that a state of one subsystem does not influence the state probabilities of other subsystems.

From the mathematical point of view statistical independence means that the probability for a subsystem which consists of two parts to be in the element of its phase space⁵ $drdk = dr_1dk_1dr_2dk_2$ is equal to the product of the probabilities for each of the two subsystems to have coordinates and quasi-momenta in dr_1dk_1 and dr_2dk_2 . Using (2.21) this gives

$$f(\mathbf{r}_1, \mathbf{r}_2, \mathbf{k}_1, \mathbf{k}_2) = f_1(\mathbf{r}_1, \mathbf{k}_1)f_2(\mathbf{r}_2, \mathbf{k}_2), \quad (2.25)$$

where $f(\mathbf{r}_1, \mathbf{r}_2, \mathbf{k}_1, \mathbf{k}_2)$ is the distribution function for the constituent subsystem and $f_1(\mathbf{r}_1, \mathbf{k}_1)$, $f_2(\mathbf{r}_2, \mathbf{k}_2)$ are the distribution functions of the two subsystems. It is obvious that the same equality (2.25) is valid for any number of subsystems.

Let two functions $g_1(\mathbf{r}_1, \mathbf{k}_1)$ and $g_2(\mathbf{r}_2, \mathbf{k}_2)$ describe the two subsystems. In this way they describe the subsystem which consists of the two subsystems. From (2.23) and (2.25) it follows that the statistical average of the product $g_1(\mathbf{r}_1, \mathbf{k}_1)g_2(\mathbf{r}_2, \mathbf{k}_2)$ is equal to the product of the statistical averages:

$$\langle g_1 g_2 \rangle = \langle g_1 \rangle \langle g_2 \rangle. \quad (2.26)$$

Considering particles as independent subsystems it is possible to determine their equilibrium distribution functions. However, these distributions depend on the wave function which describes the whole system. It can be either symmetric or antisymmetric with respect to the exchange of any two particles of the system. In turn it depends on the spin of particles. Particles with an integer spin are subject to the Bose-Einstein statistics, while particles with fractional spin are subject to the Fermi-Dirac statistics.

2.2.1.2 Distribution of Fermions

For a system of particles described by antisymmetric wave functions the Pauli exclusion principle implies that only one particle can be placed at each quantum state. To derive the distribution function the Gibbs distribution is applied to the subsystem of particles which are in the same quantum state. This is possible even in the presence of the exchange interaction because it only takes place inside the subsystem. Taking into account that the energy is equal to $n_k \epsilon_k$ the thermodynamic potential is given as:

$$\Omega_k = -k_B T \ln \sum_{n_k} \exp \left(\frac{\mu - \epsilon_k}{k_B T} \right)^{n_k}, \quad (2.27)$$

where k stands for all quantum numbers characterizing the particle state, n_k is the number of particles in state k and μ is the chemical potential of the system⁶. According to the Pauli exclusion principle occupation numbers n_k for fermions can only take values 0 or 1. Thus the thermodynamic potential has the form:

$$\Omega_k = -k_B T \ln \left[1 + \exp \left(\frac{\mu - \epsilon_k}{k_B T} \right) \right]. \quad (2.28)$$

⁴For particles this means the absence of scattering between them.

⁵Here dr_1dk_1 and dr_2dk_2 are elements of phase spaces of the two parts.

⁶In solids μ is the Fermi energy denoted as ϵ_f .

Since the average number of particles is defined through the derivative of the thermodynamic potential (2.28), with respect to the chemical potential μ by the expression:

$$\langle n_k \rangle = -\frac{\partial \Omega_k}{\partial \mu}, \quad (2.29)$$

the expression for the average fermion number in state k is:

$$\langle n_k \rangle = \frac{1}{\exp\left(\frac{\epsilon_k - \mu}{k_B T}\right) + 1}. \quad (2.30)$$

It can be seen from (2.30) that all $n_k \leq 1$ and when $\exp\{(\mu - \epsilon_k)/k_B T\} \ll 1$ the Boltzmann distribution function⁷ is obtained. The normalization is obtained from the condition that the sum over all $\langle n_k \rangle$ is equal to the total number of particles N in the system:

$$\sum_k \frac{1}{\exp\left(\frac{\epsilon_k - \mu}{k_B T}\right) + 1} = N. \quad (2.31)$$

The normalization condition gives the chemical potential μ as an implicit function of the temperature T and the total number of particles N in the system.

For example, for the equilibrium electron gas in solids the number of electrons in the phase space element $dr dk$ can now be written as⁸:

$$dN_{el} = \frac{2}{\exp\left(\frac{\epsilon(\mathbf{k}) - \epsilon_f}{k_B T}\right) + 1} \frac{d^3 k d^3 r}{(2\pi)^3}. \quad (2.32)$$

The physical meaning of the Fermi energy is that it is the largest electron energy at zero temperature. It is a boundary between occupied and free states. At non-zero temperatures electrons can also occupy states above the Fermi energy as shown in Fig. 2.4.

2.2.1.3 Distribution of Bosons

In the case of symmetric wave functions the occupation numbers of quantum states are not limited and can take on any values. The series (2.27) converges only if $\exp[(\mu - \epsilon_k)/k_B T] < 1$. This condition is valid for any ϵ_k including zero. Thus the chemical potential must be negative while for fermions it can take both positive and negative values.

The series (2.27) represents a geometric progression and its value can easily be obtained:

$$\Omega_k = k_B T \ln \left(1 - \exp\left(\frac{\mu - \epsilon_k}{k_B T}\right) \right). \quad (2.33)$$

Using (2.29) one obtains from (2.33) for the average number of bosons:

$$\langle n_k \rangle = \frac{1}{\exp\left(\frac{\epsilon_k - \mu}{k_B T}\right) - 1}. \quad (2.34)$$

⁷The Boltzmann distribution is valid when all $\langle n_k \rangle \ll 1$. Physically it corresponds to a dilute system.

⁸The factor $1/(2\pi)^3$ comes from the fact that in the quasi-classical case the phase space volume $(2\pi\hbar)^3$ corresponds to two quantum states of a particle. These states differ by spin orientation.

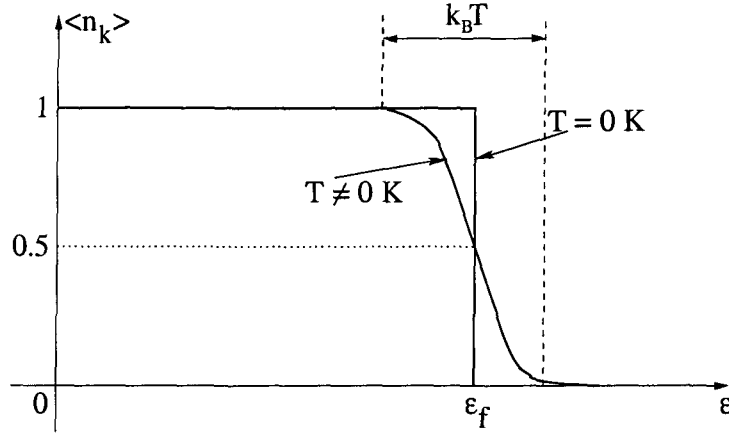


Figure 2.4: The Fermi-Dirac distribution at zero and finite temperatures.

Considering the equilibrium phonon gas the number of phonons in the phase space element $d\mathbf{r}d\mathbf{k}$ can now be written as⁹:

$$dN_{ph} = \frac{1}{\exp\left(\frac{\hbar\omega(\mathbf{k})}{k_B T}\right) - 1} \frac{d^3 k d^3 r}{(2\pi)^3}, \quad (2.35)$$

where ω is the phonon frequency.

2.2.2 Non-Equilibrium Distribution

A non-equilibrium state can be described analogously to the equilibrium state introducing a distribution function, which is called the non-equilibrium distribution function in this case.

2.2.2.1 Non-Equilibrium State

If a closed system is in a state in which some of its parts have physical quantities different from their statistical averages, the system is in a non-equilibrium state. It is assumed that a non-equilibrium state can be described by a non-equilibrium distribution function $f_n(\mathbf{r}, \mathbf{k}, t)$ which now depends on time. The electron number in band n at time t in the phase space volume $d\mathbf{r}d\mathbf{k}$ around point (\mathbf{r}, \mathbf{k}) is equal to:

$$dN_{el} = f_n(\mathbf{r}, \mathbf{k}, t) \frac{d\mathbf{r}d\mathbf{k}}{4\pi^3}. \quad (2.36)$$

When a closed system approaches its equilibrium the non-equilibrium distribution function tends to the equilibrium distribution (2.30).

⁹The spin of a phonon is taken to be zero. Thus the pre-factor $g = 2s + 1 = 1$. Since the phonon number is not fixed and determined by the equilibrium condition, the chemical potential of the phonon gas is equal to zero: $\mu = 0$.

2.2.2.2 Interpretation Within the Relaxation Time Approximation

To understand the structure of a non-equilibrium state and the difference from an equilibrium state it is useful to consider the relaxation time approximation before the general theory. The relaxation time $\tau_n(\mathbf{r}, \mathbf{k})$ is introduced in a way that the collision probability during the time interval dt for an electron in band n at phase space point (\mathbf{r}, \mathbf{k}) is equal to $dt/\tau_n(\mathbf{r}, \mathbf{k})$. In the relaxation time approximation it is inferred that some time after scattering has occurred the electron distribution does not depend on the non-equilibrium distribution just before the scattering. Additionally, if electrons have the equilibrium distribution with local temperature $T(\mathbf{r})$:

$$f_n^0(\mathbf{r}, \mathbf{k}) = \frac{1}{\exp\left(\frac{\epsilon_n(\mathbf{k}) - \mu(\mathbf{r})}{k_B T(\mathbf{r})}\right) + 1}, \quad (2.37)$$

the collisions do not affect the form of the distribution function. Therefore this approximation surmises that the information about the non-equilibrium state is completely lost due to the scattering processes¹⁰ and that the thermodynamic equilibrium corresponding to a local temperature is maintained through the scattering. This totally specifies the distribution function of those electrons, which have been scattered near point \mathbf{r} between t and $t + dt$. This distribution function is denoted as $df_n(\mathbf{r}, \mathbf{k}, t)$. It cannot depend on the non-equilibrium distribution function $f_n(\mathbf{r}, \mathbf{k}, t)$. Thus $df_n(\mathbf{r}, \mathbf{k}, t)$ can be found assuming an arbitrary form of $f_n(\mathbf{r}, \mathbf{k}, t)$. This can be done for example using expression (2.37) for the local equilibrium taking into account the fact that the collisions do not change its form. During a time interval dt an electron fraction $dt/\tau_n(\mathbf{r}, \mathbf{k})$ in band n with quasi-momentum $\hbar\mathbf{k}$ and coordinate \mathbf{r} are scattered, changing their band number and quasi-momentum¹¹. The distribution function $f_n^0(\mathbf{r}, \mathbf{k})$ cannot change which means that the distribution of those electrons which contribute to band n with quasi-momentum $\hbar\mathbf{k}$ during the same time interval dt , must exactly offset for all the losses. This leads to the following expression:

$$df_n(\mathbf{r}, \mathbf{k}, t) = \frac{dt}{\tau_n(\mathbf{r}, \mathbf{k})} f_n^0(\mathbf{r}, \mathbf{k}). \quad (2.38)$$

This equation mathematically reflects the essence of the relaxation time approximation.

The number of electrons (2.36) in band n at time t in the phase space domain $d\mathbf{r}d\mathbf{k}$ can be alternatively found selecting electrons by the time of the last collision. Let $\mathbf{r}_n(t')$ and $\mathbf{k}_n(t')$ be the solutions of the semiclassical equations of motion, (2.7) and (2.14), for band n . Let this semiclassical trajectory pass through point (\mathbf{r}, \mathbf{k}) at time $t' = t$: $\mathbf{r}_n(t) = \mathbf{r}$, $\mathbf{k}_n(t) = \mathbf{k}$. If at time t an electron was in the phase space domain $d\mathbf{r}d\mathbf{k}$ around (\mathbf{r}, \mathbf{k}) and had been scattered during the time interval $[t', t' + dt']$, it must be scattered to the phase space domain $d\mathbf{r}'d\mathbf{k}'$ around $(\mathbf{r}_n(t'), \mathbf{k}_n(t'))$ because after time t' its trajectory is completely determined by the equations of motion. Using (2.38) the total number of electrons scattered from point $(\mathbf{r}_n(t'), \mathbf{k}_n(t'))$ into the phase space domain $d\mathbf{r}'d\mathbf{k}'$ during the time interval $[t', t' + dt']$ can be written as:

$$\frac{f_n^0(\mathbf{r}_n(t'), \mathbf{k}_n(t')) dt' d\mathbf{r}d\mathbf{k}}{\tau_n(\mathbf{r}_n(t'), \mathbf{k}_n(t')) 4\pi^3}, \quad (2.39)$$

¹⁰This of course overestimates the efficiency of scattering needed to restore the equilibrium state.

¹¹In the semiclassical approach collisions are considered as instantaneous events taking place at a given point in real space. Thus the semiclassical transport model only considers changes of the non-equilibrium distribution function which happen during time intervals longer in comparison with the collision duration and at distances longer than the collision domain.

where the conservation law of the phase space volume has been used, that is, $dr'dk' = drdk$. Some of these electrons are not scattered between time moments t' and t . Let the relative number of these electrons be $P_n(\mathbf{r}, \mathbf{k}, t, t')$. Multiplying (2.39) by $P_n(\mathbf{r}, \mathbf{k}, t, t')$ and summing over all possible values of t' gives the expression for dN_{el} :

$$dN_{el} = \int_{-\infty}^t \frac{f_n^0(\mathbf{r}_n(t'), \mathbf{k}_n(t')) P_n(\mathbf{r}, \mathbf{k}, t, t') dt'}{\tau_n(\mathbf{r}_n(t'), \mathbf{k}_n(t'))}. \quad (2.40)$$

Comparison with (2.36) gives for the non-equilibrium distribution function:

$$f_n(\mathbf{r}, \mathbf{k}, t) = \int_{-\infty}^t \frac{f_n^0(\mathbf{r}_n(t'), \mathbf{k}_n(t')) P_n(\mathbf{r}, \mathbf{k}, t, t') dt'}{\tau_n(\mathbf{r}_n(t'), \mathbf{k}_n(t'))}. \quad (2.41)$$

The last expression clearly shows the structure of the non-equilibrium distribution function. The integrand includes the product of the total number of electrons scattered between t' and $t' + dt'$ and moving in such a way that they reach the phase space domain $drdk$ at time t assuming that no scattering events have occurred and the relative number of electrons which really reach the phase space domain $drdk$. The contribution from all possible time moments is taken into account by the time integration.

2.3 Boltzmann's Transport Equation

The general approach to obtain the non-equilibrium distribution function in the semiclassical approximation is based on the Boltzmann kinetic equation. The kinetic equation gives the microscopic description of the evolution process of the electron system. This description is valid at time intervals longer than the interaction duration and at distances longer than the size of the interaction domain.

2.3.1 Liouville's Theorem

The time interval during which a closed subsystem is observed can be divided into a large number of equal intervals separated by times t_1, t_2, t_3, \dots . At these moments the subsystem has corresponding phase space¹² points s_1, s_2, s_3, \dots , which are distributed in the phase space with the equilibrium distribution function¹³ $f(\mathbf{r}, \mathbf{k})$. The points s_1, s_2, s_3, \dots determine a statistical ensemble at the initial time $t = 0$. The motion of the ensemble's phase space points is governed by the semiclassical equations of motion containing coordinates and quasi-momenta of the subsystems only. At each time $t > 0$ all the phase points are distributed according to the same equilibrium distribution function. If the subsystem has l degrees of freedom, the motion can formally be considered as the stationary flow of a "phase space gas" in the $2l$ -dimensional phase space. This motion obeys a continuity equation¹⁴:

$$\text{div}(f\mathbf{v}) = 0. \quad (2.42)$$

¹²The phase space is considered in the sense of canonical conjugate variables.

¹³The fact that the equilibrium distribution is considered is shown by the absence of the time among the arguments.

¹⁴In steady state there is no any explicit time dependence. Thus $\frac{\partial f}{\partial t} = 0$.

In the case of the $2l$ -dimensional phase space the last expression gives:

$$\sum_{i=1}^l \left[\dot{r}_i \frac{\partial f}{\partial r_i} + \dot{p}_i \frac{\partial f}{\partial p_i} \right] + f \sum_{i=1}^l \left[\frac{\partial \dot{r}_i}{\partial r_i} + \frac{\partial \dot{p}_i}{\partial p_i} \right] = 0. \quad (2.43)$$

The second term in this expression is equal to zero due to the semiclassical equations of motion¹⁵. The first term the total time derivative of the distribution function. Hence (2.43) is reformulated as:

$$\frac{df}{dt} = 0, \quad (2.44)$$

where the differentiation is performed along the semiclassical phase space trajectories. This expression is called Liouville's theorem. From this theorem it follows that the equilibrium distribution function can only be expressed through such mathematical functions of coordinates and quasi-momenta which are conserved during the motion of the closed subsystem. Such functions are called *integrals of motion*. Thus the equilibrium distribution function itself represents an integral of motion.

As the equilibrium distribution function of two closed subsystems is equal to a product of the distribution functions of these subsystems (see (2.25)), the logarithm of the distribution function represents an additive integral of motion. It is well known from mechanics that there only exist seven independent integrals of motion. One of these integrals is the energy of a subsystem¹⁶. The dependence of the equilibrium distribution on the energy has already been shown for fermions (2.30) and bosons (2.34).

2.3.2 Collision Integral

If the scattering events could be neglected, each electron would represent a closed subsystem and equation (2.44) would completely determine the distribution function of an electron. The time derivative means here the differentiation along the semiclassical trajectory in the phase space of an individual electron. If an external force field acts on the electron system, the total time derivative can be expressed as:

$$\frac{df}{dt} = \frac{\partial f(\mathbf{r}, \mathbf{k}, t)}{\partial t} + \mathbf{v}(\mathbf{k}) \cdot \nabla f(\mathbf{r}, \mathbf{k}, t) + \frac{1}{\hbar} \mathbf{F}(\mathbf{r}) \cdot \frac{\partial f(\mathbf{r}, \mathbf{k}, t)}{\partial \mathbf{k}}, \quad (2.45)$$

where $\mathbf{F}(\mathbf{r})$ is the total external force given by (2.15).

If collisions are taken into consideration, Liouville's theorem is violated and the distribution function is no longer constant along semiclassical phase space trajectories. Instead of (2.44) one should write:

$$\frac{df}{dt} = \left(\frac{\partial f}{\partial t} \right)_{\text{coll}}, \quad (2.46)$$

where the right hand side is called the collision integral or scattering operator¹⁷. The collision integral is thus defined as the rate of change of the distribution function, that is, $\left(\frac{\partial f}{\partial t} \right)_{\text{coll}} \frac{d\mathbf{r} d\mathbf{k}}{(2\pi)^3}$

¹⁵This can be easily seen using the Hamiltonian form of the semiclassical equations of motion.

¹⁶The other six independent integrals of motion are the components of momentum of the subsystem and components of its angular momentum.

¹⁷The alternative symbol often used for the collision integral is $\mathbf{S}t f$.

is the change of the electron number per unit time in the phase space volume $d\mathbf{r}d\mathbf{k}$ due to scattering. Combining (2.45) and (2.46) gives the following equation:

$$\frac{\partial f(\mathbf{r}, \mathbf{k}, t)}{\partial t} + \mathbf{v}(\mathbf{k}) \cdot \nabla f(\mathbf{r}, \mathbf{k}, t) + \frac{1}{\hbar} \mathbf{F}(\mathbf{r}) \cdot \frac{\partial f(\mathbf{r}, \mathbf{k}, t)}{\partial \mathbf{k}} = \left(\frac{\partial f}{\partial t} \right)_{coll}. \quad (2.47)$$

Equations of this type represent kinetic equations in a general form. In the case of gases including the electron gas in solids it is usually called the Boltzmann kinetic equation. The kinetic equation takes a real meaning only when the form of the collisional integral is found. This form can be found accounting for electrons which are scattered in and out of a given phase space domain. The number of these electrons can be obtained introducing the scattering rate. In general each scattering mechanism is described by a scattering rate which can be found using the quantum mechanical scattering theory for an electron and the scattering center.

2.3.2.1 Scattering Probability

For a more detailed description of the collisions a probability that an electron is scattered per unit time from band n having quasi-momenta $\hbar\mathbf{k}$ to a state in band n' with quasi-momenta $\hbar\mathbf{k}'$ is assumed. This probability is obtained from the corresponding microscopic theory. The scattering probability is denoted as $S(\mathbf{k}, \mathbf{k}', \mathbf{r}, t)$ and introduced as follows¹⁸. The probability that an electron with quasi-momenta $\hbar\mathbf{k}$ and coordinate \mathbf{r} has been scattered during an infinitesimal time interval dt to an infinitesimal volume of the quasi-momenta space $d\mathbf{k}'$ around \mathbf{k}' is equal to:

$$S(\mathbf{k}, \mathbf{k}', \mathbf{r}, t) dt d\mathbf{k}'. \quad (2.48)$$

Here it is inferred that the final states are not occupied, that is, the definition of the function $S(\mathbf{k}, \mathbf{k}', \mathbf{r}, t)$ does not include the quantum mechanical Pauli exclusion principle. The form of this function depends on the type of a scattering mechanism. It can have a rather complex structure. In general it can depend on the distribution function itself.

2.3.2.2 Pauli Exclusion Principle

The quantity $S(\mathbf{k}, \mathbf{k}', \mathbf{r}, t) d\mathbf{k}'$ represents the probability per unit time that an electron with wave vector \mathbf{k} will be scattered to one of the levels in the domain $d\mathbf{k}'$ around \mathbf{k}' if the levels are not occupied. Thus the real rate of transitions should be less than this quantity by a factor given by the ratio between available levels and the total number of levels, as the Pauli principle forbids transitions to occupied levels. This is schematically shown in Fig. 2.5. The relative number of available states is equal to $1 - f(\mathbf{k}')$. The total probability that an electron will be scattered is given by the sum over all \mathbf{k}' , which can be converted to an integration over \mathbf{k}' :

$$\int (1 - f(\mathbf{r}, \mathbf{k}', t)) S(\mathbf{k}, \mathbf{k}', \mathbf{r}, t) d\mathbf{k}'. \quad (2.49)$$

¹⁸For the sake of simplicity the scattering within one band and without spin flipping is considered here.

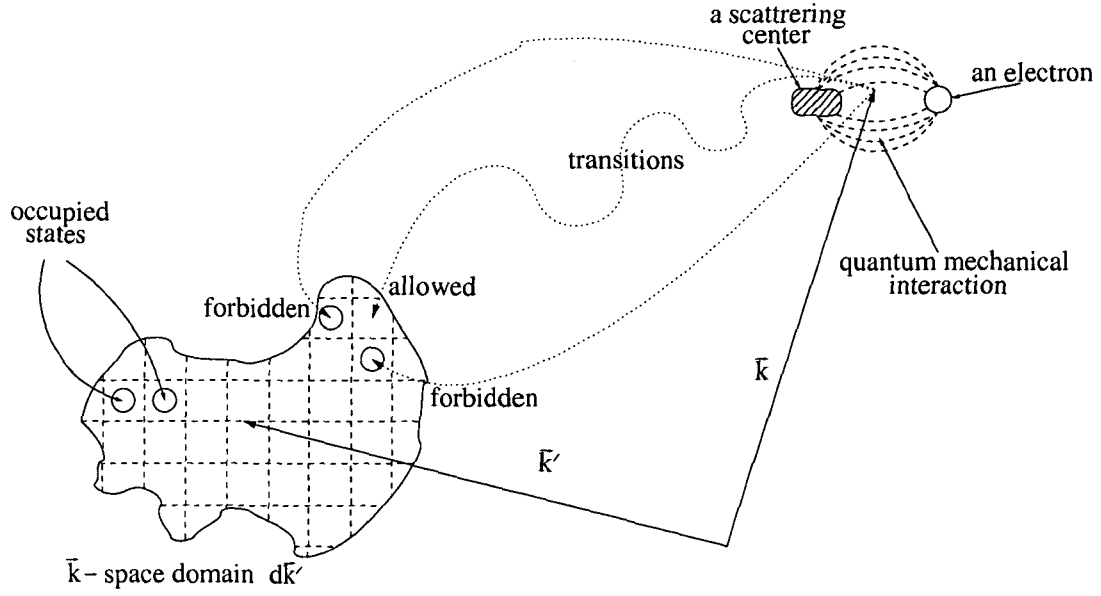


Figure 2.5: The Pauli exclusion principle forbids transitions to the states which are already occupied by electrons.

2.3.2.3 Out-Scattering and In-Scattering Terms

It is convenient to define a quantity $(\partial f(\mathbf{r}, \mathbf{k}, t)/\partial t)_{out}$ to express the electron number per unit volume with quasi-momenta in the infinitesimal volume $d\mathbf{k}$ around \mathbf{k} and which have been scattered during the infinitesimal time interval dt :

$$\left(\frac{\partial f(\mathbf{r}, \mathbf{k}, t)}{\partial t} \right)_{out} \frac{d\mathbf{k}}{(2\pi)^3} dt. \quad (2.50)$$

As the volume $d\mathbf{k}$ is infinitesimal, the scattering results in an electron being removed from this volume. Therefore (2.50) can also be considered as the number of electrons which are lost from the volume $d\mathbf{k}$ around \mathbf{k} during the time interval dt due to scattering.

The quantity $(\partial f(\mathbf{r}, \mathbf{k}, t)/\partial t)_{out}$ can be found from the fact that the expression

$$dt \int (1 - f(\mathbf{r}, \mathbf{k}', t)) S(\mathbf{k}, \mathbf{k}', \mathbf{r}, t) d\mathbf{k}'$$

is the probability that any electron from the vicinity of point \mathbf{k} has been scattered during the time interval dt and thus the total number of the scattered electrons in $d\mathbf{k}$ around \mathbf{k} is equal to

$$f(\mathbf{r}, \mathbf{k}, t) \frac{d\mathbf{k}}{(2\pi)^3} dt \int (1 - f(\mathbf{r}, \mathbf{k}', t)) S(\mathbf{k}, \mathbf{k}', \mathbf{r}, t) d\mathbf{k}'. \quad (2.51)$$

Comparison with (2.50) gives

$$\left(\frac{\partial f(\mathbf{r}, \mathbf{k}, t)}{\partial t} \right)_{out} = -f(\mathbf{r}, \mathbf{k}, t) \int (1 - f(\mathbf{r}, \mathbf{k}', t)) S(\mathbf{k}, \mathbf{k}', \mathbf{r}, t) d\mathbf{k}', \quad (2.52)$$

where the minus sign shows that this quantity describes the loss of electrons.

Scattering processes can change the distribution function in the opposite way. In addition to the scattering out of the domain $d\mathbf{k}$ there also exist scattering processes leading to a gain of electrons in $d\mathbf{k}$. To describe these processes it is natural to introduce the quantity $(\partial f(\mathbf{r}, \mathbf{k}, t)/\partial t)_{\text{in}}$ defined so that the expression

$$\left(\frac{\partial f(\mathbf{r}, \mathbf{k}, t)}{\partial t} \right)_{\text{in}} \frac{d\mathbf{k}}{(2\pi)^3} dt \quad (2.53)$$

gives the number of electrons per unit volume which are scattered into the volume $d\mathbf{k}$ around \mathbf{k} during the infinitesimal time interval dt . In order to find $(\partial f(\mathbf{r}, \mathbf{k}, t)/\partial t)_{\text{in}}$ it is necessary to consider electrons in $d\mathbf{k}'$ near \mathbf{k}' which are scattered into $d\mathbf{k}$ and sum over all possible \mathbf{k}' . The total number of electrons in $d\mathbf{k}'$ is equal to $f(\mathbf{r}, \mathbf{k}', t) d\mathbf{k}' / (2\pi)^3$. From this number of electrons only $S(\mathbf{k}', \mathbf{k}, \mathbf{r}, t) dt d\mathbf{k}$ would be scattered into $d\mathbf{k}$ around \mathbf{k} during dt if the corresponding states were not occupied. However only the fraction $1 - f(\mathbf{r}, \mathbf{k}, t)$ of the states are available. Thus, the total number of electrons per unit volume scattered into $d\mathbf{k}$ around \mathbf{k} from $d\mathbf{k}'$ around \mathbf{k}' during dt is equal to

$$f(\mathbf{r}, \mathbf{k}', t) \frac{d\mathbf{k}'}{(2\pi)^3} S(\mathbf{k}', \mathbf{k}, \mathbf{r}, t) d\mathbf{k} dt (1 - f(\mathbf{r}, \mathbf{k}, t)). \quad (2.54)$$

Summing over all possible \mathbf{k}' and comparing with (2.53) gives:

$$\left(\frac{\partial f(\mathbf{r}, \mathbf{k}, t)}{\partial t} \right)_{\text{in}} = (1 - f(\mathbf{r}, \mathbf{k}, t)) \int S(\mathbf{k}', \mathbf{k}, \mathbf{r}, t) f(\mathbf{r}, \mathbf{k}', t) d\mathbf{k}'. \quad (2.55)$$

Now the collision integral in (2.46) can be expressed as a sum of two terms:

$$\begin{aligned} \left(\frac{\partial f(\mathbf{r}, \mathbf{k}, t)}{\partial t} \right)_{\text{coll}} &= \left(\frac{\partial f(\mathbf{r}, \mathbf{k}, t)}{\partial t} \right)_{\text{in}} + \left(\frac{\partial f(\mathbf{r}, \mathbf{k}, t)}{\partial t} \right)_{\text{out}} = \\ &= (1 - f(\mathbf{r}, \mathbf{k}, t)) \int S(\mathbf{k}', \mathbf{k}, \mathbf{r}, t) f(\mathbf{r}, \mathbf{k}', t) d\mathbf{k}' - \\ &- f(\mathbf{r}, \mathbf{k}, t) \int (1 - f(\mathbf{r}, \mathbf{k}', t)) S(\mathbf{k}, \mathbf{k}', \mathbf{r}, t) d\mathbf{k}'. \end{aligned} \quad (2.56)$$

It should be noted that in the non-degenerate case when $f(\mathbf{r}, \mathbf{k}, t) \ll 1$ the scattering operator can be rewritten as:

$$\left(\frac{\partial f(\mathbf{r}, \mathbf{k}, t)}{\partial t} \right)_{\text{coll}} = \int S(\mathbf{k}', \mathbf{k}, \mathbf{r}, t) f(\mathbf{r}, \mathbf{k}', t) d\mathbf{k}' - f(\mathbf{r}, \mathbf{k}, t) \lambda(\mathbf{r}, \mathbf{k}, t), \quad (2.57)$$

where the total scattering rate $\lambda(\mathbf{r}, \mathbf{k}, t)$ is defined as follows:

$$\lambda(\mathbf{r}, \mathbf{k}, t) = \int S(\mathbf{k}, \mathbf{k}', \mathbf{r}, t) d\mathbf{k}'. \quad (2.58)$$

The Boltzmann equation takes now the form:

$$\begin{aligned} \frac{\partial f(\mathbf{r}, \mathbf{k}, t)}{\partial t} + \mathbf{v}(\mathbf{k}) \cdot \nabla f(\mathbf{r}, \mathbf{k}, t) + \frac{1}{\hbar} \mathbf{F}(\mathbf{r}) \cdot \frac{\partial f(\mathbf{r}, \mathbf{k}, t)}{\partial \mathbf{k}} = \\ = (1 - f(\mathbf{r}, \mathbf{k}, t)) \int S(\mathbf{k}', \mathbf{k}, \mathbf{r}, t) f(\mathbf{r}, \mathbf{k}', t) d\mathbf{k}' - \\ - f(\mathbf{r}, \mathbf{k}, t) \int (1 - f(\mathbf{r}, \mathbf{k}', t)) S(\mathbf{k}, \mathbf{k}', \mathbf{r}, t) d\mathbf{k}'. \end{aligned} \quad (2.59)$$

2.3.3 Principle of Detailed Balance

In equilibrium the distribution function is known and the left hand side of the Boltzmann equation is equal to zero¹⁹:

$$(1 - f_{\text{eq}}(\mathbf{r}, \mathbf{k}, t)) \int S(\mathbf{k}', \mathbf{k}, \mathbf{r}, t) f_{\text{eq}}(\mathbf{r}, \mathbf{k}', t) d\mathbf{k}' - f_{\text{eq}}(\mathbf{r}, \mathbf{k}, t) \int (1 - f_{\text{eq}}(\mathbf{r}, \mathbf{k}', t)) S(\mathbf{k}, \mathbf{k}', \mathbf{r}, t) d\mathbf{k}' = 0, \quad (2.60)$$

which is valid for any quasi-momenta $\hbar\mathbf{k}$. To satisfy this equation for all quasi-momenta $\hbar\mathbf{k}$ the following equality must be valid:

$$f_{\text{eq}}(\mathbf{r}, \mathbf{k}', t)(1 - f_{\text{eq}}(\mathbf{r}, \mathbf{k}, t))S(\mathbf{k}', \mathbf{k}, \mathbf{r}, t) = f_{\text{eq}}(\mathbf{r}, \mathbf{k}, t)(1 - f_{\text{eq}}(\mathbf{r}, \mathbf{k}', t))S(\mathbf{k}, \mathbf{k}', \mathbf{r}, t). \quad (2.61)$$

Using the explicit form of the Fermi-Dirac distribution function one obtains from (2.61):

$$S(\mathbf{k}', \mathbf{k}, \mathbf{r}, t) \exp \left[\frac{\epsilon(\mathbf{k})}{k_B T} \right] = S(\mathbf{k}, \mathbf{k}', \mathbf{r}, t) \exp \left[\frac{\epsilon(\mathbf{k}')}{k_B T} \right]. \quad (2.62)$$

Equation (2.62) is called the principle of detailed balance and relates the probabilities of forward and backward processes. For elastic processes, $\epsilon(\mathbf{k}) = \epsilon(\mathbf{k}')$, (2.62) gives:

$$S(\mathbf{k}', \mathbf{k}, \mathbf{r}, t) = S(\mathbf{k}, \mathbf{k}', \mathbf{r}, t), \quad (2.63)$$

that is for elastic processes the scattering probabilities of forward and backward processes are equal.

2.4 Band Structure

It has been pointed out in Section 2.1 that the quantum nature of the semiclassical transport model comes from the quantum mechanical consideration of a periodic crystal potential. This information is included into the electron energy dependence on the quasi-momentum $\epsilon(\mathbf{k})$. This dependence enters the Boltzmann kinetic equation (2.59) through relation (2.13) as well as through the differential scattering rates $S(\mathbf{k}, \mathbf{k}', \mathbf{r}, t)$. To solve the Boltzmann kinetic equation it is necessary to know the band structure and its specific features.

2.4.1 Electron in a Periodic Potential

In an ideal crystal the ions occupy positions which form a regular periodic structure. The potential $U(\mathbf{r})$ is thus a periodic function with the period equal to the period of the corresponding Bravais lattice:

$$U(\mathbf{r} + \mathbf{R}) = U(\mathbf{r}), \quad (2.64)$$

¹⁹This can easily be checked substituting (2.30) where $\epsilon(\mathbf{k})$ is replaced with $\epsilon(\mathbf{k}) + U(\mathbf{r})$, $U(\mathbf{r})$ is the potential energy.

where \mathbf{R} are the vectors which belong to the Bravais lattice. The period of the potential is of the same order as the de Broglie wave length which requires quantum mechanical consideration of the problem. As the total Hamiltonian for solids contains electron-electron interaction terms, the problem represents the many-body system. Within the theory of independent electrons an effective single-electron potential $U(\mathbf{r})$ is introduced. In the case of the ideal periodic crystal this potential must satisfy property (2.64). The main purpose is to analyze the periodicity²⁰ induced properties of the single-electron Schrödinger equation:

$$\left(-\frac{\hbar^2}{2m_0}\nabla^2 + U(\mathbf{r})\right)\psi(\mathbf{r}) = \epsilon\psi(\mathbf{r}). \quad (2.65)$$

Due to the potential periodicity the solution of this equation has several remarkable properties shortly given below.

2.4.1.1 Bloch's Theorem

Bloch's theorem states that the solution of equation (2.65) has the form of a plane wave multiplied by a function with the period of the Bravais lattice:

$$\psi_{n\mathbf{k}}(\mathbf{r}) = \exp(i\mathbf{k} \cdot \mathbf{r})u_{n\mathbf{k}}(\mathbf{r}), \quad (2.66)$$

where the function $u_{n\mathbf{k}}(\mathbf{r})$ satisfies the following condition:

$$u_{n\mathbf{k}}(\mathbf{r} + \mathbf{R}) = u_{n\mathbf{k}}(\mathbf{r}), \quad (2.67)$$

for all vectors lattice \mathbf{R} . Note that Bloch's theorem uses a vector \mathbf{k} . In the periodic potential this vector plays the role analogous to that of the wave vector in the theory of free electrons.

2.4.1.2 Energy Bands

In (2.66) n denotes the band index as there are several independent states for a given vector \mathbf{k} . This can be seen by substituting equation (2.66) into the Schrödinger equation (2.65) which gives:

$$\left\{\frac{\hbar^2}{2m_0}(-i\nabla + \mathbf{k})^2 + U(\mathbf{r})\right\}u_{\mathbf{k}}(\mathbf{r}) = \epsilon_{\mathbf{k}}u_{\mathbf{k}}(\mathbf{r}), \quad (2.68)$$

with the periodic boundary condition:

$$u_{\mathbf{k}}(\mathbf{r}) = u_{\mathbf{k}}(\mathbf{r} + \mathbf{R}). \quad (2.69)$$

This periodic boundary condition is very important as it allows to consider equation (2.68) as an eigenvalue problem for a finite volume, which leads to a discrete set of eigenvalues. The wave vector is only a parameter in this problem. Therefore, there are several branches²¹ of the electron energy $\epsilon_n(\mathbf{k})$.

²⁰It should be noted that the periodicity is only a simplification. Real crystals never have an ideal periodicity due to impurities, thermal vibrations and so forth.

²¹It is assumed that the discrete levels are continuous functions of the parameter \mathbf{k} .

2.4.1.3 Band Structure Periodicity

For two wave vectors \mathbf{k} and $\mathbf{k} + \mathbf{K}$ the solutions of Schrödinger equation (2.68) are equivalent because Bloch's theorem gives $\psi_{n\mathbf{k}}(\mathbf{r}) = \exp(i\mathbf{k} \cdot \mathbf{r})u_{n\mathbf{k}}(\mathbf{r})$ and $\psi_{n\mathbf{k}+\mathbf{K}}(\mathbf{r}) = \exp(i\mathbf{k} \cdot \mathbf{r})u_{n\mathbf{k}+\mathbf{K}}(\mathbf{r})$. This leads to equal eigenvalues

$$\epsilon_n(\mathbf{k}) = \epsilon_n(\mathbf{k} + \mathbf{K}), \quad (2.70)$$

and equal Bloch's amplitudes and thus equal wave functions

$$\psi_{n\mathbf{k}}(\mathbf{r}) = \psi_{n\mathbf{k}+\mathbf{K}}(\mathbf{r}). \quad (2.71)$$

It can be seen that each energy branch has the same period as the reciprocal lattice. As the functions $\epsilon_n(\mathbf{k})$ are periodic, they have maxima and minima which determine the width of the bands.

It should be noted that the wave vector \mathbf{k} in (2.66) can always be chosen in a way to belong to the first Brillouin zone because any vector \mathbf{k}' out of the first Brillouin zone can be represented as the sum $\mathbf{k}' = \mathbf{k} + \mathbf{K}$, where \mathbf{K} is a vector of the reciprocal lattice. Using the equivalent form of Bloch's theorem:

$$\psi_{n\mathbf{k}'}(\mathbf{r} + \mathbf{R}) = \exp(i\mathbf{k}' \cdot \mathbf{R})\psi_{n\mathbf{k}'}(\mathbf{r}) \quad (2.72)$$

together with (2.71) and the equality $\exp(i\mathbf{K} \cdot \mathbf{R}) = 1$ one obtains (2.72) for vector \mathbf{k} .

2.4.2 Analytical Band Structure

The full band structure gives a rather complete information about behavior of an electron in a given lattice. The determination of the band structure and its use in modeling problems are intricate problems. However, in many important physical phenomena only a small part of the Brillouin zone plays an essential role. This small part of the first Brillouin zone corresponds to energy levels near the bottom or top of some energy band. It turns out that for the description of the dispersion law in the vicinity of bands extrema it is possible to construct analytical expressions using only few parameters.

2.4.2.1 Effective Mass Tensor

If the extremum of the band n is located at the point $\mathbf{p}_0^n = \hbar\mathbf{k}_0^n$, the function $\epsilon_n(\mathbf{p})$ can be expanded into the Taylor series as follows²²

$$\epsilon_n(\mathbf{p}) = \epsilon_n(\mathbf{p}_0^n) + \frac{1}{2}m_{\alpha\beta}^{-1}(p_\alpha - p_{\alpha 0}^n)(p_\beta - p_{\beta 0}^n) + \dots \quad (2.73)$$

Here the linear terms vanish due to the definition of the point \mathbf{p}_0^n . The quantities $m_{\alpha\beta}^{-1}$ have the dimension of an inverse mass. They represent the second derivatives of the energy

$$m_{\alpha\beta}^{-1} = \left. \frac{\partial^2 \epsilon_n(\mathbf{p})}{\partial p_\alpha \partial p_\beta} \right|_{\mathbf{p}=\mathbf{p}_0^n}. \quad (2.74)$$

²²Summation is understood under repeated indices

As the value of a second derivative does not depend on the differentiation order, quantities $m_{\alpha\beta}^{-1}$ represent a symmetric tensor of the second rank²³ called the inverse effective-mass tensor. The components of this tensor depend on the coordinate system in quasi-momentum space. In particular the coordinate system can be chosen so that the non-diagonal components vanish, that is, $m_{\alpha\beta}^{-1} = 0$ for $\alpha \neq \beta$. This coordinate system is called a principle coordinate system. In the principle coordinate system (2.73) can be rewritten as:

$$\epsilon_n(\mathbf{p}) = \epsilon_n(\mathbf{p}_0^n) + \frac{1}{2} m_{\alpha}^{-1} (p_{\alpha} - p_{\alpha 0}^n)^2. \quad (2.75)$$

The equation of constant surface is obtained from the condition $\epsilon_n(\mathbf{p}) = \text{const}$ using (2.75):

$$\frac{(p_x - p_{x,0})^2}{2m_x} + \frac{(p_y - p_{y,0})^2}{2m_y} + \frac{(p_z - p_{z,0})^2}{2m_z} = \text{const}. \quad (2.76)$$

Thus the constant energy surface near a non-degenerate extremum represents an ellipsoid with the half-axes being proportional to $\sqrt{|m_x|}$, $\sqrt{|m_y|}$ and $\sqrt{|m_z|}$ and the center being placed at $\mathbf{p} = \mathbf{p}_0$. This means that the coordinate system chosen to diagonalize the tensor $m_{\alpha\beta}^{-1}$ coincides with the principle axes of an ellipsoid.

2.4.2.2 Nonparabolic Band Structures

When an electron occupies higher energy levels its dispersion law deviates from (2.75). In order to improve this situation and still use the analytical description of the band structure the $\mathbf{k} \cdot \mathbf{p}$ technique [16, 17] is employed and an additional nonparabolicity parameter is introduced for the conduction band extrema. This leads to a modified dependence of energy on the quasi-momentum in the conduction band [18, 19]:

$$\epsilon(\mathbf{k})(1 + \alpha\epsilon(\mathbf{k})) = \frac{\hbar^2}{2} \left(\frac{k_x^2}{m_x} + \frac{k_y^2}{m_y} + \frac{k_z^2}{m_z} \right), \quad (2.77)$$

where α is the nonparabolicity parameter and the energy reference point is at the band minimum.

2.4.2.3 Analytical Band Structures of Si and Ge

For Si the lowest extrema of the conduction band are located along the Δ axes near the X points of the first Brillouin zone and are called X valleys. In the case of Ge they are located exactly at the L points of the first Brillouin zone and called L valleys. Thus the surface of constant energy²⁴ for Si, equation (2.76), represents six full ellipsoids while for Ge it represents eight half-ellipsoids. This is also shown in Fig. 2.6. Two of the three effective masses are equal to each other and called transverse effective masses. The third mass is called the longitudinal effective mass. They are denoted by m_t and m_l , respectively²⁵. The numerical values [20] for the parameters of the analytical expression for the conduction band of Si and Ge are given in Table 2.1.

²³It should be noted that $m_{\alpha\beta}^{-1} > 0$ for a minimum, and $m_{\alpha\beta}^{-1} < 0$ for a maximum.

²⁴The surface in the first Brillouin zone.

²⁵For example for Si X valleys along z axes $m_x = m_y = m_t$, $m_z = m_l$.

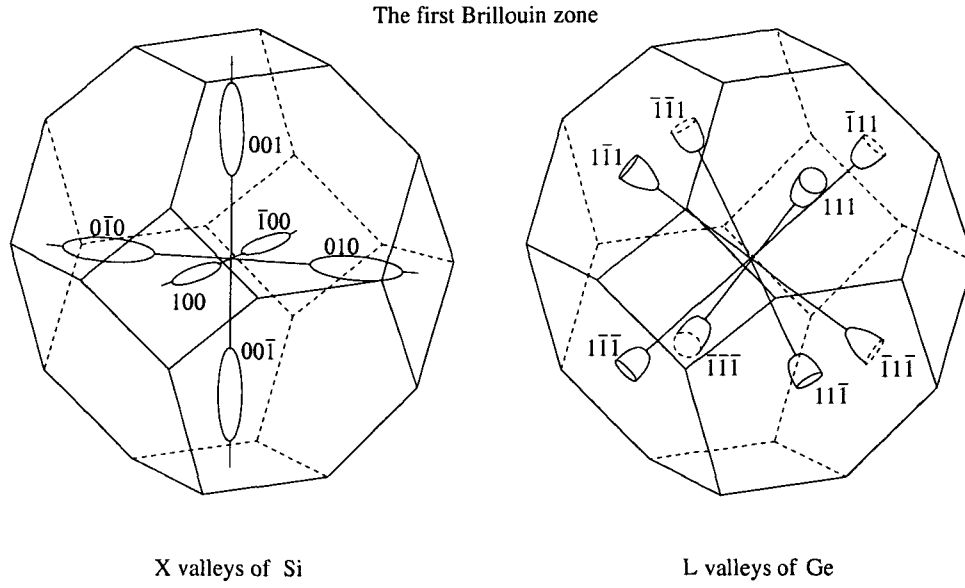


Figure 2.6: The surfaces of constant energy for Si and Ge.

	m_t^X	m_l^X	m_t^L	m_l^L	α_X	α_L
Silicon	0.191	0.903	0.126	1.634	0.5 eV^{-1}	0.3 eV^{-1}
Germanium	0.204	1.791	0.101	1.387	0.5 eV^{-1}	0.3 eV^{-1}

Table 2.1: Analytical conduction band structure parameters for Si and Ge.

2.4.2.4 Herring-Vogt Transformation

The analytical band structure given by (2.77) represents an anisotropic dispersion law. However, it is possible to transform [21] the coordinate system to obtain a spherical energy surface which is more convenient to work with. The orientation of the coordinate system is specified so that the tensors $m_{\alpha\beta}^{-1}$ for the valleys located along the Δ axes have the form:

$$m_x^{-1} = \begin{bmatrix} \frac{1}{m_{Xl}} & 0 & 0 \\ 0 & \frac{1}{m_{Xt}} & 0 \\ 0 & 0 & \frac{1}{m_{Xt}} \end{bmatrix}, \quad m_y^{-1} = \begin{bmatrix} \frac{1}{m_{Xt}} & 0 & 0 \\ 0 & \frac{1}{m_{Xl}} & 0 \\ 0 & 0 & \frac{1}{m_{Xt}} \end{bmatrix}, \quad m_z^{-1} = \begin{bmatrix} \frac{1}{m_{Xt}} & 0 & 0 \\ 0 & \frac{1}{m_{Xt}} & 0 \\ 0 & 0 & \frac{1}{m_{Xl}} \end{bmatrix}. \quad (2.78)$$

The transformation $\mathbf{w} = T\mathbf{k}$ is given by matrices T of the form:

$$T_x = \begin{bmatrix} \sqrt{\frac{m_0}{m_{Xl}}} & 0 & 0 \\ 0 & \sqrt{\frac{m_0}{m_{Xt}}} & 0 \\ 0 & 0 & \sqrt{\frac{m_0}{m_{Xt}}} \end{bmatrix}, \quad T_y = \begin{bmatrix} \sqrt{\frac{m_0}{m_{Xt}}} & 0 & 0 \\ 0 & \sqrt{\frac{m_0}{m_{Xl}}} & 0 \\ 0 & 0 & \sqrt{\frac{m_0}{m_{Xt}}} \end{bmatrix}, \quad (2.79)$$

$$T_z = \begin{bmatrix} \sqrt{\frac{m_0}{m_{Xt}}} & 0 & 0 \\ 0 & \sqrt{\frac{m_0}{m_{Xt}}} & 0 \\ 0 & 0 & \sqrt{\frac{m_0}{m_{Xl}}} \end{bmatrix}.$$

The dependence of energy on the wave-vector \mathbf{w} is now isotropic

$$\epsilon(\mathbf{k})(1 + \alpha\epsilon(\mathbf{k})) = \frac{\hbar^2 \mathbf{w}^2}{2m_0}. \quad (2.80)$$

For the valleys located at the L points the tensor $m_{\alpha\beta}^{-1}$ is not diagonal in the coordinate system chosen above. The right hand side of (2.77) can be expressed in terms of a rotation transformation D as follows:

$$\frac{\hbar^2}{2} \mathbf{k}^T D^T \begin{bmatrix} \frac{1}{m_{Li}} & 0 & 0 \\ 0 & \frac{1}{m_{Lt}} & 0 \\ 0 & 0 & \frac{1}{m_{Lt}} \end{bmatrix} D \mathbf{k}, \quad (2.81)$$

with matrix D defined as:

$$T = \begin{bmatrix} \cos \alpha \cos \beta & \sin \alpha \cos \beta & \sin \beta \\ -\sin \alpha & \cos \alpha & 0 \\ -\cos \alpha \sin \beta & -\sin \alpha \sin \beta & \cos \beta \end{bmatrix}, \quad (2.82)$$

where the angles α and β specify the longitudinal direction of an L valley as shown in Fig. 2.7. This longitudinal orientation is chosen to be x axis of the rotated coordinate system. Therefore

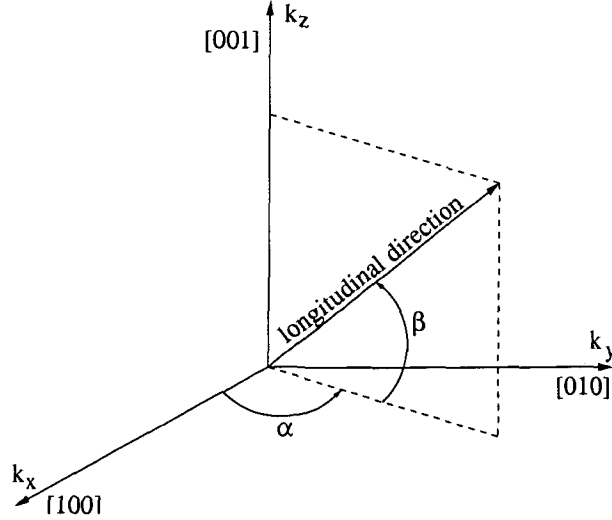


Figure 2.7: Angles α and β with respect to the coordinate system which diagonalizes m^{-1} .

the transformation matrices in this case are equal to SD , where the matrix S is given as

$$S = \begin{bmatrix} \sqrt{\frac{m_0}{m_{Li}}} & 0 & 0 \\ 0 & \sqrt{\frac{m_0}{m_{Lt}}} & 0 \\ 0 & 0 & \sqrt{\frac{m_0}{m_{Lt}}} \end{bmatrix}. \quad (2.83)$$

For example, for the $[111]$ orientation the angles are $\alpha = \frac{\pi}{4}$, $\sin \beta = \frac{1}{\sqrt{3}}$ and the matrix \mathbf{D} equals

$$D = \begin{bmatrix} \frac{1}{\sqrt{3}} & \frac{1}{\sqrt{3}} & \frac{1}{\sqrt{3}} \\ -\frac{1}{\sqrt{2}} & \frac{1}{\sqrt{2}} & 0 \\ -\frac{1}{\sqrt{6}} & -\frac{1}{\sqrt{6}} & \frac{\sqrt{2}}{\sqrt{3}} \end{bmatrix}. \quad (2.84)$$

Analogous expressions can easily be obtained for other orientations:

$$D_1 = \begin{bmatrix} -\frac{1}{\sqrt{3}} & \frac{1}{\sqrt{3}} & \frac{1}{\sqrt{3}} \\ -\frac{1}{\sqrt{2}} & -\frac{1}{\sqrt{2}} & 0 \\ \frac{1}{\sqrt{6}} & -\frac{1}{\sqrt{6}} & \frac{\sqrt{2}}{\sqrt{3}} \end{bmatrix}, \quad D_2 = \begin{bmatrix} -\frac{1}{\sqrt{3}} & -\frac{1}{\sqrt{3}} & \frac{1}{\sqrt{3}} \\ \frac{1}{\sqrt{2}} & -\frac{1}{\sqrt{2}} & 0 \\ \frac{1}{\sqrt{6}} & \frac{1}{\sqrt{6}} & \frac{\sqrt{2}}{\sqrt{3}} \end{bmatrix}, \quad D_3 = \begin{bmatrix} \frac{1}{\sqrt{3}} & -\frac{1}{\sqrt{3}} & \frac{1}{\sqrt{3}} \\ \frac{1}{\sqrt{2}} & \frac{1}{\sqrt{2}} & 0 \\ -\frac{1}{\sqrt{6}} & \frac{1}{\sqrt{6}} & \frac{\sqrt{2}}{\sqrt{3}} \end{bmatrix} \quad (2.85)$$

where indices 1, 2 and 3 specify orientations $[\bar{1}11]$, $[11\bar{1}]$, and $[1\bar{1}1]$, respectively.

2.5 Scattering Mechanisms

In an ideal periodic lattice an electron is not scattered at all. Within the approximation of independent electrons scattering occurs only due to deviations from the ideal periodicity. These deviations can be caused by various reasons, such as impurities, crystal defects, and thermal ion vibrations or phonons. Another type of scattering is due to electron-electron interactions. In this case there is a many body problem which is treated by the second quantization formalism introducing additional quasi-particles and considering scattering of electrons on these quasi-particles²⁶. Both types of scattering are used in this work and thus briefly described below.

2.5.1 Perturbation Theory

Deviations from an ideal lattice periodicity cause a deviation of the ideal crystal Hamiltonian \hat{H}_0 . The whole system is described by a new Hamiltonian \hat{H} . The new Schrödinger equation cannot be solved exactly in general²⁷. However if the deviations from the periodicity are small, it is possible to find corrections to the known solution obtained for \hat{H}_0 . Such corrections are obtained by the quantum mechanical perturbation theory.

2.5.1.1 First Order Perturbation

Let s denote a set of quantum numbers which characterize states of an unperturbed system. The corresponding wave functions are ψ_s and satisfy the unperturbed Schrödinger equation

$$\hat{H}_0 \psi_s = E_s \psi_s. \quad (2.86)$$

In the case of one electron in the lattice, s represents a band index n and the components of the quasi-momentum $\mathbf{p} = \hbar \mathbf{k}$, and ψ_s is Bloch's wave function given by (2.66). For electrons

²⁶For example electron-plasmon scattering.

²⁷In the sense that the form of its eigenstate cannot be determined in contrary to the ideal crystal case where Bloch's theorem exists.

in a vibrating lattice s includes in addition phonon numbers in all possible states and ψ_s is the product of a Bloch wave and the crystal wave function. Bloch's wave functions and the normal lattice modes are subject to the usual periodic boundary conditions in a cube. The wave functions ψ_s are ortho-normalized. Due to the interaction Hamiltonian \hat{H}_{int} the wave function ψ_s turns into a new wave function Ψ . At the initial time $t = 0$ the system is unperturbed which means $\Psi(t = 0) = \psi_s$. At $t > 0$ Ψ is determined by the equation²⁸

$$i\hbar \frac{\partial \Psi}{\partial t} = \hat{H} \Psi. \quad (2.87)$$

In the absence of the interaction equation (2.87) has the usual solution: $\Psi = \psi_s \exp(-iE_s t/\hbar)$. When the interaction is present $\Psi(t)$ can be represented as a series

$$\Psi(t) = \sum_{s''} a_{s''}(t) \psi_{s''} \exp\left(-\frac{i}{\hbar} E_{s''} t\right), \quad (2.88)$$

where $a_{s''}$ are yet unknown coefficients. Quantities $|a_{s''}(t)|^2$ are the probabilities of finding the system in state s'' at time t . They satisfy the condition

$$\sum_{s''} |a_{s''}(t)|^2 = 1. \quad (2.89)$$

Substituting (2.88) into (2.87) and forming the inner product $\langle a_{s'} | \Psi \rangle$ gives the equation for coefficients $a_{s''}$:

$$i\hbar \frac{\partial a_{s'}(t)}{\partial t} = \sum_{s''} \langle s' | H_{\text{int}} | s'' \rangle a_{s''}(t) \exp\left[\frac{i}{\hbar} (E_{s'} - E_{s''}) t\right]. \quad (2.90)$$

In the first order perturbation the unperturbed values of $a_{s''}$ are used in the right hand side²⁹ of (2.90). The unperturbed values of $a_{s''}$ follows from (2.88)³⁰:

$$i\hbar \frac{\partial a_{s'}}{\partial t} = \langle s' | H_{\text{int}} | s \rangle \exp\left[\frac{i}{\hbar} (E_{s'} - E_s) t\right]. \quad (2.91)$$

The solution of this equation is

$$a_{s'}(t) = \frac{-1 + \exp\left[\frac{i}{\hbar} (E_{s'} - E_s) t\right]}{E_s - E_{s'}} \langle s' | H_{\text{int}} | s \rangle. \quad (2.92)$$

Therefore the probability of finding a system at time t in state s' is

$$|a_{s'}(t)|^2 = \frac{2 \left[1 - \cos\left(\frac{E_{s'} - E_s}{\hbar} t\right) \right]}{(E_s - E_{s'})^2} |\langle s' | H_{\text{int}} | s \rangle|^2. \quad (2.93)$$

The transition probability per unit time is equal to the time derivative of (2.93):

$$\frac{d|a_{s'}(t)|^2}{dt} = \frac{2}{\hbar} \frac{\sin\left(\frac{E_{s'} - E_s}{\hbar} t\right)}{E_{s'} - E_s} |\langle s' | H_{\text{int}} | s \rangle|^2. \quad (2.94)$$

²⁸ \hat{H} denotes the full Hamiltonian: $\hat{H} = \hat{H}_0 + \hat{H}_{\text{int}}$.

²⁹ Matrix elements $\langle s' | H_{\text{int}} | s'' \rangle$ are considered as quantities of first order.

³⁰ The case when $s' \neq s$ is considered. The probability $|a_s(t)|^2$ is obtained from (2.89).

2.5.1.2 Fermi's Golden Rule

Expression (2.94) cannot directly be used in the kinetic equation (2.59) because of two reasons. The first reason is that it relates to transitions between states of a discrete spectrum³¹ while in the kinetic equation they are treated as continual states. The second one lies in the fact that in the semiclassical transport model scattering events are local in time. The first problem can be overcome by the fact that systems are usually macroscopic which allows to consider the discrete spectrum as quasi-continuous. The second problem is removed assuming that the free-flight time is much longer than the effective interaction time which allows to simplify (2.94) by taking the long interaction time limit³², namely for $t \rightarrow \infty$ one gets:

$$\frac{d|a_{s'}(t)|^2}{dt} = \frac{2\pi}{\hbar} |\langle s' | H_{\text{int}} | s \rangle|^2 \delta(E_{s'} - E_s). \quad (2.95)$$

This equality is called the Fermi golden rule and it shows that transitions only happen between states with equal energy $E_{s'} = E_s$. The proof that expression (2.95) can be used in the kinetic equation (2.59) represents a difficult problem. For the example of impurity scattering such proof can be found in [22, 23].

2.5.2 Scattering on Phonons

The thermal motion of atoms in the crystal may be considered as normal oscillations of the crystal lattice. The mechanical properties of this system are described by the following Lagrangian [24]:

$$L = \frac{1}{2} \sum_{\mathbf{n}s} m_s \dot{\mathbf{u}}_s^2(\mathbf{n}) - \frac{1}{2} \sum_{\mathbf{n}\mathbf{n}'s's'} \Lambda_{ik}^{ss'}(\mathbf{n} - \mathbf{n}') u_{si}(\mathbf{n}) u_{s'k}(\mathbf{n}') \quad (2.96)$$

which leads to equations of motion:

$$m_s \ddot{u}_{si} = - \sum_{\mathbf{n}'s'} \Lambda_{ik}^{ss'}(\mathbf{n} - \mathbf{n}') u_{s'k}(\mathbf{n}'). \quad (2.97)$$

Here $\mathbf{n} = (n_1, n_2, n_3)$, m_s are the atomic masses, \mathbf{u}_s are the atomic displacements. The solution of this equation represents a plane wave of the form:

$$\mathbf{u}_s(\mathbf{n}) = \mathbf{e}_s(\mathbf{k}) \exp\{i(\mathbf{k} \cdot \mathbf{r}_n - \omega t)\}, \quad (2.98)$$

where \mathbf{e}_s is the complex amplitude³³ which only depends on the position within the elementary cell.

2.5.2.1 Phonon Concept

From the quantum theory point of view instead of waves (2.98) phonons are introduced through the second quantization formalism (see Appendix A). Phonons represent quasi-particles moving

³¹Quasi-momentum components and phonon quasi-wave vectors are considered as discrete quantities.

³²Since it is assumed that an interaction decays much faster in comparison with the free-flight time, the error caused by the long interaction time limit is negligible.

³³It is also referred to as polarization.

in the crystal. The energy of a phonon is

$$\epsilon = \hbar\omega, \quad (2.99)$$

where ω is the frequency of the classical wave (2.98). The wave vector \mathbf{k} in (2.98) determines a phonon quasi-momentum as follows:

$$\mathbf{p} = \hbar\mathbf{k}. \quad (2.100)$$

This quantity is not unique as any quasi-momentum $\hbar\mathbf{k} + \hbar\mathbf{b}$, where \mathbf{b} is a reciprocal lattice vector, is physically equivalent to $\hbar\mathbf{k}$. The velocity of a phonon is determined as the group velocity of the corresponding classical waves $\mathbf{v}_{\text{gr}} = \partial\omega/\partial\mathbf{k}$ and has the form:

$$\mathbf{v} = \frac{\partial\epsilon(\mathbf{p})}{\partial\mathbf{p}}. \quad (2.101)$$

All the properties of the classical wave spectrum are valid for the energy spectrum of phonons. In particular it has $3n$ branches, three of which are acoustic ones. The wave density is now interpreted as the phonon density of states.

The free wave motion is considered as the free motion of non-interacting phonons. Inclusion of the anharmonicity leads to scattering processes in the phonon gas. These scattering processes restore the thermal equilibrium of the phonon gas. The processes conserve the quasi-momentum. However, this is only valid within an addition of a reciprocal lattice vector $\hbar\mathbf{b}$.

It should be noted that the phonon concept appears only as the quantum mechanical description of the collective atomic motion in a crystal and that phonons cannot be identified with individual atoms.

As applied to the electron transport in semiconductors the interaction between the electron gas and the phonon gas plays an important role. In this work only covalent semiconductors are considered. In this case the electron-phonon interaction can be successfully described using the deformation-potential approach [25]. In this case the interaction Hamiltonian in (2.95) is given as:

$$\hat{H}_{\text{el-ph}} = \Xi_{ij} \frac{\partial u_i}{\partial x_j}, \quad (2.102)$$

where Ξ_{ij} is the deformation-potential tensor describing the shift of a band per unit deformation. Using the continuous medium approximation the ion displacement takes the form:

$$\mathbf{u} = \sum_{\mathbf{q}} \left(\frac{\hbar}{2\rho V \omega_{\mathbf{q}}} \right)^{\frac{1}{2}} (a_{\mathbf{q}} + a_{-\mathbf{q}}^+) \exp(i\mathbf{q}\mathbf{r}) \mathbf{e}, \quad (2.103)$$

where ρ is the density of the crystal and a and a^+ stand for the phonon annihilation and creation operators, respectively. Therefore the interaction Hamiltonian is:

$$\hat{H}_{\text{el-ph}} = \sum_{\mathbf{q}} \left(\frac{\hbar}{2\rho V \omega_{\mathbf{q}}} \right)^{\frac{1}{2}} (a_{\mathbf{q}} + a_{-\mathbf{q}}^+) \exp(i\mathbf{q}\mathbf{r}) \Xi_{ij} i q_j e_i. \quad (2.104)$$

It is convenient to interpret this equation in terms of phonon emission and absorption processes. If in (2.95) $|s\rangle$ stands for $|N_{\mathbf{q}_1}, N_{\mathbf{q}_2}, \dots, N_{\mathbf{q}}, N_{\mathbf{q}'}, \dots\rangle |\mathbf{k}\rangle$ then in the sum over \mathbf{q} only two terms

will contribute: one from $\langle \dots, N_{\mathbf{q}} - 1, \dots | a_{\mathbf{q}} | \dots, N_{\mathbf{q}}, \dots \rangle$ with pre-factor $N_{\mathbf{q}}$ and the second from $\langle \dots, N_{\mathbf{q}} + 1, \dots | a_{\mathbf{q}}^\dagger | \dots, N_{\mathbf{q}}, \dots \rangle$ with pre-factor $N_{\mathbf{q}} + 1$. Thus using (2.95) the phonon differential scattering rates in the kinetic equation (2.59) take the form:

$$\begin{aligned} S^{ab}(\mathbf{k}, \mathbf{k}', \mathbf{r}, t) &= \frac{N_{\mathbf{q}} I_{ov} |\Xi_{ij} q_j e_i|^2}{8\pi^2 \rho \omega_{\mathbf{q}}} \delta[\epsilon(\mathbf{k}') - \epsilon(\mathbf{k}) - \hbar \omega_{\mathbf{q}}], \\ S^{em}(\mathbf{k}, \mathbf{k}', \mathbf{r}, t) &= \frac{(N_{\mathbf{q}} + 1) I_{ov} |\Xi_{ij} q_j e_i|^2}{8\pi^2 \rho \omega_{\mathbf{q}}} \delta[\epsilon(\mathbf{k}') - \epsilon(\mathbf{k}) + \hbar \omega_{\mathbf{q}}], \end{aligned} \quad (2.105)$$

where $N_{\mathbf{q}}$ is given by (2.34), that is, within this work the phonon gas is assumed to be in the equilibrium which is not valid in general [26–28]. I_{ov} is the overlap integral:

$$I_{ov} = \left| \int_{\text{el.cell}} d\mathbf{r} u_{\mathbf{k}'}^*(\mathbf{r}) u_{\mathbf{k}}(\mathbf{r}) \exp(i\mathbf{G} \cdot \mathbf{r}) \right|^2, \quad (2.106)$$

where \mathbf{G} is a reciprocal lattice vector. For intervalley transitions the angle between initial and final states depends mainly on the valleys involved in the transition, I_{ov} is nearly constant [29] and can be taken into account by renormalizing the corresponding coupling constant.

The most important phonon scattering processes for covalent semiconductors can be described by (2.105). Those of them which are important for Si, Ge and SiGe are briefly given below.

2.5.2.2 Intravalley Scattering by Acoustic Phonons

This type of scattering assumes that the initial and final states of an electron are within the same valley. The acoustic scattering mechanism is assumed to be elastic which is an approximation called equipartition [18]. For this type of scattering the transition probability is given by:

$$\lambda(\epsilon) = \frac{2\pi k_B T_L D_{A_i}^2}{\hbar u_s^2 \rho} g_i(\epsilon), \quad (2.107)$$

where i is the valley index, T_L is the lattice temperature, D_{A_i} is the acoustic deformation potential of the i -th valley, u_s denotes the average sound velocity, ρ is the density of the crystal and $g_i(E)$ the density of states per spin in the i -th valley which is defined by the following formula:

$$g_i(\epsilon) = \frac{1}{(2\pi)^3} \int_{BZ} \delta(\epsilon - \epsilon_i(\mathbf{k})) d^3k. \quad (2.108)$$

For the analytical band structure (2.77) it follows from (2.108):

$$g_i(\epsilon) = \frac{1}{(2\pi)^2} \frac{2m_{d_i}^*}{\hbar^2} \sqrt{\gamma_i(\epsilon)} (1 + 2\alpha_i \epsilon), \quad (2.109)$$

where $m_{d_i}^*$ is the density of states effective mass for the i -th valley, and $\gamma_i(E)$ denotes the band-form function:

$$\gamma_i(\epsilon) = \epsilon(1 + \alpha_i \epsilon). \quad (2.110)$$

The average sound velocity is defined as:

$$u_s = \frac{1}{3}(2u_t + u_l), \quad (2.111)$$

where u_t and u_l are the transverse and longitudinal components of the sound velocity.

The numerical values for the parameters [18, 20] of the acoustic phonon scattering rate are given in table Table 2.2.

	D_{AX}	D_{AL}	ρ	u_t	u_l
Silicon	7.2 eV	11.0 eV	$2.338 \times 10^{-3} \text{ kg/cm}^3$	$5.410 \times 10^5 \text{ cm/sec}$	$9.033 \times 10^5 \text{ cm/sec}$
Germanium	9.58 eV	8.84 eV	$5.32 \times 10^{-3} \text{ kg/cm}^3$	$3.61 \times 10^5 \text{ cm/sec}$	$5.31 \times 10^5 \text{ cm/sec}$

Table 2.2: Numerical values for the acoustic phonon scattering rate.

2.5.2.3 Intravalley Scattering by Optical Phonons

This scattering mechanism is divided into optical deformation potential scattering and polar optical scattering. The latter only takes place in polar semiconductors and is absent in Si, Ge and SiGe. Optical deformation potential scattering can occur in L -valleys only due to selection rules, which follow from group theory and depend on the symmetry of initial and final states and also on the symmetry of the perturbation operator [30]. In this case the transition probability for the L -valleys is:

$$\lambda(\epsilon_i) = \frac{\pi D_o^2}{\rho \omega_o} \left(N_o + \frac{1}{2} \pm \frac{1}{2} \right) g_L(\epsilon_f), \quad (2.112)$$

where ϵ_f is given as:

$$\epsilon_f = \epsilon_i \mp \hbar \omega_o. \quad (2.113)$$

The upper and lower signs refer to emission and absorption processes, respectively, D_o is the optical deformation potential, $\hbar \omega_o$ is the respective phonon energy, ϵ_i and ϵ_f are the initial and final electron energies respectively, and N_o is the equilibrium phonon distribution function given by the Bose-Einstein statistics:

$$N_o = \frac{1}{\exp\left(\frac{\hbar \omega_o}{k_B T_L}\right) - 1}. \quad (2.114)$$

The numerical values for the parameters [18, 20] of the acoustic phonon scattering rate are given in table Table 2.3.

2.5.2.4 Intervalley Phonon Scattering

An electron can be scattered from one valley to another one both by acoustical and optical phonons. Intervalley scattering can be treated as a deformation-potential interaction [30] in the same way as intravalley scattering by optical phonons.

Semiconductor	Silicon	Germanium
D_{opt}	2.2×10^8 eV/cm	5.5×10^8 eV/cm
$\hbar\omega_{opt}$	0.0612 eV	0.03704 eV

Table 2.3: Numerical values for the intravalley L-L optical deformation potential scattering rate.

Equivalent X-X Intervalley Scattering This scattering process is subdivided into f-type and g-type processes. A process is referred to as f-type, if the initial and final orientations are different, otherwise as g-type process. The transition probability of this mechanism is given by:

$$\lambda(\epsilon_i) = Z_f \frac{\pi D_{XX}^2}{\rho \omega_{XX}} \left(N_{XX} + \frac{1}{2} \pm \frac{1}{2} \right) g_X(\epsilon_f), \quad (2.115)$$

where ϵ_f is:

$$\epsilon_f = \epsilon_i \mp \hbar\omega_{XX}. \quad (2.116)$$

N_{XX} is the equilibrium phonon number of the involved phonon type:

$$N_{XX} = \frac{1}{\exp\left(\frac{\hbar\omega_{XX}}{k_B T_L}\right) - 1}. \quad (2.117)$$

Z_f is the number of possible equivalent final valleys of the same type. For f-type scattering $Z_f = 4$ and for g-type scattering $Z_f = 1$. D_{XX} is the coupling constant, $\hbar\omega_{XX}$ is the corresponding phonon energy.

The numerical values of the coupling constants and phonon energies [18, 20] are shown in Table 2.4.

	Silicon	Germanium
D_{XX}^{g1}	0.5×10^8 eV/cm	0.488×10^8 eV/cm
$\hbar\omega_{XX}^{g1}$	0.01206 eV	0.005606 eV
D_{XX}^{g2}	0.8×10^8 eV/cm	0.79×10^8 eV/cm
$\hbar\omega_{XX}^{g2}$	0.01853 eV	0.00861 eV
D_{XX}^{g3}	1.1×10^9 eV/cm	9.5×10^8 eV/cm
$\hbar\omega_{XX}^{g3}$	0.06204 eV	0.03704 eV
D_{XX}^{f1}	0.3×10^8 eV/cm	0.283×10^8 eV/cm
$\hbar\omega_{XX}^{f1}$	0.01896 eV	0.00992 eV
D_{XX}^{f2}	2.0×10^8 eV/cm	1.94×10^8 eV/cm
$\hbar\omega_{XX}^{f2}$	0.04739 eV	0.02803 eV
D_{XX}^{f3}	2.0×10^8 eV/cm	1.69×10^8 eV/cm
$\hbar\omega_{XX}^{f3}$	0.05903 eV	0.03278 eV

Table 2.4: Numerical values for the intervalley X-X scattering rate.

Equivalent L-L Intervalley Scattering For this type of scattering there is no separation into f- and g-type processes. The scattering rate is given as:

$$\lambda(\epsilon_i) = Z_L \frac{\pi D_{LL}^2}{\rho \omega_{LL}} \left(N_{LL} + \frac{1}{2} \pm \frac{1}{2} \right) g_L(\epsilon_f) \quad (2.118)$$

where ϵ_f is

$$\epsilon_f = \epsilon_i \mp \hbar \omega_{LL}. \quad (2.119)$$

N_{LL} is the equilibrium phonon number of the involved phonon type:

$$N_{LL} = \frac{1}{\exp\left(\frac{\hbar \omega_{LL}}{k_B T_L}\right) - 1}. \quad (2.120)$$

$Z_L = \frac{7}{2}$ for the transition between two different orientations and $Z_L = \frac{1}{2}$ for scattering within the same orientation, D_{LL} denotes the corresponding coupling constant and $\hbar \omega_{LL}$ is the energy of the phonon involved in the scattering process.

The numerical values of the coupling constants and phonon energies [18, 20] for this type of scattering are shown in Table 2.5.

	Silicon	Germanium
D_{LL}	5.26×10^8 eV/cm	3.0×10^8 eV/cm
$\hbar \omega_{LL}$	0.02395 eV	0.02756 eV

Table 2.5: Numerical values for the intervalley L-L scattering rate.

Non-Equivalent Intervalley Scattering This process involves transitions between all possible valleys in the conduction band. The scattering rate is given by:

$$\lambda(\epsilon_i) = Z_j \frac{\pi D_{ij}^2}{\rho \omega_{ij}} \left(N_{ij} + \frac{1}{2} \pm \frac{1}{2} \right) g_j(\epsilon_f), \quad (2.121)$$

where ϵ_f is:

$$\epsilon_f = \epsilon_i \mp \hbar \omega_{ij} - \Delta \epsilon_{ij}. \quad (2.122)$$

N_{ij} is the equilibrium phonon number of the involved phonon type:

$$N_{ij} = \frac{1}{\exp\left(\frac{\hbar \omega_{ij}}{k_B T_L}\right) - 1}, \quad (2.123)$$

and $\Delta \epsilon_{ij}$ is given as

$$\Delta \epsilon_{ij} = \epsilon_{j,\min} - \epsilon_{i,\min}. \quad (2.124)$$

Indices i and j stand for the initial and final valley, respectively, Z_j is the number of possible equivalent final valleys, D_{ij} is the corresponding coupling constant, $\hbar \omega_{ij}$ is the respective phonon energy, $\epsilon_{i,\min}$ and $\epsilon_{j,\min}$ are the energy minima of the initial and the final valley, respectively.

The numerical values of the coupling constants and phonon energies [18, 20] for this type of scattering are shown in Table 2.6.

	Silicon	Germanium
D_{GX}	0.0 eV/cm	10^9 eV/cm
$\hbar\omega_{GX}$	0.0 eV	0.02756 eV
D_{GL}	0.0 eV/cm	2.0×10^8 eV/cm
$\hbar\omega_{GL}$	0.0 eV	0.02756 eV
D_{XL}	4.65×10^8 eV/cm	4.1×10^8 eV/cm
$\hbar\omega_{XL}$	0.02283 eV	0.02756 eV

Table 2.6: Numerical values for the non-equivalent intervalley scattering rate.

2.5.3 Plasmon Scattering

In semiconductors with intermediate and high electron density an additional type of scattering is possible. The source of scattering are electron plasma oscillations, which are treated within the quasi-particle approach. In this case these quasi-particles are called plasmons.

2.5.3.1 Plasmon Concept

The plasmon concept arises from the consideration of an interacting electron gas described by the following Hamiltonian:

$$\hat{H}_{\text{el.gas}} = \sum_i \frac{\mathbf{p}_i^2}{2m} + \frac{1}{2} \sum_{i \neq j} \frac{e^2}{4\pi\epsilon |\mathbf{r}_i - \mathbf{r}_j|}, \quad (2.125)$$

where the first sum gives the kinetic energy and the second one arises from the Coulomb interaction between electrons. This Hamiltonian can be rewritten using the random phase approximation [31–34] as follows:

$$\hat{H}_{\text{el.gas}} = \hat{H}_{\text{el.gas}}^0 + \hat{H}_{\text{el.gas}}^{\text{el-el.scr}} + \hat{H}_{\text{el.gas}}^{\text{pl}} + \hat{H}_{\text{el.gas}}^{\text{el-pl}}, \quad (2.126)$$

where each contribution can be represented in the second quantized form [35]. The first term $\hat{H}_{\text{el.gas}}^0$ is the kinetic energy of the electron gas:

$$\hat{H}_{\text{el.gas}}^0 = \sum_{\mathbf{k}} \frac{\hbar^2 \mathbf{k}^2}{2m} c_{\mathbf{k}}^+ c_{\mathbf{k}}, \quad (2.127)$$

where $c_{\mathbf{k}}^+$ and $c_{\mathbf{k}}$ are the electron creation and annihilation operators, respectively, and spherical and parabolic dispersion is assumed.

The second term $\hat{H}_{\text{el.gas}}^{\text{el-el.scr}}$ gives the contribution from a two-electron screened Coulomb interaction:

$$\hat{H}_{\text{el.gas}}^{\text{el-el.scr}} = \sum_{\mathbf{k} > \mathbf{q}_c} \frac{2\pi e^2}{V\epsilon \mathbf{k}^2} \sum_{\lambda\mu} c_{\mathbf{k}_\lambda + \mathbf{k}}^+ c_{\mathbf{k}_\mu - \mathbf{k}}^+ c_{\mathbf{k}_\mu} c_{\mathbf{k}_\lambda}. \quad (2.128)$$

As can be seen, this term accounts for scattering of two electrons with the initial quasi-momenta \mathbf{k}_λ and \mathbf{k}_μ and the final quasi-momenta $\mathbf{k}_\lambda + \mathbf{k}$ and $\mathbf{k}_\mu - \mathbf{k}$ respectively. Screening is taken into

account through the cut-off wave vector q_c which separates short- and long-range parts of the Coulombic term.

The third term $\hat{H}_{\text{el.gas}}^{\text{pl}}$ describes a non-interacting plasmon gas, that is, the quantized oscillations of the electron gas³⁴:

$$\hat{H}_{\text{el.gas}}^{\text{pl}} = \sum_{\mathbf{k}} \hbar \omega_{\text{pl}} \left(a_{\mathbf{k}}^+ a_{\mathbf{k}} + \frac{1}{2} \right), \quad (2.129)$$

where $a_{\mathbf{k}}^+$, $a_{\mathbf{k}}$ are the plasmon creation and annihilation operators and $\hbar \omega_{\text{pl}}$ is the plasmon energy.

The forth term $\hat{H}_{\text{el.gas}}^{\text{el-pl}}$ represents the electron-plasmon interaction:

$$\hat{H}_{\text{el.gas}}^{\text{el-pl}} = \sum_{\mathbf{k} < \mathbf{q}_c} \left(\frac{\pi e^2 \hbar^3}{2V 4\pi \epsilon \omega_{\text{pl}} m^2 \mathbf{k}^2} \right)^{\frac{1}{2}} \sum_{\mathbf{k}} (2\mathbf{k} \cdot \mathbf{q} + \mathbf{q}^2) (a_{\mathbf{q}} c_{\mathbf{k}+\mathbf{q}}^+ c_{\mathbf{k}} + a_{-\mathbf{q}}^+ c_{\mathbf{k}+\mathbf{q}}^+ c_{\mathbf{k}}), \quad (2.130)$$

where two terms in the second sum can conveniently be treated in terms of absorption and emission of a plasmon in the same way as it has been shown above for phonons.

The possible plasmon-phonon coupling [36–38] is not considered in this work as it plays an important role only in polar semiconductors where in the degenerate case the frequencies of the charge density fluctuations are comparable to the optical frequencies.

2.5.3.2 Scattering Rate

The scattering rate due to electron-plasmon interaction can be obtained using Fermi's golden rule (2.95) and the Hamiltonian (2.130). Plasmon scattering of electrons represents the long-range part of the electron-electron interaction [39]. Assuming a nonparabolic and spherical analytical band structure (2.77), the scattering rate is given by:

$$\lambda_{\text{plas}}(k) = \frac{e^2 \hbar}{16\pi \epsilon (m_d^*)^2 \omega_{\text{pl}} v_g(k)} \left(N(\omega_{\text{pl}}) + \frac{1}{2} \pm \frac{1}{2} \right) (k^2 - k_f^2)^2 \ln \frac{q_c}{q_{\text{min}}}, \quad (2.131)$$

The final electron energy is given as:

$$\epsilon_f = \epsilon_i \mp \hbar \omega_{\text{pl}}, \quad (2.132)$$

where the plasma frequency is (see Appendix B):

$$\omega_{\text{pl}} = \sqrt{\frac{e^2}{\epsilon} \sum_v \frac{n_v}{(m_d^*)_v}}. \quad (2.133)$$

Here the summation over all possible valleys is assumed, and n_v stands for the contribution from valley v to the electron density.

The cut-off wave vector q_c is defined as follows:

$$q_c = \min(q_{\text{max}}, \beta_s). \quad (2.134)$$

³⁴Similarly to phonons plasmons represent bosons.

q_{\min} and q_{\max} stand for the boundaries of the momentum transfer:

$$\begin{aligned} q_{\min} &= |k - k_f|, \\ q_{\max} &= |k + k_f|. \end{aligned} \quad (2.135)$$

k_f is the final wave vector defined by the equation:

$$\epsilon(k_f) = \epsilon_f, \quad (2.136)$$

$N(\omega_{pl})$ is the average number of the plasmon excitations defined by the equilibrium Bose-Einstein statistics:

$$N(\omega_{pl}) = \frac{1}{\exp\left(\frac{\hbar\omega_{pl}}{k_B T_L}\right) - 1}. \quad (2.137)$$

2.5.4 Alloy Scattering

When an alloy of Si and Ge is considered, there is an additional scattering mechanism due to the atomic disorder. To describe this mechanism it is necessary to define the model of disorder and the scattering potential.

The model used in this work for the SiGe alloy is that of Harrison-Hauser [40], which uses Warren-Cowley's approach for the disorder model [41] and Mott's inner-potential model for the scattering potential. The resulting scattering rate is given by the following expression which takes both intravalley and intervalley scattering into account:

$$\lambda_{\text{alloy}}(\epsilon) = \frac{\pi}{\hbar}(1-x)x\Omega_{\text{cell}}U^2g(\epsilon), \quad (2.138)$$

where x is the mole fraction of one of the materials, Ω_{cell} is the volume of the elementary cell, and U is the alloy scattering potential.

2.5.5 Ionized Impurity Scattering

The scattering by ionized impurities represents an elastic process. The most popular models for this type of scattering are due to Brooks and Herring [42] and Conwell and Weisskopf [43]. The difference between the two approaches lies in the treatment of the screening effect. In this work we adopt the Brooks-Herring model with some refinements described below.

2.5.5.1 Brooks-Herring Model

Within this model the scattering potential is given by

$$V(r) = \frac{Ze^2}{4\pi\epsilon r} \exp(-\beta r), \quad (2.139)$$

where β^{-1} is the screening length and Z denotes the number of charge units of the impurity.

Using Fermi's golden rule (2.95) together with the nonparabolic band structure (2.77) one obtains for the total scattering rate:

$$\lambda_{BH}(\epsilon) = \frac{\sqrt{2}N_I Z^2 e^4}{\epsilon^2 \sqrt{m_d^* \epsilon_\beta}} \sqrt{\epsilon(1 + \alpha\epsilon)} \frac{1 + 2\alpha\epsilon}{1 + 4 \frac{\epsilon(1 + \alpha\epsilon)}{\epsilon_\beta}}, \quad (2.140)$$

where parameter ϵ_β is defined by

$$\epsilon_\beta = \frac{\hbar^2 \beta^2}{2m_d^*}. \quad (2.141)$$

The important improvements to this model are shortly described below.

2.5.5.2 Two-Ion Scattering

This correction [44, 45] to the Brooks-Herring model takes into account the fact that at high impurity concentration the scattering on two ions becomes important. The bare scattering potential is given as:

$$V_0(\mathbf{r}) = \frac{Ze}{4\pi\epsilon} \left(\frac{1}{|\mathbf{r}|} + \frac{1}{|\mathbf{r} - \mathbf{R}|} \right), \quad (2.142)$$

where $|\mathbf{R}|$ is the average distance between impurity centers. The Fourier transform of this potential is equal to:

$$V_0(\mathbf{q}) = \int \exp(-i\mathbf{q} \cdot \mathbf{r}) V_0(\mathbf{r}) d\mathbf{r} = \frac{Ze}{\epsilon \mathbf{q}^2} (1 + \exp(-i\mathbf{q} \cdot \mathbf{R})). \quad (2.143)$$

Electrons respond to this potential forming a self-consistent potential which can be described by screening theory. The general screening theory in the presence of the periodic crystal potential is rather complicated. Thus the screening theory for the electron gas is employed here.

2.5.5.3 Screening Theory

The screening effect is the most important manifestation of the electron-electron interaction. In this work only linear screening is considered. Nonlinear effects which require the solution of the nonlinear Poisson equation either analytically [46, 47] or numerically [48] are neglected here.

A positively charged particle introduced into the electron gas will create an excess of negative charge in its vicinity which screen its electric field³⁵. The bare potential (2.142) satisfies the Poisson equation:

$$\epsilon \nabla^2 V_0(\mathbf{r}) = -\rho_0(\mathbf{r}), \quad (2.144)$$

where $\rho_0(\mathbf{r}) = Ze[\delta(\mathbf{r}) + \delta(\mathbf{r} - \mathbf{R})]$ is the volume density of the particle charge³⁶. The total physical potential $V_t(\mathbf{r})$, which is produced both by the particle and the electron cloud, is described by the Poisson equation of the form:

$$\epsilon \nabla^2 V_t(\mathbf{r}) = -\rho(\mathbf{r}), \quad (2.145)$$

³⁵The same is valid for two positively charged particles.

³⁶In our case the charge density of two ions.

where $\rho(\mathbf{r})$ is the total volume charge density:

$$\rho(\mathbf{r}) = \rho_0(\mathbf{r}) + \rho_{\text{ind}}(\mathbf{r}). \quad (2.146)$$

Here $\rho_{\text{ind}}(\mathbf{r})$ denotes the volume density of the charge induced in the electron gas by the positive particle. From the electrodynamics of continuous media [49] it is known that $V_0(\mathbf{r})$ and $V_t(\mathbf{r})$ are linearly related to each other:

$$V_0(\mathbf{r}) = \int \varepsilon(\mathbf{r}, \mathbf{r}') V_t(\mathbf{r}') d\mathbf{r}'. \quad (2.147)$$

For the homogeneous electron gas function $\varepsilon(\mathbf{r}, \mathbf{r}')$ can only depend on the distance between the two points \mathbf{r} and \mathbf{r}' :

$$\varepsilon(\mathbf{r}, \mathbf{r}') = \varepsilon(\mathbf{r} - \mathbf{r}'). \quad (2.148)$$

This gives the following relation between the Fourier components of $V_0(\mathbf{r})$ and $V_t(\mathbf{r})$:

$$V_t(\mathbf{q}) = \frac{V_0(\mathbf{q})}{\varepsilon(\mathbf{q})}. \quad (2.149)$$

In the linear screening theory it is assumed that $\rho_{\text{ind}}(\mathbf{r})$ and $V_t(\mathbf{r})$ are linearly related to each other³⁷ which implies for Fourier components:

$$\rho_{\text{ind}}(\mathbf{q}) = \chi(\mathbf{q}) V_t(\mathbf{q}). \quad (2.150)$$

The Fourier transform of the Poisson equations (2.144) and (2.145) together with (2.150) leads to the relation:

$$\varepsilon(\mathbf{q}) = 1 - \frac{1}{q^2} \chi(\mathbf{q}). \quad (2.151)$$

To calculate the quantity $\chi(\mathbf{q})$ some approximations are necessary. In this work we use the so called Lindhard screening theory³⁸. Within this model the expression for the dielectric function [50] is:

$$\varepsilon(\mathbf{q}, 0) = 1 + \frac{\beta_s^2}{q^2} G(\xi, \eta), \quad (2.152)$$

with the inverse screening length given by the Thomas-Fermi theory:

$$\beta_s^2 = \frac{e^2 n}{\varepsilon k_B T_L} \frac{\mathcal{F}_{-1/2}(\eta)}{\mathcal{F}_{1/2}(\eta)}. \quad (2.153)$$

Here \mathcal{F}_i stands for the Fermi integral of the i -th order, and η is the reduced Fermi energy:

$$\eta = \frac{E_F - E_C}{k_B T_L}. \quad (2.154)$$

³⁷This is valid for a rather weak potential V_t .

³⁸Sometimes it is called the Random Phase Approximation (RPA).

G represents the screening function given by the following expression:

$$G(\xi, \eta) = \frac{1}{\mathcal{F}_{-1/2}(\eta)} \frac{1}{\xi \sqrt{\pi}} \int_0^\infty \frac{x}{1 + \exp(x^2 - \eta)} \ln \left| \frac{x + \xi}{x - \xi} \right| dx, \quad (2.155)$$

where the argument ξ is:

$$\xi^2 = \frac{\hbar^2 q^2}{8m^* k_B T_L}. \quad (2.156)$$

The corrections described above can be taken into account within the first Born approximation. In this approximation the scattering amplitude is given as:

$$f(\mathbf{q}) = -\frac{1}{4\pi} U(\mathbf{q}), \quad (2.157)$$

where $U(\mathbf{q})$ is defined by

$$U(\mathbf{q}) = -\frac{2eV_t(\mathbf{q})m^*}{\hbar^2}. \quad (2.158)$$

The differential cross section is defined as:

$$\sigma(\mathbf{q}) = \frac{(2\pi\hbar)^3}{m^{*2}|\mathbf{v}(\mathbf{k})|} |f(\mathbf{q})|^2 \rho(\epsilon). \quad (2.159)$$

Now the total scattering rate is obtained through

$$\lambda(\mathbf{k}) = N_p |\mathbf{v}(\mathbf{k})| \sigma_{\text{tot}}(\mathbf{k}), \quad (2.160)$$

where $N_p = N_I/2$ is the density of scattering pairs and $\sigma_{\text{tot}}(\mathbf{k})$ is equal to:

$$\sigma_{\text{tot}}(\mathbf{k}) = \frac{2\pi}{k^2} \int \sigma(\mathbf{q}) q dq. \quad (2.161)$$

The simple calculations give the final total ionized impurity scattering rate taking into account the momentum dependent screening and the two-ion correction:

$$\lambda(\mathbf{k}) = C(k) \int_0^{2k} \frac{1}{(q^2 + \beta_s^2 G(\xi, \eta))^2} \left(1 + \frac{\sin(qR)}{qR} \right) dq, \quad (2.162)$$

$$C(k) = \frac{N_i Z^2 e^4}{2\pi \hbar^2 \epsilon^2 |\mathbf{v}(\mathbf{k})|}.$$

2.5.5.4 Second Born Correction

The additional correction applied to the ionized impurity scattering rate results from the second Born approximation. The Schwinger scattering amplitude is used to obtain a correction to the first Born approximation. The second Born correction is given by:

$$\Delta\lambda(k) = s_0(k) C(k) \int_0^{2k} \frac{q}{(q^2 + \beta_s^2)^2} dq, \quad (2.163)$$

where the expression for $s_0(k)$ is

$$s_0(k) = \frac{a}{1 + \frac{4k^2}{\beta_s^2} - a}, \quad (2.164)$$

with the parameters a and U_0 defined as:

$$a = \frac{U_0}{\beta_s} \left(1 - \frac{U_0}{4\beta_s} \right), \quad (2.165)$$

$$U_0 = \frac{2m_d^* Ze^2}{\hbar^2 4\pi\epsilon}. \quad (2.166)$$

The first Born approximation is valid when $|U_0|/\beta_s \ll 1$ [51]. This inequality is violated at low and intermediate doping levels, where the second Born correction thus plays an important role.

2.5.5.5 Ridley's Model

The ionized impurity scattering rate has a sharp peak at very low energies. This can cause very high self-scattering rates in Monte Carlo methods described later in this work and long computational times. Although the comprehensive ionized impurity scattering model described above is mostly used in the present work, in some cases it is useful to employ simpler models. One such model is briefly described here.

Assuming statistical screening avoids the problem of the sharp behavior at low energies[52]. In this approach an additional statistical screening mechanism is introduced to cut off the long-range part of the screened Coulomb interaction. The resulting scattering rate is:

$$\lambda_{st.sc}(\mathbf{k}) = \frac{|\mathbf{v}(\mathbf{k})|}{R} \left(1 - \exp \left(-\lambda_{BH}(\mathbf{k}) \frac{R}{|\mathbf{v}(\mathbf{k})|} \right) \right), \quad (2.167)$$

where λ_{BH} stands for the scattering rate of the Brooks-Herring model (2.140). This approach allows the number of small-angle scattering events to be reduced and thus reduces the amount of scattering events to be simulated.

Chapter 3

Strain Effects in $\text{Si}_{1-x}\text{Ge}_x$ Grown on a $\text{Si}_{1-y}\text{Ge}_y$ Substrate

3.1 SiGe Strained Layers

SiGe active layers are used to create advanced semiconductor devices. These layers must be sufficiently thin to avoid generation of dislocations which will negatively affect transport properties of the devices.

3.1.1 Critical Thickness and Dislocations

The basic principle of strained-layer epitaxy is that a certain amount of elastic strain can be accommodated by any material without generating dislocations or defects. It takes energy to accommodate an epitaxial layer of lattice-mismatched material. The energy depends on both the thickness and the size of the lattice mismatch. It also requires energy to create a dislocation that will relieve the lattice mismatch strain. If the thickness of the epitaxial layer is kept small enough to maintain the elastic strain energy below the energy of dislocation formation, the strained-layer structure will be thermodynamically stable against dislocation formation. The unstrained state of the lattice-mismatched layer is energetically most favorable, but the strained structure is stable against transformation to the unstrained state by the energy barrier associated with the generation of enough dislocations to relieve the strain.

The most important types are edge and screw dislocations. Edge dislocation can be represented by an extra half plane inserted into a crystal as illustrated in Fig. 3.1. The edge of this half plane is called an edge dislocation. In the vicinity of the dislocation the deviation of the crystal structure from the ideal one is rather strong. But already at distances of a few lattice periods the crystal planes touch each other almost as in the perfect crystal structure. However, the deformation also exists at great distance from the dislocation. It can be clearly found by

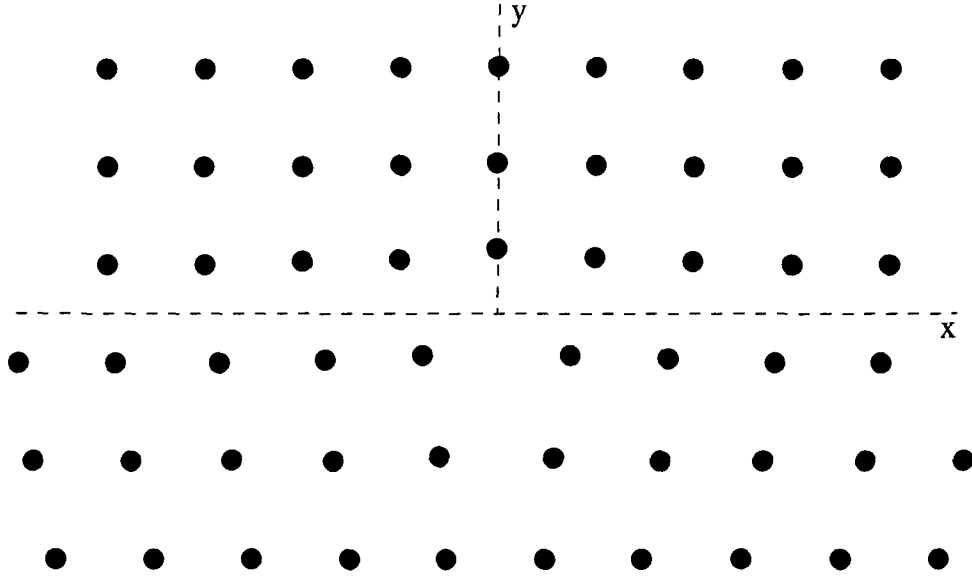


Figure 3.1: Edge dislocation.

traversing a closed contour through the lattice nodes in $x - y$ plane containing the origin of the coordinates. If \mathbf{u} stands for the displacement of an atom from its position in the ideal structure, the total change of this vector for the whole contour is not equal to zero. Instead it is equal to the lattice period along x .

Screw dislocations can be viewed as a result of cutting a lattice along a half plane with a subsequent one period relative shift of the two parts of the lattice on each side of the cut as depicted in Fig. 3.2. The edge of the cut is called the screw dislocation. Traversing a contour around the dislocation line the vector \mathbf{u} gains one period along this axis. From the macroscopic point of view a dislocation deformation of a crystal considered as a continuous media has a general property: traversing a closed contour L containing the dislocation line D , the vector of the elastic shift \mathbf{u} gains a finite addition \mathbf{b} equal to one of the periods of a given crystal lattice. The constant vector \mathbf{b} is called Burger's vector of a given dislocation. This property is mathematically written as:

$$\oint_L du_i = \oint_L \frac{\partial u_i}{\partial x_k} dx_k = -b_i, \quad (3.1)$$

where it is understood that the traversing direction of the contour is clockwise with respect to the chosen direction of the tangent vector $\boldsymbol{\tau}$ of the dislocation line. The dislocation line itself represents a line of peculiar points of the deformation field. In the case of edge and screw dislocations the dislocation lines D represent straight lines with $\boldsymbol{\tau} \perp \mathbf{b}$ and $\boldsymbol{\tau} \parallel \mathbf{b}$, respectively. In the general case a dislocation is a curve along which the angle between $\boldsymbol{\tau}$ and \mathbf{b} can change. A dislocation line cannot stop inside a crystal. The two ends must be on the surface of a crystal or the dislocation represents a loop. Condition (3.1) means that the displacement vector is a non-unique function of coordinates. It gains an additional vector after traversing a contour around a dislocation line. Physically there does not exist any non-uniqueness: an additional vector \mathbf{b} means an additional one period shift of the lattice nodes which cannot change the lattice state.

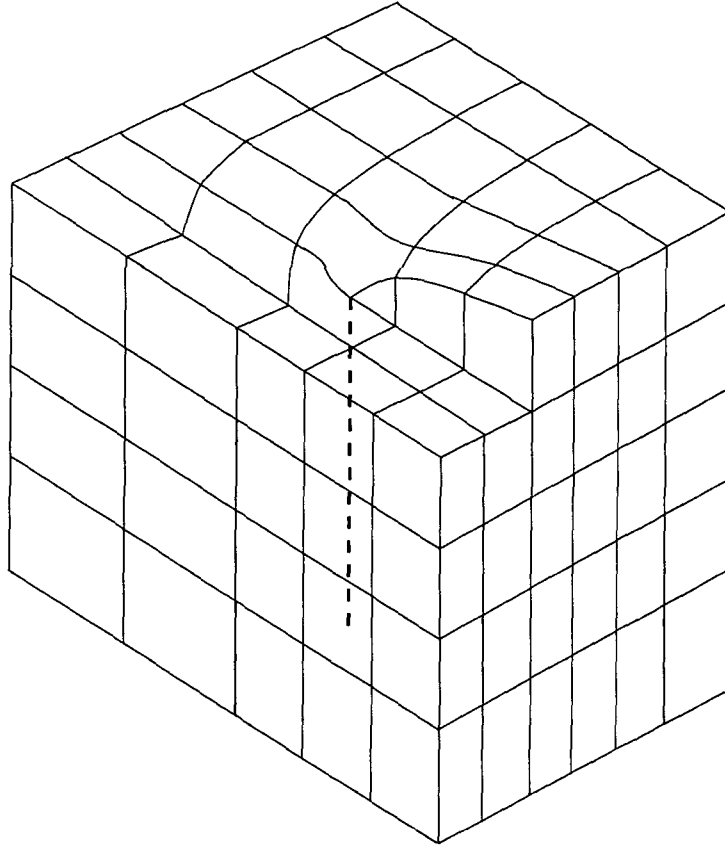


Figure 3.2: Screw dislocation.

In particular, the stress tensor is a unique and continuous function of coordinates.

A fundamental assumption underlying many of the critical thickness calculations is the a priori assumption that the equilibrium configuration of the strain induced dislocations is that of a regular, non-interacting, rectangular array. Critical layer thicknesses are then computed by requiring that the total strain energy per unit area ϵ_T be a minimum with respect to the in-plane strain e

$$\frac{\partial \epsilon_T}{\partial |e|} = 0 \quad (3.2)$$

evaluated at $|e| = f$, where f is the mismatch between the film and the substrate. Here ϵ_T is defined as a sum

$$\epsilon_T = \epsilon_H + \epsilon_D \quad (3.3)$$

of the homogeneous strain energy density ϵ_H :

$$\epsilon_H = 2G \left(\frac{1+\nu}{1-\nu} \right) e^2 h \quad (3.4)$$

and the areal energy density of the dislocation ϵ_D :

$$\epsilon_D \equiv \frac{E_l}{p}. \quad (3.5)$$

Here G is the shear modulus, h is the film thickness, E_l the energy per unit length of a given dislocation line, and p is the spacing between the dislocations in the assumed rectangular array. It should be noted that E_l is independent of the in-plane strain e in the film [53] and in fact ϵ_D only depends on the strain in the film through of the strain-dependence of the effective interfacial width p . The spacing between dislocations in the array is given by

$$p = \frac{b}{f - |e|} \quad (3.6)$$

where b is the magnitude of Burger's vector. Equations (3.4)-(3.6) in conjunction with the mechanical equilibrium condition (3.2) give the following equation [54] for the critical thickness h_c :

$$h_c = \frac{b}{4\pi f(1 + \nu)} \left[\ln \left(\frac{h_c}{b} \right) + 1 \right]. \quad (3.7)$$

However there are other models for the critical thickness h_c . One of them can be described by the expression [55]:

$$h_c = \frac{b^2(1 - \nu)}{20\pi\sqrt{2}f^2\langle a(x) \rangle(1 + \nu)} \ln \left(\frac{h_c}{b} \right). \quad (3.8)$$

The difference between the models (3.7) and (3.8) lies in the fact that in deriving (3.8) it is not assumed that initial dislocations appear in a regular rectangular array. Here dislocations are generated in a stochastic fashion. This is an attempt to deal with the relaxation kinetics in contrast to the equilibrium based derivation (3.7). It is assumed that dislocation formation requires in a dislocation formation energy ϵ_D . As the thickness of a film approaches its critical value, some fraction of the homogeneous strain energy ϵ_H will be used to supply this dislocation formation energy.

3.1.2 Applications of Strain

The study of lattice-mismatched epitaxy gained much attention when it was recognized that strained-layer structures might display new electronic and optical properties not seen in the unstrained-constituent materials [3, 56]. The strain is unavoidable in semiconductor heterostructures. However it can be a tool for modifying the band structure of semiconductors in a useful and predictable fashion. The strain is imposed internally, as a consequence of lattice-mismatch and it may be compressive or tensile. To modify the band structure by more than 100 meV it is necessary to create a lattice mismatch greater than about 2%. This in turn means that a careful control over the layer thickness is required to produce extended strained structures that meet the critical thickness requirement.

3.1.3 Strained Layers in Semiconductor Devices

Strained SiGe layers are used in modern semiconductor devices, such as the strained-layer modulation doped field-effect transistor (S-MODFET) and the strained metal-oxide-semiconductor field-effect transistor (S-MOSFET).

3.1.3.1 Modulation-Doped FET

The typical layer structure of an n-S-MODFET [57] is shown in Fig. 3.3. It is grown by molecular beam epitaxy on a p^- -substrate with $\rho \geq 1000 \Omega \cdot \text{cm}$ starting with a relaxed SiGe buffer layer whose Ge content is linearly graded to 40-50%. The core of the layer structure is the 7-10 nm thick biaxially strained Si channel embedded in undoped $\text{Si}_{1-x}\text{Ge}_x$ spacers which separate the following carrier supply layers from the channel. Due to a Ge content of 40-50% in the SiGe layers, a high conduction band offset is achieved and the resultant quantum well enables sheet carrier densities up to $n_s = 7 \times 10^{12} \text{ cm}^{-2}$.

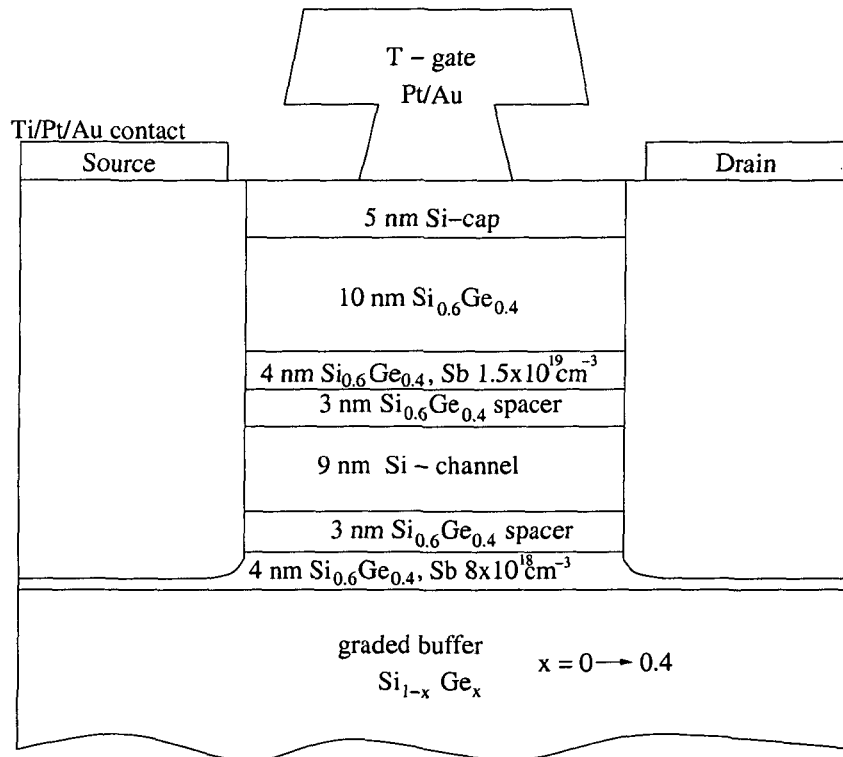


Figure 3.3: S-MODFET structure.

3.1.3.2 Strained MOSFET

The strained Si layer is also used as the channel in the usual n-MOSFET structure where, it is grown on a SiGe substrate. The in-plane electron mobility increase is used to improve the device performance.

3.2 Linear Deformation-Potential Theory

Linear deformation potential theory has been first justified within the effective mass approximation by Bardeen and Shockley [58] and thus is usually referred to as the Bardeen-Shockley theory. Originally this method has been applied to study the interaction of electrons and acoustic phonons, and later in the theory of strained materials, in particular for thin strained SiGe layers. Within this theory the energy is expanded into a Taylor series in powers of a quantity characterizing the strength of the lattice strain. The expansion is truncated after the first power of this parameter, which renders the theory linear. Neglecting terms of the second order is equivalent to the effective masses being unchanged by the induced strain.

3.2.1 General Description of the Conduction Band Splitting in Strained SiGe

In this work the linear deformation potential theory is used to calculate the conduction band splitting in thin strained SiGe layers. As Si and Ge have their conduction band extrema at quasi-momenta $\mathbf{k} \neq 0$, the applied stress reduces the original degeneracy¹ of band states with different quasi-momenta. This reduction depends on the relative orientation of the quasi-momentum for a given conduction band extremum and the applied forces as schematically illustrated in Fig. 3.4 and Fig. 3.5. For a general orientation of applied forces all band extrema can be split. However, if the forces are applied along some axes with high symmetry the degeneracy reduction can be partial. Extrema are forming subsets within which the degeneracy is conserved, but extrema from different subsets are no longer degenerate. In $\text{Si}_{1-x}\text{Ge}_x$ layers grown on relaxed $\text{Si}_{1-y}\text{Ge}_y$ substrates stress due to lattice mismatch always arises when the Ge compositions are different, $x \neq y$. The direction and the magnitude of the applied forces in such a system depend on the orientation of the $\text{Si}_{1-y}\text{Ge}_y$ substrate and the Ge compositions x and y . This stress leads to a deformation of the perfect crystal. It is assumed that the thickness is below the critical value which implies absence of dislocations. As a result the degeneracy of the conduction band is reduced. The splitting of the conduction band minima has a strong impact on the transport properties of strained SiGe active layers in comparison with unstrained ones. In particular it causes anisotropy of transport quantities such as electron mobility. For Si, Ge and SiGe the low field electron mobility is represented by a scalar, that is, the mobility tensor is diagonal with equal diagonal elements. In the strained layer the diagonal elements are in general different. The difference of the kinetic properties for different orientations can be significant and can be used to optimize the characteristics of advanced semiconductor devices.

3.2.2 Strain Tensor

Under applied forces solids are strained resulting in a change of volume and shape. In the approximation of the elastic continuum, the position of each point of a solid is described by the vector \mathbf{r} which in some Cartesian coordinate system has the components x_1, x_2, x_3 . Under strain all points of a solid are in general shifted. If the position of a given point before strain was \mathbf{r} , then after strain it is \mathbf{r}' with components $x'_i, i = 1, 2, 3$. The displacement of the point is

¹The original degeneracy is related to the symmetry of the unstrained Si and Ge crystals.

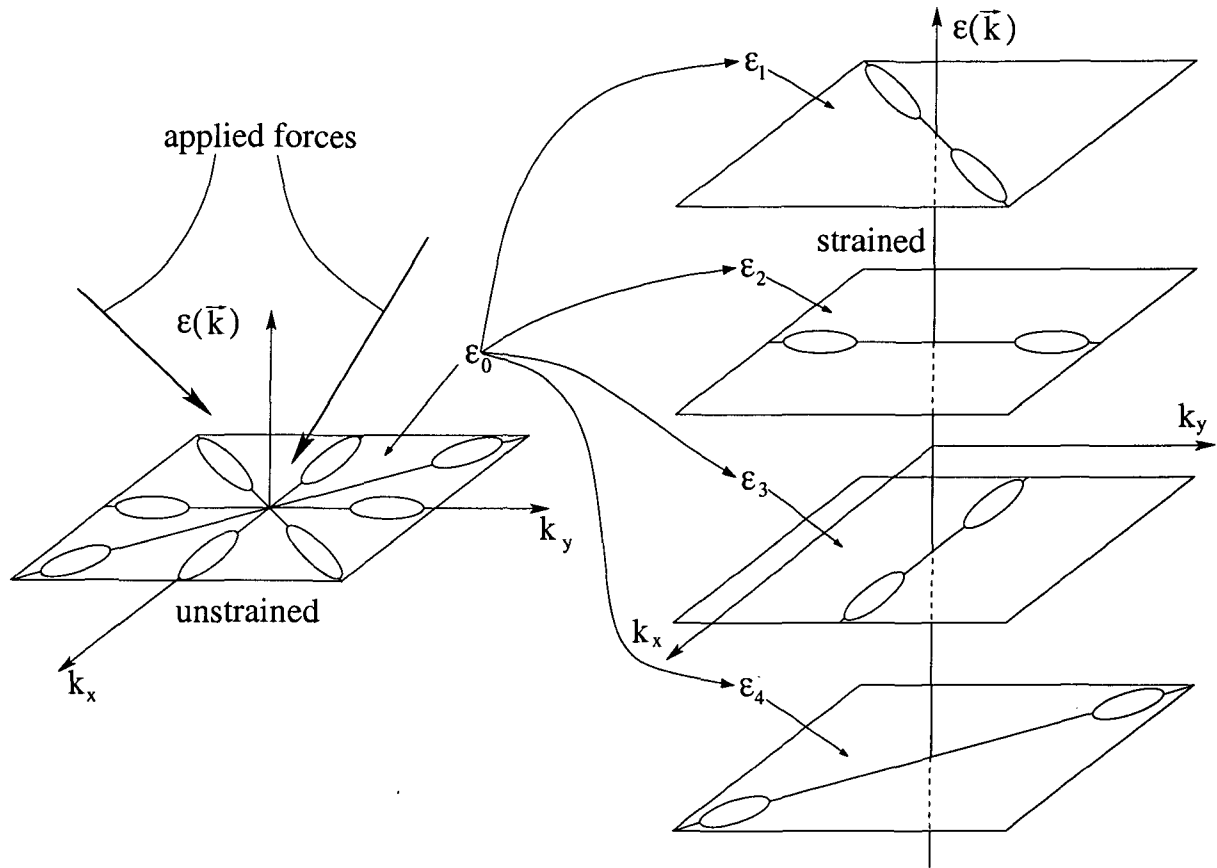


Figure 3.4: Full degeneracy reduction due to the applied stress for a hypothetical band structure. For a general orientation of applied forces $\epsilon_1 \neq \epsilon_2 \neq \epsilon_3 \neq \epsilon_4$.

characterized by the displacement vector defined as

$$\mathbf{u} = \mathbf{r}' - \mathbf{r}. \quad (3.9)$$

The coordinates x'_i of a shifted point are functions of the coordinates x_i of the same point before strain. This means that the displacement vector \mathbf{u} is also a function of x'_i . This function completely determines the strained state of a solid.

When a solid is strained, the distances between points change. If before strain the distance between two infinitely close points was dx_i , then after strain it is equal to $dx'_i = dx_i + du_i$. The distance between these two points before strain is

$$dl = \sqrt{dx_1^2 + dx_2^2 + dx_3^2} \quad (3.10)$$

and after strain:

$$dl' = \sqrt{dx_1'^2 + dx_2'^2 + dx_3'^2}. \quad (3.11)$$

Substituting the expressions for dx'_i through du_i the following expression for dl'^2 is obtained:

$$dl'^2 = dl^2 + 2 \frac{\partial u_i}{\partial x_k} dx_i dx_k + \frac{\partial u_i}{\partial x_k} \frac{\partial u_i}{\partial x_l} dx_k dx_l. \quad (3.12)$$

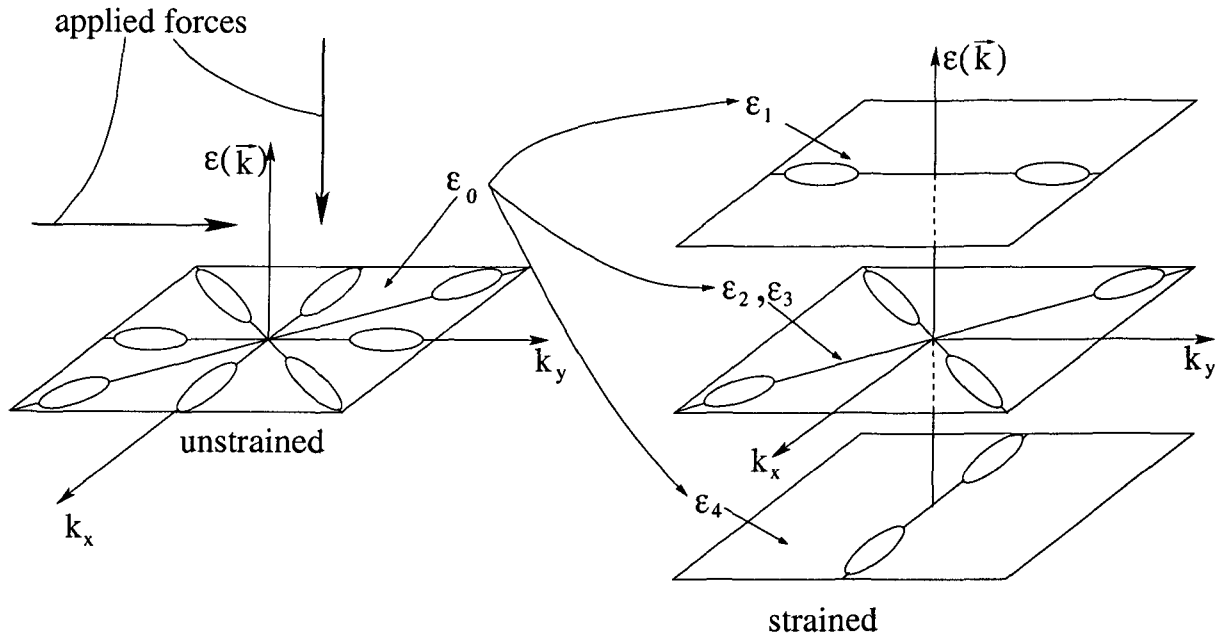


Figure 3.5: Partial degeneracy reduction due to the applied stress for a hypothetical band structure. For applied forces oriented along high symmetry axes $\epsilon_1 \neq \epsilon_2 = \epsilon_3 \neq \epsilon_4$.

Since indices in the double sum can be exchanged, the last expression can be rearranged and rewritten as:

$$dl'^2 = dl^2 + 2\epsilon_{ik}dx_i dx_k, \quad (3.13)$$

where a tensor of the second rank has been introduced:

$$\epsilon_{ik} = \frac{1}{2} \left(\frac{\partial u_i}{\partial x_k} + \frac{\partial u_k}{\partial x_i} + \frac{\partial u_l}{\partial x_i} \frac{\partial u_l}{\partial x_k} \right). \quad (3.14)$$

The second rank tensor ϵ_{ik} is called the strain tensor. As can be seen from the definition (3.14), it represents a symmetric tensor:

$$\epsilon_{ik} = \epsilon_{ki}, \quad \forall i, k = 1, 2, 3. \quad (3.15)$$

Any symmetric tensor can be reduced to the principle axes. This means that at each given point the coordinate system can be chosen in such a way that only diagonal elements ϵ_{11} , ϵ_{22} and ϵ_{33} will be non-zero and all non-diagonal elements vanish. It should be noted that if a tensor is reduced to the diagonal form at a given point, it will be in general non-diagonal at all other points of a given solid considered as continuum.

If the strain tensor is reduced at a given point to its principle axes, in the elementary volume built around this point the element of the length (3.13) takes the form:

$$dl'^2 = (1 + 2\epsilon_{11})dx_1^2 + (1 + 2\epsilon_{22})dx_2^2 + (1 + 2\epsilon_{33})dx_3^2. \quad (3.16)$$

This expression is decomposed into three independent terms. This means that at any given elementary volume of a solid the strain can be considered as a set of three independent deformations along three relatively orthogonal directions - the principal axes of the tensor. Each of these

deformations represents a simple stretching or compressing along the corresponding direction: the length dx_i along the i -th principle axis turns into the length dx'_i :

$$dx'_i = \sqrt{1 + 2\varepsilon_{ii}} dx_i. \quad (3.17)$$

The relative elongation along the i -th axis is thus given as:

$$\frac{dx'_i - dx_i}{dx_i} = \sqrt{1 + 2\varepsilon_{ii}} - 1. \quad (3.18)$$

A deformation is considered small if the change of any distance in a solid turns out to be much less than the distance itself. In other words all relative elongations are much less than unity. In this work only strain of this kind is considered.

When strain is weak in the sense mentioned above, the displacements u_i and their derivatives are small. Thus, in the general expression (3.14) the last term is negligible and can be omitted. Therefore, in the case of weak strain, the components ε_{ik} of the strain tensor are determined by the following expression:

$$\varepsilon_{ik} = \frac{1}{2} \left(\frac{\partial u_i}{\partial x_k} + \frac{\partial u_k}{\partial x_i} \right). \quad (3.19)$$

In this case the relative elongations are thus equal:

$$\sqrt{1 + 2\varepsilon_{ii}} - 1 \approx \varepsilon_{ii}, \quad (3.20)$$

and given by the eigen values of the strain tensor.

3.2.3 Stress Tensor

When a solid is strained by external forces the positions between atoms change and it is in a non-equilibrium state. As a result some internal forces appear. These forces tend to return the strained solid to its equilibrium state. The induced forces are called the internal stresses. If a solid is not strained, the internal stresses vanish.

Considering some volume of a solid the total force applied to it can be written as an integral over the same volume:

$$\int \mathbf{F} dV, \quad (3.21)$$

where \mathbf{F} is the force applied to a unit volume of the solid. As the forces between internal parts of the volume are balanced, only external parts contribute. Further the macroscopic principle² means that the total force can only be expressed as a surface integral.

Therefore each of the three components of the total force (3.21) should be a surface integral. This fact implies that the vector \mathbf{F} must be the divergence of a tensor of rank two. Denoting this tensor as σ_{ik} , $i, k = 1, 2, 3$, \mathbf{F} can be expressed as:

$$F_i = \frac{\partial \sigma_{ik}}{\partial x_k}. \quad (3.22)$$

²That is the statement about the radius of the atomic forces. This radius must be considered to be zero in the macroscopic theory.

From this expression the following formula is obtained:

$$\int F_i dV = \oint \sigma_{ik} df_k, \quad (3.23)$$

which is only valid for the weak strain condition³.

The tensor σ_{ik} is called the stress tensor. As it can be seen from (3.23), $\sigma_{ik} df_k$ is the i -th component of the force applied to the surface element df . Choosing a surface element in the x, y ; y, z and x, z planes it can be seen that the component σ_{ik} of the stress tensor is the i -th component of the force applied to a unit area perpendicular to the x_k axis. For example, the normal component of the force applied to a unit area perpendicular to x is equal to σ_{xx} and the forces tangential to it are equal to σ_{yx} and σ_{zx} as it is shown in Fig. 3.6.

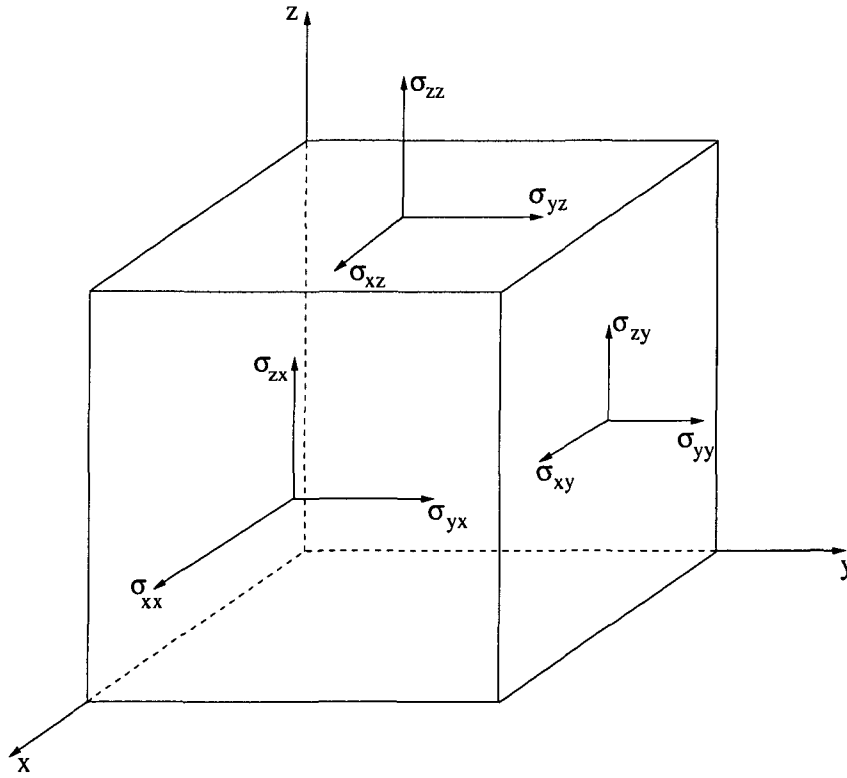


Figure 3.6: The stress tensor components in terms of the applied forces.

It is well known that the moment of force can be written as an antisymmetric tensor of rank two⁴. Thus the total moment of force applied to the volume under consideration is:

$$M_{ik} = \int (F_i x_k - F_k x_i) dV. \quad (3.24)$$

³The integration variables must be x' . However, due to weak strain the derivative in (3.22) differs from the derivative with respect to x' by higher order terms.

⁴Moment of force is a vector. Its components can be expressed as $M_i = \frac{1}{2} e_{ijk} M_{jk}$, where e is the unit antisymmetric tensor of rank three and M_{jk} is the antisymmetric tensor of rank two which is integrand in (3.24).

Like the total force the moment of force also must be expressed through a surface integral. Substituting (3.22) into (3.24) gives:

$$M_{ik} = \oint (\sigma_{il}x_k - \sigma_{kl}x_i)df_l + \int (\sigma_{ki} - \sigma_{ik})dV. \quad (3.25)$$

This expression represents a surface integral only if the following equality is satisfied:

$$\sigma_{ik} = \sigma_{ki}, \quad (3.26)$$

which removes the volume integral in (3.25). Hence an important property of the stress tensor is its symmetry. In principle the integrand in the volume integral in (3.25) can be a complete divergence of a tensor of rank three which is antisymmetric in the first two indices. This tensor must be expressed through derivatives like $\partial u_i / \partial x_k$. Thus the stress tensor would contain terms of higher order derivatives of the displacement vector \mathbf{u} . Within this work such terms are considered negligible. Hence the symmetry of the stress tensor is again justified.

It should be noted that the stress tensor can be transformed into diagonal form even without this approximation. The point is that its definition (3.22) is not unique. Any transformation

$$\tilde{\sigma}_{ik} - \sigma_{ik} = \frac{\partial \chi_{ikl}}{\partial x_l}, \quad (3.27)$$

where the tensor χ_{ikl} is antisymmetric with respect to the last two indices, does not change the force \mathbf{F} .

3.2.4 Energy Shift

As it has been pointed out above in a strained solid the energy of an extremum is expanded into the Taylor series in powers of some small quantity characterizing the strength of the lattice strain. For weak strain it is natural to perform the expansion in powers of the strain tensor components around the unstrained point. The energy shift of the k -th non-degenerate band extremum is in general expressed as:

$$\Delta \epsilon^{(k)} = \sum_{ij} \Xi_{ij}^{(k)} \epsilon_{ij}. \quad (3.28)$$

The coefficients of this expansion form a second rank tensor called the deformation potential tensor. This tensor is a characteristic of a given non-degenerate band of a solid. Due to the symmetry property of the strain tensor the deformation potential tensor is also symmetric:

$$\Xi_{ij}^{(k)} = \Xi_{ji}^{(k)}. \quad (3.29)$$

Such tensor has only six independent components. For cubic crystals the number of independent components reduces to three, denoted as Ξ_u , Ξ_d and Ξ_p .

3.2.4.1 Shift of Conduction Band Minima

In this work the X and L valleys of Si, Ge, and SiGe are considered. The symmetry of these valleys further reduces the number of independent components of the deformation potential

tensor to two, namely Ξ_u and Ξ_d . The deformation potential Ξ_d relates to pure dilatation while Ξ_u is associated with a pure shear involving a uniaxial stretch along the major axis plus a symmetrical compression along the minor axis [59].

Linear deformation-potential theory implies that for conduction band extrema not located in the center of the Brillouin zone the shape of the equal energy surface does not change to the first order in strain. However, a particular extremum of the conduction band shifts under strain. The shift depends on the magnitude of applied forces and their orientation with respect to the quasi-momentum of a given extremum. The degenerate extrema are in general split. This splitting is completely determined by the deformation potentials Ξ_d and Ξ_u .

The general form of the energy shift (3.28) of valley i of type $k = X, L$ for an arbitrary homogeneous deformation can be written in the following form [60]:

$$\Delta\epsilon_c^{(i,k)} = \Xi_d^{(k)} \text{Tr}(\hat{\epsilon}) + \Xi_u^{(k)} \mathbf{a}_i^T \hat{\epsilon} \mathbf{a}_i, \quad (3.30)$$

where \mathbf{a}_i is a unit vector parallel to the \mathbf{k} vector of valley i . From (3.30) it follows that degeneracy is reduced by shear strain.

3.2.4.2 Shift of the Mean Energy

The shift of the mean energy of the conduction band extrema of type k is expressed as:

$$\Delta\epsilon_{c,av}^{(k)} = \left(\Xi_d^k + \frac{1}{3} \Xi_u^k \right) \text{Tr}(\hat{\epsilon}). \quad (3.31)$$

This shift can become important when more than one type of valley is taken into account as in general the deformation potentials Ξ_d and Ξ_u have different values for different valley types. The relative shift of the mean energy for valleys of different type can cause a repopulation between these valleys as schematically shown in Fig. 3.7 for the case of X and L valleys. Expression (3.31) is derived as an average of particular shifts given by (3.30). Thus some valleys of a given type can still significantly move which will cause a repopulation between particular extrema of different type while the transitions between other extrema will be reduced.

3.3 Substrate Orientation and Strain Tensor

The energy splitting and the shift of the mean energy depend on the orientation of the applied forces. In the case of strained SiGe active layers grown on relaxed SiGe substrates this orientation is determined by the orientation of a substrate.

3.3.1 Strain Tensor in the Interface Coordinate System

The energy splitting and the hydrostatic shift of the mean energy depend on the orientation of the applied forces.

The interface coordinate system is specified as a system with its z -axis perpendicular to the hetero-interface. The form of the strain tensor $\hat{\epsilon}'$ in this coordinate system can be found as follows.

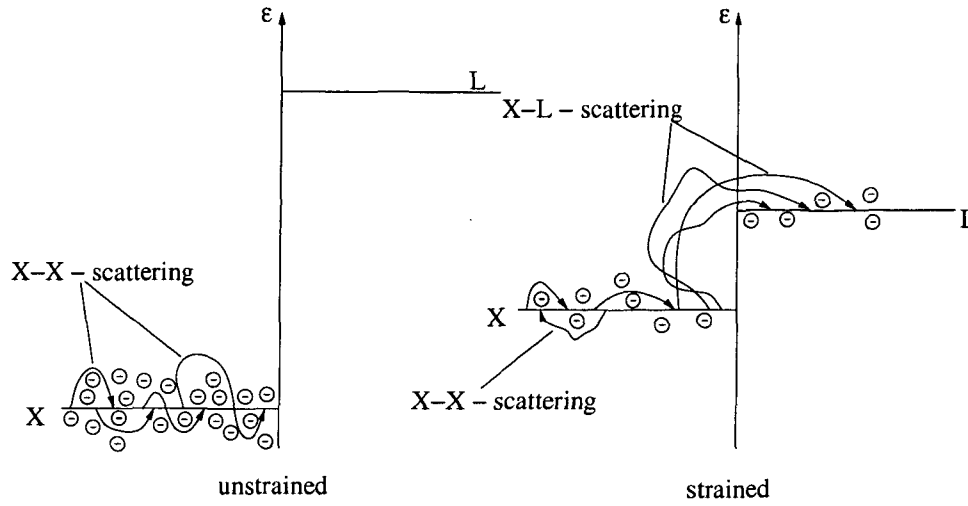


Figure 3.7: Repopulation effect between X and L valleys in strained material.

The condition of biaxial dilatation or contraction gives:

$$\varepsilon'_{11} = \varepsilon'_{22} = \varepsilon_{\parallel}, \quad (3.32)$$

where ε_{\parallel} is the in-plane strain given as the relative lattice mismatch:

$$\varepsilon_{\parallel} = \frac{a_s - a_l}{a_l}. \quad (3.33)$$

Here a_l is the lattice constant of the layer and a_s that of the substrate. The substrate is assumed to be thick enough to remain unstrained. Further, the condition of vanishing in-plane shear implies:

$$\varepsilon'_{12} = 0. \quad (3.34)$$

It is also assumed that there is no any film distortion which means the following conditions:

$$\varepsilon'_{13} = \varepsilon'_{23} = 0. \quad (3.35)$$

This is justified for the case of substrates with high rotational symmetry. In other cases it is relatively weak for SiGe structures.

Thus under these conditions the strain tensor for the SiGe active layer is diagonal in the interface coordinate system. The two diagonal elements are known to be equal to ε_{\parallel} . To determine the third diagonal element Hooke's law is applied. It linearly relates the components of the stress and the strain tensors σ_{ik} and ε_{jl} :

$$\sigma'_{\alpha\beta} = c'_{\alpha\beta ij} \varepsilon'_{ij}, \quad (3.36)$$

where c_{ijkl} is a tensor of rank four called the elastic stiffness tensor. As the only external stress is in-plane, the out-of-plane component vanishes

$$\sigma'_{33} = 0 \quad (3.37)$$

which gives for the third diagonal component of the strain tensor:

$$\varepsilon'_{33} = -\frac{c'_{3311} + c'_{3322}}{c'_{3333}} \varepsilon_{\parallel}. \quad (3.38)$$

3.3.2 Coordinate System Transformation

To find the components of the elastic stiffness tensor it is necessary to perform a coordinate transformation.

3.3.2.1 Euler's Angles

The angles which specify the relative orientation of the two coordinate systems are called Euler's angles. They are defined by the following rules. First a clockwise rotation around the z -axis is performed. This angle is usually denoted as α . Then a clockwise rotation around the new y -axis follows. This second angle is denoted as β . Finally, a clockwise rotation around the new z -axis finishes the transformation. The last angle is denoted as γ . The range of these angles are determined as follows:

$$\begin{aligned} 0 &\leq \alpha \leq 2\pi, \\ 0 &\leq \beta \leq \pi, \\ 0 &\leq \gamma \leq 2\pi. \end{aligned} \quad (3.39)$$

3.3.2.2 Transformation Operator

The transformation operator describing three successive rotations with Euler's Angles α , β and γ is given as a product of three rotations:

$$\hat{U}(\alpha, \beta, \gamma) = \hat{U}_z(\alpha) \hat{U}_{y'}(\beta) \hat{U}_{z'}(\gamma), \quad (3.40)$$

where the unitary operators $\hat{U}_z(\alpha)$, $\hat{U}_{y'}(\beta)$ and $\hat{U}_{z'}(\gamma)$ are given through the expressions:

$$\hat{U}_z(\alpha) = \begin{pmatrix} \cos \alpha & -\sin \alpha & 0 \\ \sin \alpha & \cos \alpha & 0 \\ 0 & 0 & 1 \end{pmatrix}, \quad (3.41)$$

$$\hat{U}_{y'}(\beta) = \begin{pmatrix} \cos \beta & 0 & \sin \beta \\ 0 & 1 & 0 \\ -\sin \beta & 0 & \cos \beta \end{pmatrix}, \quad (3.42)$$

$$\hat{U}_{z'}(\gamma) = \begin{pmatrix} \cos \gamma & -\sin \gamma & 0 \\ \sin \gamma & \cos \gamma & 0 \\ 0 & 0 & 1 \end{pmatrix}. \quad (3.43)$$

Thus the transformation operator (3.40) takes the form:

$$\hat{U}(\alpha, \beta, \gamma) = \begin{pmatrix} \cos \alpha \cos \beta \cos \gamma - \sin \alpha \sin \gamma & -\cos \alpha \cos \beta \sin \gamma - \sin \alpha \cos \gamma & \cos \alpha \sin \beta \\ \sin \alpha \cos \beta \cos \gamma + \cos \alpha \sin \gamma & -\sin \alpha \cos \beta \sin \gamma + \cos \alpha \cos \gamma & \sin \alpha \sin \beta \\ -\sin \beta \cos \gamma & \sin \beta \sin \gamma & \cos \beta \end{pmatrix}. \quad (3.44)$$

Due to the symmetry property (3.32) the transformed strain tensor will not depend on γ . So γ is arbitrary and can be set to zero. The transformation operator takes the final form:

$$\hat{U}(\alpha, \beta) = \begin{pmatrix} \cos \alpha \cos \beta & -\sin \alpha & \cos \alpha \sin \beta \\ \sin \alpha \cos \beta & \cos \alpha & \sin \alpha \sin \beta \\ -\sin \beta & 0 & \cos \beta \end{pmatrix}. \quad (3.45)$$

3.3.2.3 Tensor Transformations

Using the transformation operator $\hat{U}(\alpha, \beta)$ the strain tensor elements are transformed as follows:

$$\varepsilon'_{\alpha\beta} = U_{i\alpha} U_{j\beta} \varepsilon_{ij}. \quad (3.46)$$

Therefore the main task is to determine the elements of the strain tensor in the interface coordinate system. The strain tensor elements in the principle coordinate system are then obtained as:

$$\varepsilon_{\alpha\beta} = U_{\alpha i} U_{\beta j} \varepsilon'_{ij}. \quad (3.47)$$

The elastic stiffness tensor is transformed analogously:

$$c'_{\alpha\beta\delta\gamma} = U_{i\alpha} U_{j\beta} U_{k\delta} U_{l\gamma} c_{ijkl} \quad (3.48)$$

3.3.3 Strain Tensor Elements in the Principle Coordinate System

Due to the cubic symmetry of Si and Ge there are only three non-zero components of the elastic stiffness tensor, namely c_{11} , c_{12} and c_{44} in the short-hand notation [50]. This fact allows to significantly simplify the calculations of ε'_{33} which are given below for the three substrate orientations [001], [110] and [111]. The calculations for an arbitrary substrate orientation are performed in the same manner. For these three substrate orientations the transformation operator takes the form:

$$\hat{U}_{(001)} = \begin{pmatrix} 1 & 0 & 0 \\ 0 & 1 & 0 \\ 0 & 0 & 1 \end{pmatrix}, \quad (3.49)$$

$$\hat{U}_{(110)} = \begin{pmatrix} 0 & -\frac{1}{\sqrt{2}} & \frac{1}{\sqrt{2}} \\ 0 & \frac{1}{\sqrt{2}} & \frac{1}{\sqrt{2}} \\ -1 & 0 & 0 \end{pmatrix}, \quad (3.50)$$

$$\hat{U}_{(111)} = \begin{pmatrix} \frac{1}{\sqrt{6}} & -\frac{1}{\sqrt{2}} & \frac{1}{\sqrt{3}} \\ \frac{1}{\sqrt{6}} & \frac{1}{\sqrt{2}} & \frac{1}{\sqrt{3}} \\ \sqrt{\frac{2}{3}} & 0 & \frac{1}{\sqrt{3}} \end{pmatrix}. \quad (3.51)$$

Using (3.48) and (3.38) one obtains:

$$\varepsilon'_{33}^{(001)} = -\frac{2c_{12}}{c_{11}} \varepsilon_{\parallel}, \quad (3.52)$$

$$\varepsilon'_{33}^{(110)} = -\frac{c_{11} + 3c_{12} - 2c_{44}}{c_{11} + c_{12} + 2c_{44}} \varepsilon_{\parallel}, \quad (3.53)$$

$$\varepsilon'_{33}^{(111)} = -\frac{2c_{11} + 4c_{12} - 4c_{44}}{c_{11} + 2c_{12} + 4c_{44}} \varepsilon_{\parallel}. \quad (3.54)$$

Now the transformation of the strain tensor according to (3.47) gives for the elements of the strain tensor in the principle coordinate system the following expressions.

[001]:

$$\begin{aligned}
\varepsilon_{11}^{(001)} &= \varepsilon_{22}^{(001)} = \varepsilon_{\parallel}, \\
\varepsilon_{33}^{(001)} &= -\frac{2c_{12}}{c_{11}}\varepsilon_{\parallel}, \\
\varepsilon_{12}^{(001)} &= \varepsilon_{13}^{(001)} = \varepsilon_{23}^{(001)} = 0.
\end{aligned} \tag{3.55}$$

[110]:

$$\begin{aligned}
\varepsilon_{11}^{(110)} &= \varepsilon_{22}^{(110)} = \frac{2c_{44} - c_{12}}{c_{11} + c_{12} + 2c_{44}}\varepsilon_{\parallel}, \\
\varepsilon_{33}^{(110)} &= \varepsilon_{\parallel}, \\
\varepsilon_{12}^{(110)} &= -\frac{c_{11} + 2c_{12}}{c_{11} + c_{12} + 2c_{44}}\varepsilon_{\parallel}, \\
\varepsilon_{13}^{(110)} &= \varepsilon_{23}^{(110)} = 0.
\end{aligned} \tag{3.56}$$

[111]:

$$\begin{aligned}
\varepsilon_{11}^{(111)} &= \varepsilon_{22}^{(111)} = \varepsilon_{33}^{(111)} = \frac{4c_{44}}{c_{11} + 2c_{12} + 4c_{44}}\varepsilon_{\parallel}, \\
\varepsilon_{12}^{(111)} &= \varepsilon_{13}^{(111)} = \varepsilon_{23}^{(111)} = -\frac{c_{11} + 2c_{12}}{c_{11} + 2c_{12} + 4c_{44}}\varepsilon_{\parallel}.
\end{aligned} \tag{3.57}$$

3.4 Band Structure of Strained SiGe layers

Within linear deformation-potential theory only shift of valleys is taken into account whereas their shape is unchanged. This shift is described by general expressions (3.30) and (3.31). These expressions are used to calculate the energy splitting and the shift of the mean energy of the X and L valleys for the three most important substrate orientations. Generalization for the case of an arbitrary substrate orientation is straightforward.

3.4.1 Hydrostatic Strain

Expression (3.31) gives the hydrostatic shift of the mean energy of both X and L valleys:

$$\Delta\epsilon_{c,av}^{X,L} = \left(\Xi_d^{X,L} + \frac{1}{3}\Xi_u^{X,L} \right) (\varepsilon_{11} + \varepsilon_{22} + \varepsilon_{33}). \tag{3.58}$$

Note that the deformation potentials for X and L valleys are different.

3.4.2 Uniaxial Strain

The splitting of equivalent valleys is given by the difference of (3.30) and (3.31) and depends on both valley type and substrate orientation.

3.4.2.1 Splitting of the X Valleys

For [001] and [110] substrates the splitting is given as:

$$\begin{aligned}\Delta\epsilon^{(100)} &= \Delta\epsilon^{(010)} = \frac{1}{3}\Xi_u^X(\epsilon_{11} - \epsilon_{33}), \\ \Delta\epsilon^{(001)} &= \frac{2}{3}\Xi_u^X(\epsilon_{33} - \epsilon_{11}).\end{aligned}\tag{3.59}$$

For [111] substrate it becomes:

$$\Delta\epsilon^{(100)} = \Delta\epsilon^{(010)} = \Delta\epsilon^{(001)} = 0.\tag{3.60}$$

Expression (3.60) means that for [111] substrates the X valleys remain degenerate.

3.4.2.2 Splitting of the L Valleys

For [001] substrate the splitting becomes:

$$\Delta\epsilon^{(111)} = \Delta\epsilon^{(\bar{1}\bar{1}1)} = \Delta\epsilon^{(\bar{1}\bar{1}\bar{1})} = \Delta\epsilon^{(1\bar{1}\bar{1})} = 0.\tag{3.61}$$

For [110]:

$$\begin{aligned}\Delta\epsilon^{(111)} &= \Delta\epsilon^{(\bar{1}\bar{1}1)} = \frac{2}{3}\Xi_u^L\epsilon_{12}, \\ \Delta\epsilon^{(\bar{1}\bar{1}\bar{1})} &= \Delta\epsilon^{(1\bar{1}\bar{1})} = -\frac{2}{3}\Xi_u^L\epsilon_{12}.\end{aligned}\tag{3.62}$$

For [111]:

$$\begin{aligned}\Delta\epsilon^{(111)} &= 2\Xi_u^L\epsilon_{12}, \\ \Delta\epsilon^{(\bar{1}\bar{1}\bar{1})} &= \Delta\epsilon^{(\bar{1}\bar{1}1)} = \Delta\epsilon^{(1\bar{1}\bar{1})} = -\frac{2}{3}\Xi_u^L\epsilon_{12}.\end{aligned}\tag{3.63}$$

Expression (3.61) shows that the L valleys are degenerate for the substrate orientation [001]. For [110] and [111] substrates they are split. This splitting is symmetric with respect to the mean energy for the substrate oriented along [110] while it is asymmetric for the case of the substrate oriented along [111].

3.4.3 Effective Masses in Strained SiGe

To take into account effects beyond the linear deformation-potential theory the model of Rieger and Vogl [61] is used for the substrate orientation [001]. This model gives the effective masses versus Ge mole compositions in the active layer and the substrate:

$$m^*(x, y) = (1, \quad (x - y), \quad (x - y)^2) \mathbf{W} \begin{pmatrix} 1 \\ (x + y) \end{pmatrix}\tag{3.64}$$

where \mathbf{W} contains parameterized transverse and longitudinal effective masses for the perpendicular and parallel X valleys, and x and y denote the Ge mole fractions of the active layer and the substrate, respectively.

For substrate orientations different from [001] a linear interpolation

$$m_{\text{SiGe}}^* = m_{\text{Si}}^*(1 - x) + m_{\text{Ge}}^*x. \quad (3.65)$$

is used for the effective masses in the active layer.

3.5 Scattering Mechanisms in Strained SiGe

The changes in the band structure of strained SiGe affects the scattering processes in the active layer. These modification are discussed in the following for the main scattering processes in SiGe such as the electron-phonon and the ionized impurity scattering.

3.5.1 Electron-Phonon Scattering

The influence of strain on acoustic phonon scattering is taken into account through the modification of the number of final equivalent valleys and the final electron energy.

The final energy is given by the following expression:

$$\begin{aligned} E_{fin} &= E_{in} \mp \hbar\omega_{V_1V_2} + \Delta E_{ij}^{(V_1, V_2)}, \\ \Delta E_{ij}^{(V_1, V_2)} &= \Delta E_j^{(V_1)} - \Delta E_i^{(V_2)}, \end{aligned} \quad (3.66)$$

where $\Delta E_{ij}^{(V_1, V_2)}$ is the difference between the minima of the valleys V_1 and V_2 , $V_k = X, L$ is the valley type and indices i and j denote the initial and final orientations of the valleys, respectively.

3.5.2 Ionized Impurity Scattering

The influence of strain on the Fermi level and the screening parameters of the ionized impurity scattering model [44] is considered. The effects of strain on impurity centers [62] in doped layers, however, are neglected.

For an analytical band structure taking into account nonparabolicity and anisotropy the density of states of one valley is given by

$$g(\epsilon) = \frac{\sqrt{2}m_d^{\frac{3}{2}}\sqrt{\epsilon}}{\pi^2\hbar^3} \sqrt{1 + \alpha\epsilon} \cdot (1 + 2\alpha\epsilon) \quad (3.67)$$

In order to calculate the Fermi energy in the strained material only terms up to the second order in the nonparabolicity coefficient are kept. A nonlinear equation for the Fermi energy E_f is obtained:

$$n = \sum_i N_{c_i}^{(or)} \sum_j \left[\mathcal{F}_{1/2}(\eta_{ij}) + \frac{15}{4} \alpha k_B T_0 \mathcal{F}_{3/2}(\eta_{ij}) + \frac{105}{32} \alpha^2 k_B^2 T_0^2 \mathcal{F}_{5/2}(\eta_{ij}) \right] \quad (3.68)$$

where $\eta_{ij} = (E_f - E_{c_i} - \Delta E_{c_{ij}})/k_B T_0$, $N_{c_i}^{(or)}$ stands for the effective density of states of valley i with orientation j , $\Delta E_{c_{ij}}$ is the energy splitting of that valley and T_0 is the lattice temperature.

The linear and quadratic terms in (3.68) play an important role as carriers can populate higher energy levels in highly degenerate semiconductors. (3.68) is solved by Newton iteration using as an initial guess the solution obtained for non-degenerate statistics and parabolic bands.

Including nonparabolicity up to the second order the contribution of valley i with orientation j to the inverse screening length takes the following form:

$$\beta_{sij}^2 = \frac{e^2}{\epsilon_s \epsilon_0 k_B T_0} N_{c_i}^{(or)} \cdot \left[\mathcal{F}_{-1/2}(\eta_{ij}) + \frac{15}{4} \alpha K_B T_0 \cdot \mathcal{F}_{1/2}(\eta_{ij}) + \frac{105}{32} \alpha^2 K_B^2 T_0^2 \cdot \mathcal{F}_{3/2}(\eta_{ij}) \right], \quad (3.69)$$

It should be noted that in semiconductors with non-parabolic bands the inverse screening length increases which may weaken the ionized impurity scattering rate in particular for a high doping level when due to the Pauli exclusion principle the population of higher energies increases significantly. Thus there are two opposite factors which determine the strength of ionized impurity scattering. Another interesting effect occurs in strained doped materials. Due to strain some valleys shift up and do not contribute to the kinetics. However, this may change at high degeneracy when the Pauli principle causes the upper split bands to be populated, which then also give a contribution to the transport properties. The repopulation may be significant leading to a reduction of the valley splitting effect.

In case of momentum-dependent screening the dielectric function is modified to take into account the strain induced splitting of the conduction band minima for different valleys and orientations:

$$\epsilon(q) = \epsilon(0) \cdot \left(1 + \frac{1}{q^2} \sum_{ij} \beta_{sij}^2 G_{ij}(\xi, \eta_{ij}) \right), \quad (3.70)$$

where G_{ij} stands for the screening function in valley i with orientation j . The momentum transfer $\mathbf{q} = \mathbf{p}' - \mathbf{p}$ and the temperature dependence enters through ξ .

3.5.3 Plasmon Scattering

In the case of plasmon scattering the strain effects enter through the screening length β_s which determines the cut-off wave vector (2.134). Additionally the plasmon frequency in the strained case is given as:

$$\omega_{pl} = e \sqrt{\frac{1}{\epsilon} \sum_{ij} \frac{n_{ij}}{(m_d^*)_i}}, \quad (3.71)$$

where n_{ij} is the contribution to the electron density from valley i with orientation j :

$$n_{ij} = N_{c_i}^{(or)} \left[\mathcal{F}_{1/2}(\eta_{ij}) + \frac{15}{4} \alpha k_B T_0 \mathcal{F}_{3/2}(\eta_{ij}) + \frac{105}{32} \alpha^2 k_B^2 T_0^2 \mathcal{F}_{5/2}(\eta_{ij}) \right]. \quad (3.72)$$

It should be noted that this result as well as the expression (2.133) for the unstrained material is only valid within the Random Phase Approximation (see Appendix B).

Chapter 4

Monte Carlo Methods for the Solution of the Boltzmann Equation

To analyze the semiclassical kinetics in semiconductors described in Chapter 2 in a comprehensive manner it is necessary to solve the Boltzmann kinetic equation (2.59). This equation mathematically represents an integro-differential equation. In general the exact solution cannot be obtained analytically. Thus approximate solution techniques have been developed. They can be divided into three classes which are analytical techniques, deterministic numerical methods, and Monte Carlo approaches.

Analytical techniques were the first attempt to understand the semiclassical transport in semiconductors. Some of these techniques assume an analytical form of the distribution function which contains parameters. These parameters are obtained from the Boltzmann kinetic equation. For example, for a heated and drifted normalized Maxwellian distribution

$$f(\mathbf{k}) = A \exp \left\{ -\frac{\hbar^2(\mathbf{k} - \mathbf{k}_d)^2}{2mk_B T_e} \right\}, \quad (4.1)$$

where A is the normalization constant, two parameters \mathbf{k}_d and T_e are introduced. The first parameter, $\hbar\mathbf{k}_d$ is the average quasi-momentum of the distribution. The second one, T_e , is the electron temperature. These two parameters are obtained from the equations which represent the first three moments of the Boltzmann transport equation which are coupled. Despite this approach is restricted to simple cases it turned out to be very useful for the hot-electron problem [63]. Another analytical approach is related to an expansion of the distribution function in spherical harmonics [64–67]. If a problem has a cylindrical symmetry around the direction of the electric field, the Legendre polynomial expansion can be written as:

$$f(\mathbf{k}) = f_0(\epsilon) + f_1(\epsilon)P_1(\cos\theta) + \dots, \quad (4.2)$$

where ϵ is the electron energy, θ stands for the angle between the electron quasi-momentum

$\hbar\mathbf{k}$ and electric field¹, f_0 denotes the symmetrical part of the distribution function and f_1 is the anti-symmetrical contribution to the distribution. Expansion (4.2) is substituted into the kinetic equation. Making use of the orthogonality of the Legendre polynomials a coupled system of equations for the coefficients f_0, f_1, \dots is derived. This system can then be solved numerically. However, the treatment of general band structures is quite difficult within this approach.

Iterative techniques [68–70] are based on the following equality for the distribution function for a homogenous system²:

$$f(\mathbf{k}, t) = \int_0^\infty dt' \int d\mathbf{k}' \exp\left\{-\int_0^{t'} \lambda[\mathbf{K}(y)] dy\right\} f(\mathbf{k}', t-t') S(\mathbf{K}(t'), \mathbf{k}'). \quad (4.3)$$

The iterative method consists of substituting an initial distribution function $f_0(\mathbf{k}, t)$ into the right-hand side of (4.3) and evaluating $f(\mathbf{k}, t)$. The new distribution function is again substituted into the right-hand side of (4.3) and this procedure is repeated until $f(\mathbf{k}, t)$ has converged to its solution with a given accuracy.

The Monte Carlo method simulates the electron's motion in a crystal under external forces. Within this technique a particle trajectory is constructed as a sequence of free flights and scattering events³. The free flight times between collisions and the parameters of the scattering events are generated stochastically using probabilities of microscopic processes. Thus the main advantage of this approach is the direct description of the microscopic particle dynamics. This allows to incorporate within the same technique very complicated kinetic phenomena. General band structures of different semiconductors can be taken into account. In addition the implementation is simpler compared to other numerical methods.

In this work preference is given to the Monte Carlo approach. In the following new Monte Carlo algorithms are developed for modeling of strained bulk SiGe, and known Monte Carlo techniques and their aspects are also described.

4.1 Perturbation Approach to the Boltzmann Equation Including the Pauli Principle

In the following a homogenous semiconductor is considered. Then the distribution function and the differential scattering rate are independent on position. It is also assumed that the differential scattering rate is time invariant. With these conditions the time dependent Boltzmann equation (2.59) taking into account the Pauli exclusion principle takes the following form:

$$\frac{\partial f(\mathbf{k}, t)}{\partial t} + \frac{q\mathbf{E}(t)}{\hbar} \nabla f(\mathbf{k}, t) = Q[f](\mathbf{k}, t), \quad (4.4)$$

¹The quasi-momentum and electric field are assumed to be transformed to the Herring-Vogt space to spherical constant energy surfaces instead of ellipsoidal ones which are the case for Si and Ge.

²This is just an integral form of the Boltzmann kinetic equation discussed later in this chapter.

³In general a Monte Carlo trajectory is not identical with a real trajectory and depends on a specific Monte Carlo algorithm.

where $\mathbf{E}(t)$ is an electric field and q is the particle charge. $Q[f](\mathbf{k}, t)$ represents the scattering operator which is given by the following expression:

$$Q[f](\mathbf{k}, t) = \int f(\mathbf{k}', t)[1 - f(\mathbf{k}, t)]S(\mathbf{k}', \mathbf{k}) d\mathbf{k}' - \int f(\mathbf{k}, t)[1 - f(\mathbf{k}', t)]S(\mathbf{k}, \mathbf{k}') d\mathbf{k}', \quad (4.5)$$

where $S(\mathbf{k}', \mathbf{k})$ stands for the differential scattering rate. Thus $S(\mathbf{k}', \mathbf{k})d\mathbf{k}$ is the scattering rate from a state with wave vector \mathbf{k}' to states in $d\mathbf{k}$ around \mathbf{k} , $f(\mathbf{k}, t)$ is the distribution function, and the factors $[1 - f(\mathbf{k}, t)]$ mean that the final state must not be occupied according to the Pauli exclusion principle. As can be seen from (4.5), there are terms $f(\mathbf{k}, t)f(\mathbf{k}', t)$ which render the equation nonlinear. Only when the condition $f(\mathbf{k}, t) \ll 1$ is valid the factors $[1 - f(\mathbf{k}, t)]$ can be replaced by unity and the equation takes the usual linear form.

To linearize (4.4) the electric field is written in the form:

$$\mathbf{E}(t) = \mathbf{E}_s + \mathbf{E}_1(t), \quad (4.6)$$

where \mathbf{E}_s stands for a stationary field and $\mathbf{E}_1(t)$ denotes a small perturbation which is superimposed on a stationary field. It is assumed that this small perturbation of the electric field causes a small perturbation of the distribution function which can be written as follows:

$$f(\mathbf{k}, t) = f_s(\mathbf{k}) + f_1(\mathbf{k}, t), \quad (4.7)$$

where $f_s(\mathbf{k})$ is a stationary distribution function and $f_1(\mathbf{k}, t)$ is a small deviation from a stationary distribution. Substituting (4.7) into (4.5) the scattering operator $Q[f](\mathbf{k}, t)$ takes the form:

$$Q[f](\mathbf{k}, t) = \int (f_s(\mathbf{k}') + f_1(\mathbf{k}', t))[1 - f_s(\mathbf{k}) - f_1(\mathbf{k}, t)]S(\mathbf{k}', \mathbf{k}) d\mathbf{k}' - \int (f_s(\mathbf{k}) + f_1(\mathbf{k}, t))[1 - f_s(\mathbf{k}') - f_1(\mathbf{k}', t)]S(\mathbf{k}, \mathbf{k}') d\mathbf{k}'. \quad (4.8)$$

It should be noted that in spite of the fact that $f_1(\mathbf{k}, t) \ll 1$ one should take care when linearizing terms such as $1 - f_s(\mathbf{k}) - f_1(\mathbf{k}, t)$. Especially in the degenerate case it may happen that $1 - f_s(\mathbf{k}) \ll f_1(\mathbf{k}, t)$ because of $[1 - f_s(\mathbf{k})] \rightarrow 0$.

4.1.1 The Zeroth Order Equation

Neglecting terms of the first and the second order in (4.4) the zeroth order equation is derived:

$$\frac{q}{\hbar} \mathbf{E}_s \nabla f_s(\mathbf{k}) = [1 - f_s(\mathbf{k})] \int f_s(\mathbf{k}') S(\mathbf{k}', \mathbf{k}) d\mathbf{k}' - f_s(\mathbf{k}) \int [1 - f_s(\mathbf{k}')] S(\mathbf{k}, \mathbf{k}') d\mathbf{k}'. \quad (4.9)$$

(4.9) represents the nonlinear stationary Boltzmann equation for the stationary distribution function $f_s(\mathbf{k})$.

4.1.2 The First Order Equation

Collecting terms of the first order gives the following equation:

$$\frac{\partial f_1(\mathbf{k}, t)}{\partial t} + \frac{q}{\hbar} \mathbf{E}_s \cdot \nabla f_1(\mathbf{k}, t) = -\frac{q}{\hbar} \mathbf{E}_1(t) \cdot \nabla f_s(\mathbf{k}) + Q^{(1)}[f](\mathbf{k}, t), \quad (4.10)$$

where the notation $Q^{(1)}[f](\mathbf{k}, t)$ has been introduced for the first order scattering operator which has the form

$$\begin{aligned} Q^{(1)}[f](\mathbf{k}, t) = & [1 - f_s(\mathbf{k})] \int f_1(\mathbf{k}', t) S(\mathbf{k}', \mathbf{k}) d\mathbf{k}' - \\ & - f_1(\mathbf{k}, t) \int [1 - f_s(\mathbf{k}')] S(\mathbf{k}, \mathbf{k}') d\mathbf{k}' - f_1(\mathbf{k}, t) \int f_s(\mathbf{k}') S(\mathbf{k}', \mathbf{k}) d\mathbf{k}' + \\ & + f_s(\mathbf{k}) \int f_1(\mathbf{k}', t) S(\mathbf{k}, \mathbf{k}') d\mathbf{k}'. \end{aligned} \quad (4.11)$$

Equation (4.10) is linear with respect to $f_1(\mathbf{k}, t)$, but it is a kinetic equation different from the usual form of the Boltzmann equation. The first difference is the additional term on the right hand side being the term proportional to \mathbf{E}_1 which additionally depends on the stationary distribution $f_s(\mathbf{k})$ determined by (4.9). The second difference is the expression for the scattering operator which now has a more complex form and also depends on the stationary distribution $f_s(\mathbf{k})$.

4.2 Integral Form of the First Order Equation

To construct a new Monte Carlo algorithm the Boltzmann kinetic equation of the first order is reformulated as an integral equation.

4.2.1 New Differential and Total Scattering Rates

For this purpose a new differential scattering rate and new total scattering rate are introduced, as defined by the following expressions:

$$\tilde{S}(\mathbf{k}', \mathbf{k}) = [1 - f_s(\mathbf{k})] S(\mathbf{k}', \mathbf{k}) + f_s(\mathbf{k}) S(\mathbf{k}, \mathbf{k}'), \quad (4.12)$$

$$\tilde{\lambda}(\mathbf{k}) = \int ([1 - f_s(\mathbf{k})] S(\mathbf{k}, \mathbf{k}') + f_s(\mathbf{k}') S(\mathbf{k}', \mathbf{k})) d\mathbf{k}' = \int \tilde{S}(\mathbf{k}, \mathbf{k}') d\mathbf{k}'. \quad (4.13)$$

The differential scattering rate and total scattering rate are now functionals of the stationary distribution function which is the solution of the equation of zero order (4.9).

With these definitions the scattering operator of the first order $Q^{(1)}[f](\mathbf{k}, t)$ takes the form:

$$Q^{(1)}[f](\mathbf{k}, t) = \int f_1(\mathbf{k}', t) \tilde{S}(\mathbf{k}', \mathbf{k}) d\mathbf{k}' - f_1(\mathbf{k}, t) \tilde{\lambda}(\mathbf{k}), \quad (4.14)$$

and the Boltzmann-like equation can be rewritten as follows:

$$\begin{aligned} \frac{\partial f_1(\mathbf{k}, t)}{\partial t} + \frac{q}{\hbar} \mathbf{E}_s \cdot \nabla f_1(\mathbf{k}, t) = & \int f_1(\mathbf{k}', t) \tilde{S}(\mathbf{k}', \mathbf{k}) d\mathbf{k}' - \\ & - f_1(\mathbf{k}, t) \tilde{\lambda}(\mathbf{k}) - \frac{q}{\hbar} \mathbf{E}_1(t) \cdot \nabla f_s(\mathbf{k}). \end{aligned} \quad (4.15)$$

4.2.2 Integral Form for the Distribution Function Perturbation

The integral form of this equation is derived using techniques described in [71]. Introducing a quasi-momentum space trajectory $\mathbf{K}(t') = \mathbf{k} - \frac{q}{\hbar} \mathbf{E}_s(t - t')$ which is the solution of Newton's equation it is possible to replace the left-hand side of (4.15) by the total derivative:

$$\frac{\partial f_1(\mathbf{K}(t), t)}{\partial t} + \frac{q}{\hbar} \mathbf{E}_s \cdot \nabla f_1(\mathbf{K}(t), t) = \frac{df_1(\mathbf{K}(t), t)}{dt}. \quad (4.16)$$

Introducing function $g(t)$:

$$g(t) = \int f_1(\mathbf{k}', t) \tilde{S}(\mathbf{k}', \mathbf{K}(t)) d\mathbf{k}' - \frac{q}{\hbar} \mathbf{E}_1 \cdot \nabla f_s(\mathbf{K}(t)), \quad (4.17)$$

the first order equation can be written as:

$$\frac{df_1(\mathbf{K}(t), t)}{dt} + \tilde{\lambda}(\mathbf{K}(t)) f_1(\mathbf{k}, t) = g(t). \quad (4.18)$$

This is an ordinary differential equation which can be solved by multiplying both sides by a function $h(t)$. This function has to fulfill the condition:

$$\frac{dh(t)}{dt} = h(t) \tilde{\lambda}(t) \quad (4.19)$$

with the particular solution:

$$h(t) = \exp \left[\int_0^t \tilde{\lambda}(y) dy \right]. \quad (4.20)$$

Then the left-hand side of (4.18) is the total derivative of the product $f_1(t)h(t)$. Taking into account that $f_1(\mathbf{K}(t_0), t_0) = 0$ for $t_0 < 0$ because of $E_1(t) = 0$ for $t < 0$ the solution is obtained:

$$f_1(\mathbf{K}(t), t) = \int_0^t g(t') \exp \left\{ - \int_{t'}^t \tilde{\lambda}[\mathbf{K}(y)] dy \right\} dt'. \quad (4.21)$$

Substituting (4.17) into (4.21) the following integral form is obtained as:

$$\begin{aligned} f_1(\mathbf{K}(t), t) = & \int_0^t dt' \int d\mathbf{k}' f_1(\mathbf{k}', t') \tilde{S}(\mathbf{k}', \mathbf{K}(t')) \exp \left(- \int_{t'}^t \tilde{\lambda}[\mathbf{K}(y)] dy \right) - \\ & - \frac{q}{\hbar} \int_0^t \mathbf{E}_1(t') \cdot [\nabla f_s](\mathbf{K}(t')) \exp \left(- \int_{t'}^t \tilde{\lambda}[\mathbf{K}(y)] dy \right) dt'. \end{aligned} \quad (4.22)$$

4.2.3 Free Term and Initial Distribution

Assuming an impulse like excitation of the electric field, $\mathbf{E}_1(t) = \delta(t)\mathbf{E}_{im}$, gives:

$$f_1(\mathbf{K}(t), t) = \int_0^t dt' \int d\mathbf{k}' f_1(\mathbf{k}', t') \tilde{S}(\mathbf{k}', \mathbf{K}(t')) \cdot \exp\left(-\int_{t'}^t \tilde{\lambda}[\mathbf{K}(y)] dy\right) + G(\mathbf{K}(0)) \exp\left(-\int_0^t \tilde{\lambda}[\mathbf{K}(y)] dy\right), \quad (4.23)$$

where

$$G(\mathbf{k}) = -\frac{q}{\hbar} \mathbf{E}_{im} \cdot \nabla f_s(\mathbf{k}). \quad (4.24)$$

The essential difference of this integral representation from the one of the non-degenerate approach consists in the appearance of the new differential scattering rate $\tilde{S}(\mathbf{k}', \mathbf{k})$ and of the total scattering rate $\tilde{\lambda}(\mathbf{k})$. The Boltzmann-like equation (4.10) differs from the Boltzmann equation (4.4) by the additional free term on the right hand side which in general cannot be treated as an initial distribution because it also takes negative values.

4.2.4 The Resolvent Series

Equation (4.23) represents a Fredholm integral equation of second kind with a free term determined by function $G(\mathbf{k})$. This equation can be rewritten⁴:

$$f(x) = \int f(x') K(x', x) dx' + g(x), \quad (4.25)$$

where the $K(x', x)$ and the free term are given functions. The multidimensional variable x stands for (\mathbf{k}, t) ⁵. The resolvent series⁶ of a Fredholm integral equation is obtained by replacement of its right hand side into itself:

$$f(x) = g(x) + \int g(x_1) K(x_1, x) dx_1 + \int dx_1 \int dx_2 g(x_1) K(x_1, x_2) K(x_2, x) + \dots \quad (4.26)$$

This means that the solution of (4.23) can be written as consecutive iterations of the free term:

$$f(x) = f^0(x) + f^1(x) + f^2(x) + \dots \quad (4.27)$$

To find the iteration terms explicitly (4.23) is rewritten as:

$$f_1(\mathbf{k}, t) = \int_0^t dt_1 \int d\mathbf{k}_1 f_1(\mathbf{k}_1, t_1) \tilde{S}(\mathbf{k}_1, \mathbf{K}(t_1)) \cdot \exp\left(-\int_{t_1}^t \tilde{\lambda}[\mathbf{K}(y)] dy\right) + G(\mathbf{K}(0)) \exp\left(-\int_0^t \tilde{\lambda}[\mathbf{K}(y)] dy\right), \quad (4.28)$$

⁴This is the standard form from the theory of integral equations.

⁵For inhomogeneous case it stands for $(\mathbf{k}, \mathbf{r}, t)$ that is a point in the seven dimensional space.

⁶Also known as the Neumann series [72].

where (\mathbf{k}', t') has been replaced by (\mathbf{k}_1, t_1) and the respective quasi-momentum space trajectory is:

$$\begin{aligned} \mathbf{K}(t_1) &= \mathbf{k} - \frac{q}{\hbar} \mathbf{E}_s(t - t_1), \\ \mathbf{K}(t) &= \mathbf{k}, \\ 0 < t_1 < t. \end{aligned} \quad (4.29)$$

Introducing a quasi-momentum space trajectory for the time interval $0 < t_2 < t_1$:

$$\begin{aligned} \mathbf{K}_1(t_2) &= \mathbf{k}_1 - \frac{q}{\hbar} \mathbf{E}_s(t_1 - t_2), \\ \mathbf{K}_1(t_1) &= \mathbf{k}_1, \end{aligned} \quad (4.30)$$

one obtains for $f_1(\mathbf{k}_1, t_1)$:

$$\begin{aligned} f_1(\mathbf{k}_1, t_1) &= \int_0^{t_1} dt_2 \int d\mathbf{k}_2 f_1(\mathbf{k}_2, t_2) \tilde{S}(\mathbf{k}_2, \mathbf{K}_1(t_2)) \cdot \exp\left(-\int_{t_2}^{t_1} \tilde{\lambda}[\mathbf{K}_1(y)] dy\right) + \\ &+ G(\mathbf{K}_1(0)) \exp\left(-\int_0^{t_1} \tilde{\lambda}[\mathbf{K}_1(y)] dy\right). \end{aligned} \quad (4.31)$$

Substituting (4.31) into (4.28) gives:

$$\begin{aligned} f_1(\mathbf{k}, t) &= \int_0^t dt_1 \int d\mathbf{k}_1 \int_0^{t_1} dt_2 \int d\mathbf{k}_2 f_1(\mathbf{k}_2, t_2) \tilde{S}(\mathbf{k}_2, \mathbf{K}_1(t_2)) \exp\left(-\int_{t_2}^{t_1} \tilde{\lambda}[\mathbf{K}_1(y)] dy\right) \times \\ &\times \tilde{S}(\mathbf{k}_1, \mathbf{K}(t_1)) \exp\left(-\int_{t_1}^t \tilde{\lambda}[\mathbf{K}(y)] dy\right) + \\ &+ \int_0^t dt_1 \int d\mathbf{k}_1 G(\mathbf{K}_1(0)) \exp\left(-\int_0^{t_1} \tilde{\lambda}[\mathbf{K}_1(y)] dy\right) \tilde{S}(\mathbf{k}_1, \mathbf{K}(t_1)) \exp\left(-\int_{t_1}^t \tilde{\lambda}[\mathbf{K}(y)] dy\right) + \\ &+ G(\mathbf{K}(0)) \exp\left(-\int_0^t \tilde{\lambda}[\mathbf{K}(y)] dy\right). \end{aligned} \quad (4.32)$$

From (4.32) the first iteration term is obtained:

$$\begin{aligned} f_1^{(1)}(\mathbf{k}, t) &= \\ &\int_0^t dt_1 \int d\mathbf{k}_1 G(\mathbf{K}_1(0)) \exp\left(-\int_0^{t_1} \tilde{\lambda}[\mathbf{K}_1(y)] dy\right) \tilde{S}(\mathbf{k}_1, \mathbf{K}(t_1)) \exp\left(-\int_{t_1}^t \tilde{\lambda}[\mathbf{K}(y)] dy\right). \end{aligned} \quad (4.33)$$

which is also schematically shown in Fig. 4.1.

In order to obtain the second iteration term the third quasi-momentum space trajectory is introduced for $0 < t_3 < t_2$

$$\begin{aligned} \mathbf{K}_2(t_3) &= \mathbf{k}_2 - \frac{q}{\hbar} \mathbf{E}_s(t_2 - t_3), \\ \mathbf{K}_2(t_2) &= \mathbf{k}_2. \end{aligned} \quad (4.34)$$

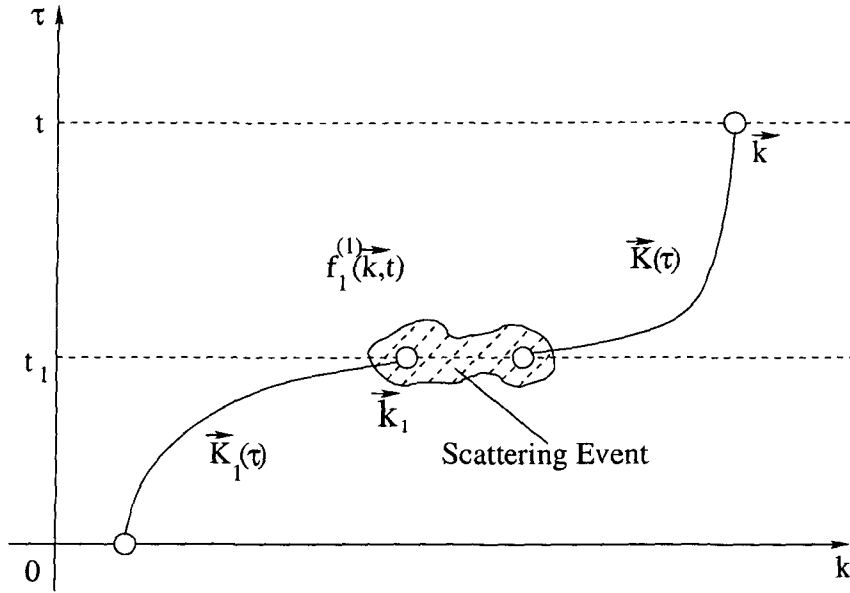


Figure 4.1: Graphical representation of the first iteration term.

Then for $f_1(\mathbf{k}_2, t_2)$ in (4.31) one obtained:

$$f_1(\mathbf{k}_2, t_2) = \int_0^{t_2} dt_3 \int d\mathbf{k}_3 f_1(\mathbf{k}_3, t_3) \tilde{S}(\mathbf{k}_3, \mathbf{K}_2(t_3)) \cdot \exp\left(-\int_{t_3}^{t_2} \tilde{\lambda}[\mathbf{K}_2(y)] dy\right) + G(\mathbf{K}_2(0)) \exp\left(-\int_0^{t_2} \tilde{\lambda}[\mathbf{K}_2(y)] dy\right). \quad (4.35)$$

The second iteration term is obtained from (4.35) by replacing $f_1(\mathbf{k}_3, t_3)$ with the free term of (4.28):

$$f_1^{(2)}(\mathbf{k}, t) = \int_0^t dt_1 \int d\mathbf{k}_1 \int_0^{t_1} dt_2 \int d\mathbf{k}_2 G(\mathbf{K}_2(0)) \exp\left(-\int_0^{t_2} \tilde{\lambda}[\mathbf{K}_2(y)] dy\right) \times \tilde{S}(\mathbf{k}_2, \mathbf{K}_1(t_2)) \exp\left(-\int_{t_2}^{t_1} \tilde{\lambda}[\mathbf{K}_1(y)] dy\right) \tilde{S}(\mathbf{k}_1, \mathbf{K}(t_1)) \exp\left(-\int_{t_1}^t \tilde{\lambda}[\mathbf{K}(y)] dy\right). \quad (4.36)$$

This term is displayed graphically in Fig. 4.2.

4.2.5 The Second Iteration of the Forward Resolvent Series

The structure of the algorithm can be seen by derivation of the second iteration term of the Neumann series for (4.23) using the forward formulation to obtain the ensemble Monte Carlo algorithm. This algorithm does not give the distribution function value at a given point, but

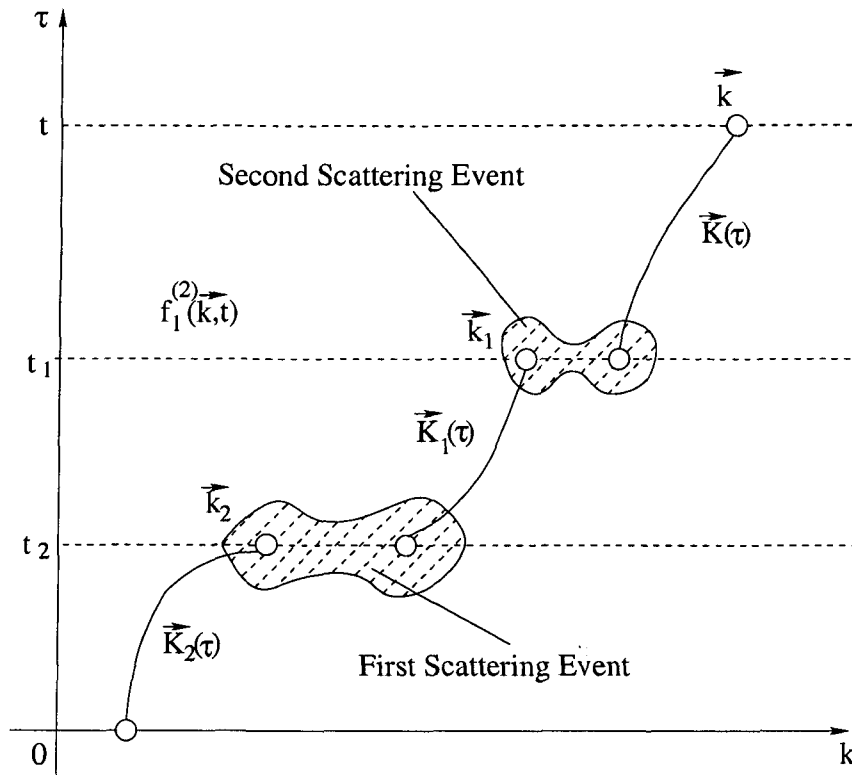


Figure 4.2: Graphical representation of the second iteration term.

instead the relative number of carriers in a region Ω with volume $\Delta \mathbf{k}$ around point \mathbf{k} in the quasi-momentum space⁷.

The relative number of carriers in Ω determined by the small perturbation $f_1(\mathbf{k}, t)$ is defined as:

$$(f_1)_\Omega = \int_{\Delta \mathbf{k}} f_1(\mathbf{k}, t) d\mathbf{k} = \int f_1(\mathbf{k}, t) \theta_\Omega(\mathbf{k}) d\mathbf{k}, \quad (4.37)$$

where the domain indicator $\theta_\Omega(\mathbf{k})$ has been introduced as a function which evaluates to one if $\mathbf{k} \in \Omega$ and zero otherwise. In order to use the phase space volume conservation law described in Section 2.1.3, an additional integral over the real space is added and (4.37) is rewritten as

$$(f_1)_\Omega = \frac{1}{V_{cr}} \int d\mathbf{k} \int d\mathbf{r} f_1(\mathbf{k}, t) \theta_\Omega(\mathbf{k}), \quad (4.38)$$

⁷It should be noted that in our case this is the relative number of carriers determined by the perturbation $f_1(\mathbf{k}, t)$.

where V_{cr} is a crystal volume. From (4.36) the second iteration term is obtained:

$$(f_1^{(2)})_{\Omega} = \frac{1}{V_{cr}} \int_0^t dt_1 \int_0^{t_1} dt_2 \int d\mathbf{k} \int d\mathbf{r} \int d\mathbf{k}_2 \int d\mathbf{k}_1 G(\mathbf{K}_2(0)) \exp\left(-\int_0^{t_2} \tilde{\lambda}[\mathbf{K}_2(y)] dy\right) \times \quad (4.39)$$

$$\times \tilde{S}(\mathbf{k}_2, \mathbf{K}_1(t_2)) \exp\left(-\int_{t_2}^{t_1} \tilde{\lambda}[\mathbf{K}_1(y)] dy\right) \tilde{S}(\mathbf{k}_1, \mathbf{K}(t_1)) \exp\left(-\int_{t_1}^t \tilde{\lambda}[\mathbf{K}(y)] dy\right) \theta_{\Omega}(\mathbf{k}).$$

Considering \mathbf{r} as $\mathbf{R}(t)$ which is the real space trajectory corresponding to the quasi-momentum trajectory (4.29) it follows from the phase space volume conservation⁸ that $d\mathbf{k}d\mathbf{r} = d\mathbf{K}(t_1)d\mathbf{R}(t_1)$. Denoting $\mathbf{K}(t_1)$ with \mathbf{k}_1^a (4.29) can be rewritten in a forward initialization:

$$\mathbf{K}(t) = \mathbf{k}_1^a + \frac{q}{\hbar} \mathbf{E}_s(t - t_1). \quad (4.40)$$

In the same manner combining $d\mathbf{k}_1$ with $d\mathbf{R}(t_1)$ gives $d\mathbf{k}_1d\mathbf{R}(t_1) = d\mathbf{K}_1(t_2)d\mathbf{R}_1(t_2)$. Denoting $\mathbf{K}_1(t_2)$ with \mathbf{k}_2^a (4.30) can be rewritten in a forward initialization:

$$\mathbf{K}_1(t_1) = \mathbf{k}_2^a + \frac{q}{\hbar} \mathbf{E}_s(t_1 - t_2). \quad (4.41)$$

Finally $d\mathbf{k}_2d\mathbf{R}_1(t_2) = d\mathbf{K}_2(0)d\mathbf{R}_2(0)$. Denoting $\mathbf{K}_2(0)$ as \mathbf{k}_i one obtains for the corresponding forward initialization:

$$\mathbf{K}_2(t_2) = \mathbf{k}_i + \frac{q}{\hbar} \mathbf{E}_s t_2. \quad (4.42)$$

Integrating out $\mathbf{R}_2(0)$ cancels the crystal volume V_{cr} and the final expression is:

$$(f_1^{(2)})_{\Omega} = \int_0^t dt_1 \int_0^{t_1} dt_2 \int d\mathbf{k}_2^a \int d\mathbf{k}_1^a \int d\mathbf{k}_i G(\mathbf{k}_i) \exp\left(-\int_0^{t_2} \tilde{\lambda}[\mathbf{K}_2(y)] dy\right) \times \quad (4.43)$$

$$\times \tilde{S}(\mathbf{K}_2(t_2), \mathbf{k}_2^a) \exp\left(-\int_{t_2}^{t_1} \tilde{\lambda}[\mathbf{K}_1(y)] dy\right) \tilde{S}(\mathbf{K}_1(t_1), \mathbf{k}_1^a) \exp\left(-\int_{t_1}^t \tilde{\lambda}[\mathbf{K}(y)] dy\right) \theta_{\Omega}(\mathbf{K}(t)).$$

To express the time integrals in a forward way the following identity is used:

$$\int_0^t dt_1 \int_0^{t_1} dt_2 = \int_0^t dt_2 \int_{t_2}^t dt_1, \quad (4.44)$$

which is schematically shown in Fig. 4.3.

⁸Or from the incompressibility of the phase space liquid.

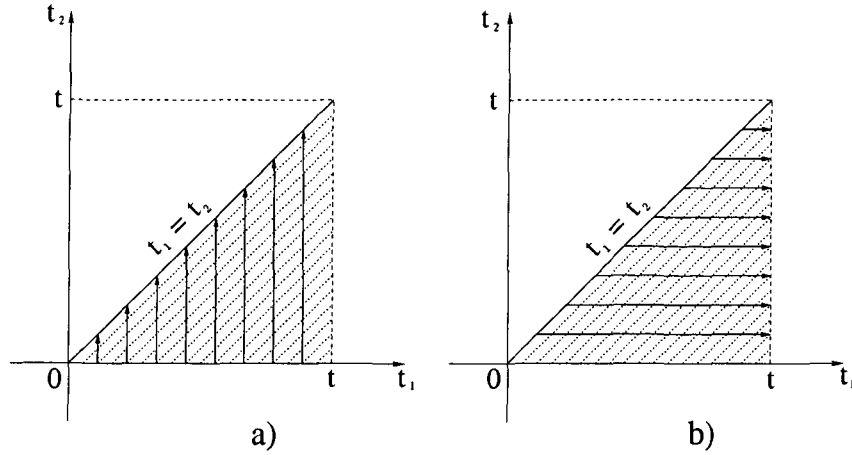


Figure 4.3: The same integration area can be covered either vertically a) or horizontally b).

Now the second iteration term has the form:

$$\begin{aligned}
 (f_1^{(2)})_{\Omega} = & \int_0^t dt_2 \int_{t_2}^t dt_1 \int d\mathbf{k}_2^a \int d\mathbf{k}_1^a \int d\mathbf{k}_i \{G(\mathbf{k}_i)\} \times \\
 & \times \left\{ \exp\left(-\int_0^{t_2} \tilde{\lambda}[\mathbf{K}_2(y)] dy\right) \tilde{\lambda}[\mathbf{K}_2(t_2)] \right\} \left\{ \frac{\tilde{S}[\mathbf{K}_2(t_2), \mathbf{k}_2^a]}{\tilde{\lambda}[\mathbf{K}_2(t_2)]} \right\} \times \\
 & \times \left\{ \exp\left(-\int_{t_2}^{t_1} \tilde{\lambda}[\mathbf{K}_1(y)] dy\right) \tilde{\lambda}[\mathbf{K}_1(t_1)] \right\} \left\{ \frac{\tilde{S}[\mathbf{K}_1(t_1), \mathbf{k}_1^a]}{\tilde{\lambda}[\mathbf{K}_1(t_1)]} \right\} \times \\
 & \times \exp\left(-\int_{t_1}^t \tilde{\lambda}[\mathbf{K}(y)] dy\right) \theta_{\Omega}(\mathbf{K}(t)),
 \end{aligned} \tag{4.45}$$

where \mathbf{k}^a stands for an after-scattering wave vector and \mathbf{k}_i denotes an initial wave vector. The quantity $\tilde{S}[\mathbf{k}, \mathbf{k}']/\tilde{\lambda}[\mathbf{k}]$ represents a normalized after-scattering distribution. As can be seen from (4.12) and (4.13) it is normalized to unity. It follows from (4.45), that during Monte Carlo simulation a particle trajectory is constructed in terms of new quantities \tilde{S} and $\tilde{\lambda}$.

4.3 Zero Field Monte Carlo Algorithm Including the Pauli Principle

At zero electric field the free term can be calculated explicitly which simplifies the construction of the algorithm.

4.3.1 Low Field Carrier Mobility and Monte Carlo Techniques

The low field carrier mobility is an important kinetic property of a bulk semiconductor. It is used to analyze carrier transport in semiconductor devices at low applied voltages and enters expressions for high field mobility models as an additional parameter. Thus the knowledge of the low field carrier mobility and its correct dependence on the material properties such as the doping concentration are necessary to adequately simulate carrier transport in semiconductor devices.

The standard Monte Carlo approach for obtaining the low field carrier mobility is a single particle Monte Carlo method. In order to calculate the low field mobility along the direction of the electric field one has to carefully choose the magnitude of the applied electric field. On the one hand, the magnitude of the electric field must be as low as possible. In principle it is desirable to have zero electric field. However, there exist limitations related to the increase of the variance of standard Monte Carlo methods. On the other hand, the field must not be too high to avoid a mobility reduction due to carrier heating.

In addition to these disadvantages, the standard approaches only give one component of the carrier mobility, namely the component in the direction of the electric field. For isotropic conditions it does not make any difference since the mobility tensor is diagonal and all diagonal values are equal. However, when anisotropy is present, for example in strained semiconductors, the mobility tensor elements may be different and several Monte Carlo simulations are required to obtain all the components of the tensor.

To overcome these problems associated with the standard Monte Carlo methods a new Monte Carlo algorithm has been suggested recently [73], which solves the Boltzmann equation for zero electric field and represents a limiting case of the small signal algorithm obtained in [74]. One of the most remarkable properties of the algorithm is the absence of self-scattering that allows to significantly reduce calculation time and achieve very good accuracy of the results. This method is restricted to the simulation of lowly doped semiconductors. The quantum mechanical Pauli exclusion principle is not included in the scattering term of the Boltzmann equation used for the derivation of the algorithm. As a result there are limitations on the doping level of the materials analyzed by this technique. It allows to obtain excellent results at low and intermediate doping levels while results obtained for higher doping levels, where the effects of degenerate statistics are more pronounced, are incorrect. As the standard Monte Carlo methods exhibit a very high variance especially in the degenerate case, it is thus desirable to have a powerful technique to analyze the carrier mobility at high doping levels.

In this chapter a zero field algorithm [75] used to account for degenerate statistics in strained SiGe layers is described. The Pauli exclusion principle is taken into consideration in the scattering term of the Boltzmann equation. As a result the Boltzmann equation becomes nonlinear. Using this nonlinear equation a generalized zero field algorithm applicable for the analysis of highly doped materials is derived.

4.3.2 Specific of the Equilibrium Distribution

When the electric field tends to zero, the distribution function approaches the equilibrium distribution which is in the case of particles with fractional spin represented by the Fermi-Dirac

distribution function (2.30). It has the form

$$f_{FD}(\epsilon(\mathbf{k})) = \frac{1}{\exp\left(-\frac{E_f - \epsilon(\mathbf{k})}{k_B T_0}\right) + 1}, \quad (4.46)$$

where E_f denotes the Fermi energy, ϵ stands for the electron energy and T_0 is the equilibrium temperature equal to the lattice temperature. Since the stationary distribution is known, there is no need to solve the zeroth order equation (4.9). As can be seen from (4.46), in equilibrium the distribution function depends only on the carrier energy, and the dependence on the quasi-momentum is only introduced through the dispersion law $\epsilon(\mathbf{k})$.

4.3.3 Total Scattering Rate

The fact that the dependence on the quasi-momentum enters (4.46) only through the dispersion law allows one to significantly simplify (4.13) using the Fermi golden rule [76]:

$$S(\mathbf{k}, \mathbf{k}') = \frac{V}{2\pi^2\hbar} |V_{\mathbf{k}\mathbf{k}'}|^2 \delta[\epsilon(\mathbf{k}') - \epsilon(\mathbf{k}) \pm \Delta\epsilon]. \quad (4.47)$$

Making use of the delta function in the last expression (4.13) can be rewritten in the following manner:

$$\tilde{\lambda}(\mathbf{k}) = [1 - f_{FD}(\epsilon_f)]\lambda(\mathbf{k}) + f_{FD}(\epsilon_f)\lambda^*(\mathbf{k}), \quad (4.48)$$

where ϵ_f denotes the final carrier energy $\epsilon(\mathbf{k}_f)$. The backward scattering rate has been introduced as $S^*(\mathbf{k}, \mathbf{k}') = S(\mathbf{k}', \mathbf{k})$ and the total backward scattering rate as $\lambda^*(\mathbf{k}) = \int S^*(\mathbf{k}, \mathbf{k}') d\mathbf{k}'$. (4.48) represents a linear combination of the forward and backward total scattering rates. In the

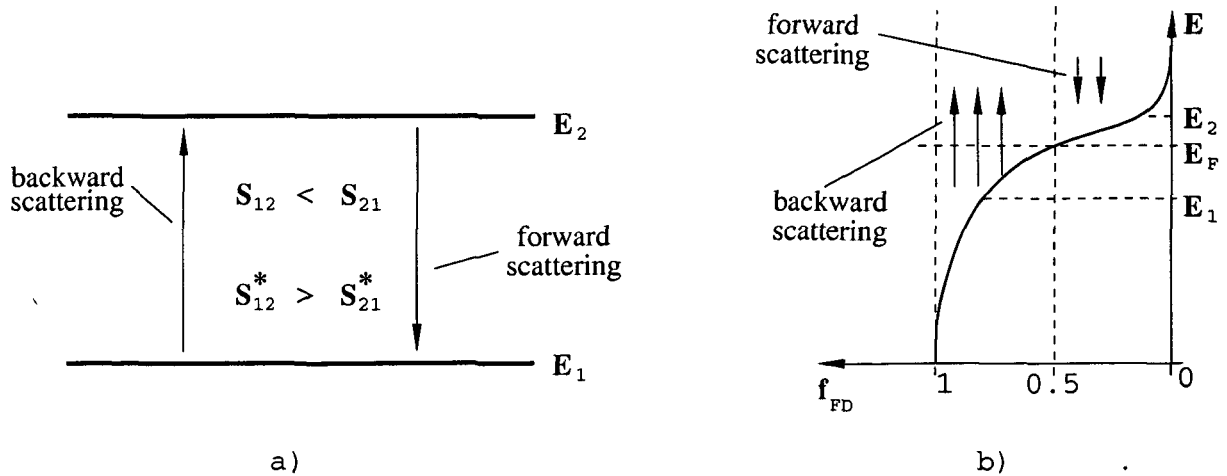


Figure 4.4: Schematic illustration of the scattering processes at high degeneracy.

non-degenerate case, $f_{FD}(\epsilon) \ll 1$, we obtain $\tilde{\lambda}(\mathbf{k}) = \lambda(\mathbf{k})$ which means that scattering processes are mostly determined by the forward-scattering rate and thus the algorithm developed in [73]

for non-degenerate statistics is restored. On the other hand, for highly degenerate semiconductors, $f_{FD}(\epsilon) \sim 1$, scattering processes are dominantly backward $\tilde{\lambda}(\mathbf{k}) = \lambda^*(\mathbf{k})$. In the case of intermediate degeneracy both forward-scattering and backward-scattering contributes to the kinetics.

The fact that backward-scattering is dominant in processes where an initial state of an electron has lower energy than in its final state can formally be explained by the principle of detailed balance, given by the symmetry relation (see also (2.62))

$$S(\mathbf{k}, \mathbf{k}') \cdot \exp\left(\frac{\epsilon(\mathbf{k}')}{k_B T_0}\right) = S^*(\mathbf{k}, \mathbf{k}') \cdot \exp\left(\frac{\epsilon(\mathbf{k})}{k_B T_0}\right). \quad (4.49)$$

As can be seen from (4.49), forward transitions from high to low energy levels are preferred and backward transitions from low to high energy levels prevail.

It should be mentioned that at high degeneracy the backward scattering rate is dominant, and thus the probability of scattering to higher energy levels is larger than to lower energy levels as schematically shown in Fig. 4.4(a). Physically this means that lower energy levels are already occupied by particles, $f_{FD}(\epsilon) \approx 1$ (see Fig. 4.4(b)) and, due to the Pauli exclusion principle, scattering to these energy levels is quantum mechanically forbidden.

4.3.4 Expression for the Initial Distribution

The additional free term in (4.23) cannot be considered an initial distribution because the function $G(\mathbf{k})$ may take on negative values. However, in the case of zero electric field the stationary distribution is known analytically and $G(\mathbf{k})$ can be evaluated explicitly:

$$G(\mathbf{k}) = \frac{q}{k_B T_0} \mathbf{E}_{im} \cdot \mathbf{v} \frac{\exp\left(-\frac{E_f - \epsilon}{k_B T_0}\right)}{\left(\exp\left(-\frac{E_f - \epsilon}{k_B T_0}\right) + 1\right)^2}, \quad (4.50)$$

where \mathbf{v} denotes the group velocity. This expression can be rewritten in the following manner:

$$G(\mathbf{k}) = \frac{q \mathbf{E}_{im} \langle \tilde{\lambda} \rangle}{k_B T_0} \frac{\mathbf{v}(\mathbf{k}) [1 - f_{FD}(\epsilon(\mathbf{k}))]}{\tilde{\lambda}(\mathbf{k})} \left\{ \frac{\tilde{\lambda}(\mathbf{k}) f_{FD}(\epsilon(\mathbf{k}))}{\langle \tilde{\lambda} \rangle} \right\} \quad (4.51)$$

where the term in curly brackets represents the normalized distribution function of the before-scattering states.

The Monte Carlo algorithm contains the same steps as that in [73] except that the whole kinetics is now determined by $\tilde{S}(\mathbf{k}, \mathbf{k}')$ and $\tilde{\lambda}(\mathbf{k})$ instead of $S(\mathbf{k}, \mathbf{k}')$ and $\lambda(\mathbf{k})$.

Another difference from the non-degenerate zero field algorithm is that the weight coefficient $\mathbf{v}(\mathbf{k})/\tilde{\lambda}(\mathbf{k})$ must be multiplied by the factor $[1 - f_{FD}(\epsilon(\mathbf{k}))]$.

With the modifications described above the zero-field algorithm for the time discrete impulse response of a physical quantity $A(\mathbf{k})$ of interest becomes:

1. Follow a main trajectory for one free flight and store the before-scattering state \mathbf{k} .

2. Compute the weight $w = [1 - f_{FD}(\epsilon(\mathbf{k}))]\mathbf{v}(\mathbf{k})/\tilde{\lambda}(\mathbf{k})$.
3. Start a trajectory $\mathbf{K}(t)$ from \mathbf{k} and follow it for time T . At equidistant times t_i add $w\mathbf{A}(\mathbf{K}(t_i))$ to a histogram ν_i .
4. Continue with the first step until N \mathbf{k} -points have been generated.
5. Calculate the time discrete impulse response as $\langle A \rangle_{im}(t_i) = q\mathbf{E}_{im}\langle \tilde{\lambda} \rangle \nu_i / k_B T_0 N$.

This algorithm is also depicted in Fig. 4.5.

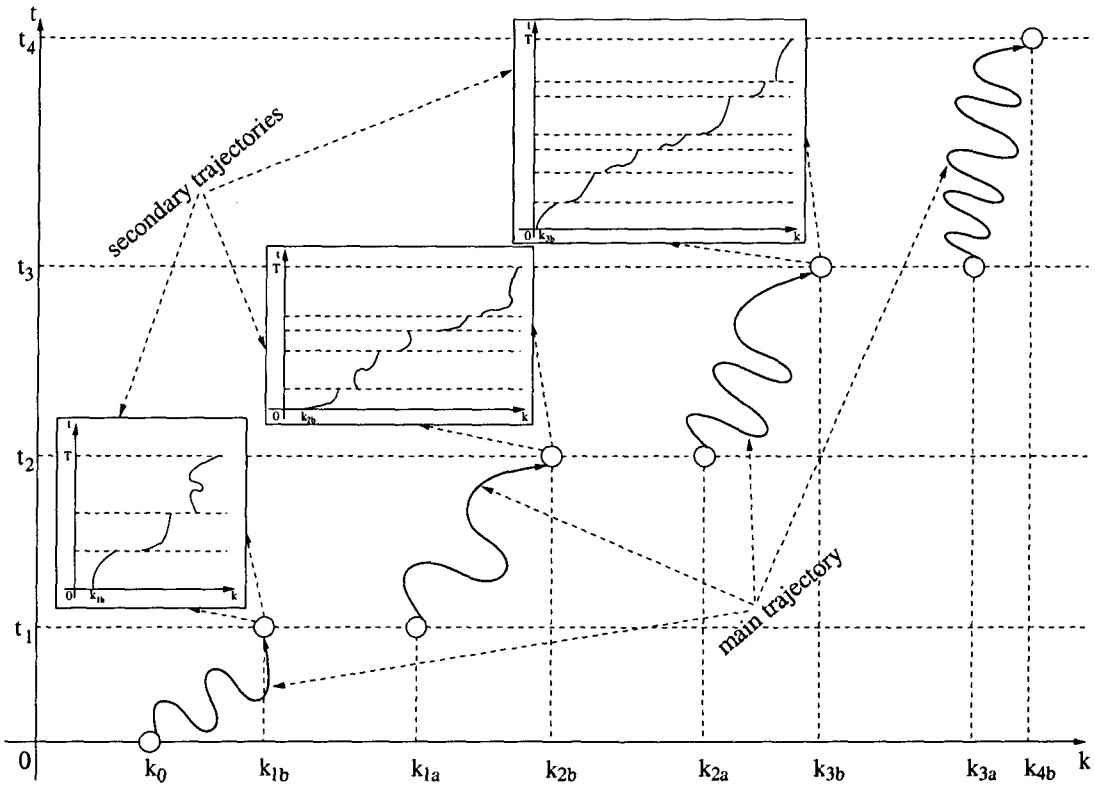


Figure 4.5: Schematic representation of the zero field Monte Carlo algorithm. Here \mathbf{k}_b and \mathbf{k}_a denote before- and after-scattering states, respectively.

4.3.5 Monte Carlo Algorithm for the Mobility Tensor

The response to small signals with a general time dependence can be obtained from the knowledge of the impulse response. The static zero field mobility is given by the long time limit of the differential velocity step response. This is exploited to derive a zero field Monte Carlo algorithm for the mobility tensor from the algorithm presented in the previous section. For a vector-valued physical quantity \mathbf{A} elements of the differential step response tensor are related

to the differential impulse response tensor in the following manner:

$$[K_A^{\text{step}}(t)]_{ij} = \int_0^t [K_A^{\text{imp}}(t')]_{ij} dt', \quad (4.52)$$

where the differential impulse $[K_A^{\text{imp}}(t')]_{ij}$ and step $[K_A^{\text{step}}(t)]_{ij}$ response tensors are defined through the following relations:

$$\begin{aligned} \langle A_i \rangle_{\text{imp}}(t) &= \sum_j [K_A^{\text{imp}}(t)]_{ij} (F_{\text{imp}})_j \\ \langle A_i \rangle_{\text{step}}(t) &= \sum_j [K_A^{\text{step}}(t)]_{ij} (F_1)_j. \end{aligned} \quad (4.53)$$

In order to obtain the zero field mobility tensor it is necessary to integrate the differential velocity impulse response over a secondary trajectory for a sufficiently long time. However, the time integration can be stopped after the first velocity randomizing scattering event has occurred, because in this case the correlation of the trajectory's initial velocity with the after-scattering velocity is lost. Since in the thermodynamic equilibrium the before and after-scattering distributions are equal, the secondary trajectories can be mapped onto the main trajectory. As a result the algorithm schematically depicted in Fig. 4.6 is obtained.

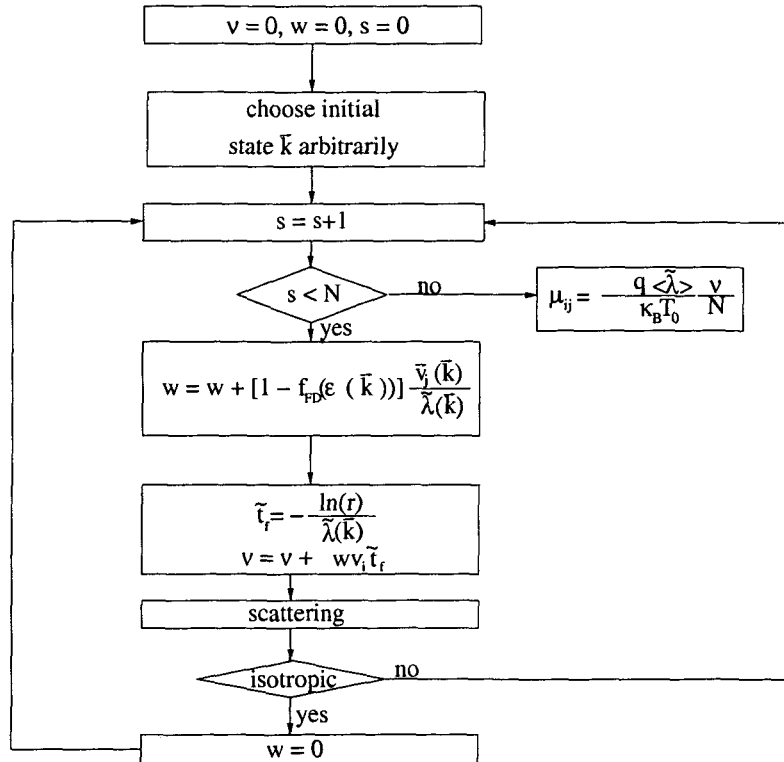


Figure 4.6: Zero field Monte Carlo flow chart.

1. Set $\nu = 0$, $w = 0$.
2. Select initial state \mathbf{k} arbitrarily.
3. Compute a sum of weights: $w = w + [1 - f_{\text{FD}}(\epsilon(\mathbf{k}))][v_j(\mathbf{k})/\tilde{\lambda}(\mathbf{k})]$.
4. Select a free-flight time $\tilde{t}_f = -\ln(r)/\tilde{\lambda}(\mathbf{k})$ and add time integral to estimator: $\nu = \nu + wv_i\tilde{t}_f$ or use the expected value of the time integral: $\nu = \nu + w[v_i/\tilde{\lambda}(\mathbf{k})]$.
5. Perform scattering. If mechanism was isotropic, reset weight: $w = 0$.
6. Continue with step 3 until N \mathbf{k} -points have been generated.
7. Calculate component of zero field mobility tensor as $\mu_{ij} = q\langle\tilde{\lambda}\rangle\nu/(k_B T_0 N)$.

Especially the diagonal elements can be calculated very efficiently using this algorithm. Consider a system where only isotropic scattering events take place. Then the product wv_i is always positive, independent of the sign of v_i . Therefore, only positive values are added to the estimator, which leads to a low variance.

4.4 The High Field Small Signal Monte Carlo Algorithm

To investigate the small signal response of the carriers in semiconductors different Monte Carlo techniques are widely applied to solve the time-dependent Boltzmann equation [73, 74, 77–79]. There are also small signal approaches based on the velocity and energy balance equations [80, 81]. However, a significant advantage of Monte Carlo methods based on the Boltzmann kinetic equation is that they allow a comprehensive treatment of kinetic phenomena within the quasi-classical approach and to account for accurate band structures. Additionally, the quantum mechanical Pauli exclusion principle can be taken into consideration to study the small signal response of carriers in degenerate semiconductors.

When the carrier density is very high the Pauli exclusion principle becomes important and may have a strong influence on various differential response functions which relate a small perturbation of the electric field and a mean value of some physical quantity. The influence is expected to be strong and it has been pointed out [74] that the behavior of impulse response functions is determined by the overlap of the distributions of two carrier ensembles introduced in the formalism. This overlap is much stronger when the Pauli exclusion principle is included due to the additional statistical broadening. When degenerate statistics is taken into account, the Boltzmann equation is nonlinear which makes its solution more difficult. One of the possible solution methods is based on a Legendre polynomial expansion [65]. In this work however, the Monte Carlo method is employed.

In this section the approach presented in [74] is extended and a Monte Carlo algorithm for small signal analysis of degenerate electron gases in homogeneous bulk semiconductors is constructed.

4.4.1 Solution of the Zeroth Order Equation

To solve the nonlinear Boltzmann equation including the Pauli exclusion principle Monte Carlo algorithms based on a rejection technique have been developed by Bosi and Jacoboni [82] and

later by Lugli and Ferry [83]. The first algorithm is adopted in this work to solve the zeroth order equation. In what follows it is shown that this algorithm can also be used to generate the initial distributions G^+ and G^- of the two carrier ensembles which appear when solving the first order equation. The normalization of the stationary distribution required for the correct rejection is presented.

4.4.1.1 Initial Distributions of the Two Ensembles

Using the same method as suggested in [74] the free term in (4.23) is split into two positive functions G^+ and G^- which are related to G through the relation: $G = G^+ - G^-$. These two positive functions are considered as initial distributions of two carrier ensembles which contain the same numbers of particles. This follows from the following equality:

$$\int G(\mathbf{k}) d\mathbf{k} = 0. \quad (4.54)$$

To find the initial distributions for the case of a longitudinal perturbation the zeroth order equation (4.9) is used. This equation gives together with (4.12):

$$G(\mathbf{k}) = \frac{E_{im}}{E_s} \cdot \left(\lambda(\mathbf{k}) f_s(\mathbf{k}) - \int f_s(\mathbf{k}') \tilde{S}(\mathbf{k}', \mathbf{k}) d\mathbf{k}' \right), \quad (4.55)$$

where $\lambda(\mathbf{k}) = \int S(\mathbf{k}, \mathbf{k}') d\mathbf{k}'$. The last expression provides a splitting of G into two positive functions. From the balance condition stated by the zeroth order equation (4.9) it follows $\langle \tilde{\lambda} \rangle_s = \langle \lambda \rangle_s$, where the stationary statistical average is defined as $\langle \cdots \rangle_s = \int f_s(\mathbf{k}) \cdots d\mathbf{k}$. Then the initial distributions can be written as:

$$\begin{aligned} G^+ &= \frac{E_{im}}{E_s} \langle \tilde{\lambda} \rangle_s \left\{ \frac{\lambda(\mathbf{k}) f_s(\mathbf{k})}{\langle \lambda \rangle_s} \right\}, \\ G^- &= \frac{E_{im}}{E_s} \langle \tilde{\lambda} \rangle_s \int \left\{ \frac{\tilde{\lambda}(\mathbf{k}) f_s(\mathbf{k})}{\langle \tilde{\lambda} \rangle_s} \right\} \left\{ \frac{\tilde{S}(\mathbf{k}, \mathbf{k}')}{\tilde{\lambda}(\mathbf{k})} \right\} d\mathbf{k}. \end{aligned} \quad (4.56)$$

In (4.56), G^+ represents the normalized before-scattering distribution function for a particle trajectory whose free-flight times are determined by the conventional scattering rate $\lambda(\mathbf{k})$, while G^- gives the normalized after-scattering distribution function for a particle trajectory constructed using $\tilde{S}(\mathbf{k}, \mathbf{k}')$ and $\tilde{\lambda}(\mathbf{k})$, respectively.

4.4.1.2 Normalization of the Stationary Distribution Function

The stationary distribution function $f_s(\mathbf{k})$ must be normalized as a probability, $0 < f_s(\mathbf{k}) < 1$ to guarantee the correct rejection of scattering events. The \mathbf{k} space is divided into sub-domains Ω of size $V_\Omega = (\Delta k)^3$. In the following \bar{f}_Ω stands for the average distribution function in Ω for a given valley and n is the contribution to the electron density from the same valley. In each sub-domain the electron density is

$$n_\Omega = \frac{1}{4\pi^3} \int_\Omega f_s(\mathbf{k}) d\mathbf{k}. \quad (4.57)$$

and the average distribution function is given as:

$$\bar{f}_\Omega = \frac{\int_\Omega f_s(\mathbf{k}) d\mathbf{k}}{V_\Omega} = \frac{4\pi^3 n_\Omega}{V_\Omega}. \quad (4.58)$$

Using the before-scattering estimation for the statistical average

$$\langle\langle A \rangle\rangle = C \frac{1}{N} \sum_b \frac{A(\mathbf{k}_b)}{\lambda(\mathbf{k}_b)}, \quad (4.59)$$

where N is the number of electron free-flights and the normalization constant C is given as

$$C = \frac{4\pi^3 N \cdot n}{\sum_b \frac{1}{\lambda(\mathbf{k}_b)}}, \quad (4.60)$$

one obtains for n_Ω :

$$n_\Omega = \frac{1}{4\pi^3} \int \Theta_\Omega(\mathbf{k}) f_s(\mathbf{k}) d\mathbf{k} = \frac{\langle\langle \Theta_\Omega \rangle\rangle}{4\pi^3} = n \cdot \frac{\sum_b \Theta_\Omega(\mathbf{k}_b)/\lambda(\mathbf{k}_b)}{\sum_b 1/\lambda(\mathbf{k}_b)}, \quad (4.61)$$

where the indicator function $\Theta_\Omega(\mathbf{k})$ of sub-domain Ω has been introduced. Substituting (4.61) into (4.58) the average distribution function is finally obtained:

$$\bar{f}_\Omega = \frac{4\pi^3 n}{V_\Omega} \cdot \frac{\sum_b \Theta_\Omega(\mathbf{k}_b)/\lambda(\mathbf{k}_b)}{\sum_b 1/\lambda(\mathbf{k}_b)}. \quad (4.62)$$

4.4.1.3 Integral Form of the Nonlinear Boltzmann Equation

To show the generation of the distributions G^+ and G^- the integral representation of the stationary Boltzmann equation (4.9) is used. First, the scattering operator in (4.9) is reformulated as:

$$\begin{aligned} Q[f_s] = & [1 - f_s(\mathbf{k})] \int f_s(\mathbf{k}') S(\mathbf{k}', \mathbf{k}) d\mathbf{k}' + \int f_s(\mathbf{k}') \alpha(\mathbf{k}') \lambda(\mathbf{k}') \delta(\mathbf{k} - \mathbf{k}') d\mathbf{k}' - \\ & - f_s(\mathbf{k}) \left\{ \int [1 - f_s(\mathbf{k}')] S(\mathbf{k}, \mathbf{k}') d\mathbf{k}' + \alpha(\mathbf{k}) \lambda(\mathbf{k}) \right\}, \end{aligned} \quad (4.63)$$

where the self-scattering rate $\alpha(\mathbf{k})$ has been introduced. Note that the delta function guarantees that the self-scattering does not change an electron state. Free-flight times are generated using the total scattering rate $\lambda(\mathbf{k})$. Thus the self-scattering rate has to satisfy the equality

$$\lambda(\mathbf{k}) = \int [1 - f_s(\mathbf{k}')] S(\mathbf{k}, \mathbf{k}') d\mathbf{k}' + \alpha(\mathbf{k}) \lambda(\mathbf{k}). \quad (4.64)$$

This gives for the self-scattering rate the following expression:

$$\alpha(\mathbf{k}) = \frac{1}{\lambda(\mathbf{k})} \int f_s(\mathbf{k}') S(\mathbf{k}, \mathbf{k}') d\mathbf{k}'. \quad (4.65)$$

Further, an additional differential scattering rate $\hat{S}(\mathbf{k}, \mathbf{k}')$ is introduced

$$\hat{S}(\mathbf{k}, \mathbf{k}') = [1 - f_s(\mathbf{k}')] S(\mathbf{k}, \mathbf{k}') + \alpha(\mathbf{k}) \lambda(\mathbf{k}) \delta(\mathbf{k} - \mathbf{k}'), \quad (4.66)$$

$$\int \frac{\widehat{S}(\mathbf{k}, \mathbf{k}')}{\lambda(\mathbf{k})} d\mathbf{k}' = 1. \quad (4.67)$$

Now taking into account (4.64) and (4.66) the scattering operator (4.63) takes the conventional form:

$$Q[f_s] = \int f_s(\mathbf{k}') \widehat{S}(\mathbf{k}', \mathbf{k}) d\mathbf{k}' - f_s(\mathbf{k}) \lambda(\mathbf{k}). \quad (4.68)$$

Using the Neumann series of the forward equation the second iteration term (4.45) is derived as an example:

$$\begin{aligned} f_{\Omega}^{(2)} = & \int_0^{\infty} dt_2 \int_{t_2}^{\infty} dt_1 \int_{t_1}^{\infty} dt_0 \int d\mathbf{k}_2^a \int d\mathbf{k}_1^a \int d\mathbf{k}_i \cdot \{f_0(\mathbf{k}_i)\} \times \\ & \times \left\{ \exp\left(-\int_0^{t_2} \lambda[\mathbf{K}_2(y)] dy\right) \lambda(\mathbf{K}_2(t_2)) \frac{\widehat{S}(\mathbf{K}_2(t_2), \mathbf{k}_2^a)}{\lambda(\mathbf{K}_2(t_2))} \right\} \times \\ & \times \left\{ \exp\left(-\int_{t_2}^{t_1} \lambda[\mathbf{K}_1(y)] dy\right) \lambda(\mathbf{K}_1(t_1)) \frac{\widehat{S}(\mathbf{K}_1(t_1), \mathbf{k}_1^a)}{\lambda(\mathbf{K}_1(t_1))} \right\} \times \\ & \times \left\{ \exp\left(-\int_{t_1}^{t_0} \lambda[\mathbf{K}(y)] dy\right) \lambda(\mathbf{K}(t_0)) \right\} \Theta(t - t_1) \Theta_{\Omega}(\mathbf{K}(t)) \Theta(t_0 - t). \end{aligned} \quad (4.69)$$

Here $\Theta(t)$ is the step function and $f_{\Omega}^{(2)} = \int f^{(2)}(\mathbf{k}, t) \Theta_{\Omega}(\mathbf{k}) d\mathbf{k}$. From (4.69) it is seen that if the free-flight time is calculated from the exponential distribution according to the scattering rate $\lambda(\mathbf{k})$, the conditional probability density for an after-scattering state \mathbf{k}' from the initial state \mathbf{k} is equal to $\widehat{S}(\mathbf{k}, \mathbf{k}')/\lambda(\mathbf{k})$.

Within the algorithm presented in [82] the before-scattering distribution function is equal to $\lambda(\mathbf{k}) f_s(\mathbf{k}) / \langle \lambda \rangle_s$ which gives the distribution G^+ . In order to find the distribution function of the after-scattering states the before-scattering distribution function should be multiplied by the conditional probability density for an after-scattering state and this product is integrated over all before-scattering states. Using (4.66) and (4.65) one obtains for the after-scattering distribution:

$$\begin{aligned} & \int \left\{ \frac{\lambda(\mathbf{k}) f_s(\mathbf{k})}{\langle \lambda \rangle_s} \right\} \left\{ \frac{\widehat{S}(\mathbf{k}, \mathbf{k}')}{\lambda(\mathbf{k})} \right\} d\mathbf{k} = \int \left\{ \frac{\lambda(\mathbf{k}) f_s(\mathbf{k})}{\langle \lambda \rangle_s} \right\} \frac{[1 - f_s(\mathbf{k}')] S(\mathbf{k}, \mathbf{k}')}{\lambda(\mathbf{k})} d\mathbf{k} + \\ & + \frac{\lambda(\mathbf{k}') f_s(\mathbf{k}')}{\langle \lambda \rangle_s} \alpha(\mathbf{k}') = \int \left\{ \frac{\lambda(\mathbf{k}) f_s(\mathbf{k})}{\langle \lambda \rangle_s} \right\} \frac{[1 - f_s(\mathbf{k}')] S(\mathbf{k}, \mathbf{k}')}{\lambda(\mathbf{k})} d\mathbf{k} + \\ & + \int \left\{ \frac{\lambda(\mathbf{k}) f_s(\mathbf{k})}{\langle \lambda \rangle_s} \right\} \frac{f_s(\mathbf{k}') S(\mathbf{k}', \mathbf{k})}{\lambda(\mathbf{k})} d\mathbf{k} = \\ & = \int \left\{ \frac{\widetilde{\lambda}(\mathbf{k}) f_s(\mathbf{k})}{\langle \widetilde{\lambda} \rangle_s} \right\} \left\{ \frac{\widetilde{S}(\mathbf{k}, \mathbf{k}')}{\widetilde{\lambda}(\mathbf{k})} \right\} d\mathbf{k} = \frac{E_s}{E_{im} \langle \widetilde{\lambda} \rangle_s} G^-(\mathbf{k}'). \end{aligned} \quad (4.70)$$

Note that the after-scattering distribution is normalized to unity. Now it is obvious that the initial distributions G^+ and G^- can be generated by introduction the main trajectory which

is constructed using the algorithm from [82] to solve (4.9). Then for each main iteration two carrier ensembles with initial distributions G^+ and G^- evolve in time according to (4.10) for the secondary trajectories.

4.4.2 Solution of the First Order Equation

(4.10) contains terms which depend on the stationary distribution function $f_s(\mathbf{k})$. These are the free term and the scattering term. The stationary distribution function is the solution of (4.9). This fact prevents an analytical solution for $\tilde{\lambda}$, and a numerical integration is necessary. However, in this work a rejection technique is applied to solve (4.10). In Section 4.2.1 a new differential scattering rate \tilde{S} has been introduced (see (4.12)). Here another differential scattering rate is defined according to the following expression:

$$\tilde{S}_0(\mathbf{k}', \mathbf{k}) = S(\mathbf{k}', \mathbf{k}) + S(\mathbf{k}, \mathbf{k}'). \quad (4.71)$$

The corresponding total scattering rate is

$$\tilde{\lambda}_0(\mathbf{k}) = \lambda(\mathbf{k}) + \lambda^*(\mathbf{k}), \quad (4.72)$$

where λ^* stands for the total backward-scattering rate

$$\begin{aligned} S^*(\mathbf{k}, \mathbf{k}') &= S(\mathbf{k}', \mathbf{k}), \\ \lambda^*(\mathbf{k}) &= \int S^*(\mathbf{k}, \mathbf{k}') d\mathbf{k}'. \end{aligned} \quad (4.73)$$

From (4.12) and (4.71) it follows that

$$\tilde{S}_0(\mathbf{k}', \mathbf{k}) \geq \tilde{S}(\mathbf{k}', \mathbf{k}). \quad (4.74)$$

To solve (4.10) a wave vector \mathbf{k} is generated using the differential scattering rate $S_0(\mathbf{k}', \mathbf{k})$. The condition of acceptance takes the following form

$$r\tilde{S}_0(\mathbf{k}', \mathbf{k}) < \tilde{S}(\mathbf{k}', \mathbf{k}), \quad (4.75)$$

where r is a random number evenly distributed between 0 and 1. The last inequality may be rewritten as follows:

$$r[S(\mathbf{k}', \mathbf{k}) + S(\mathbf{k}, \mathbf{k}')] < (1 - f_s(\mathbf{k}))S(\mathbf{k}', \mathbf{k}) + f_s(\mathbf{k})S(\mathbf{k}, \mathbf{k}'). \quad (4.76)$$

When the scattering process can be split into the sum of the emission and absorption of some quasi-particles such as phonons and plasmons, this condition can be rewritten. Considering a forward transition from \mathbf{k}' to \mathbf{k} it can be easily shown that one of the following rejection conditions has to be checked depending on whether an absorption or emission process has occurred. For absorption processes it takes the form:

$$r[1 + \frac{N_{eq}}{N_{eq} + 1}] < [1 - f_s(\mathbf{k})]\frac{N_{eq}}{N_{eq} + 1} + f_s(\mathbf{k}), \quad (4.77)$$

whereas for emission processes the following condition is checked

$$r[1 + \frac{N_{eq}}{N_{eq} + 1}] < 1 - f_s(\mathbf{k}) + f_s(\mathbf{k})\frac{N_{eq}}{N_{eq} + 1}, \quad (4.78)$$

where N_{eq} denotes the equilibrium number of quasi-particles. For example, when $N_{eq}/(N_{eq} + 1) \ll 1$ it follows from (4.77) and (4.78) that for the non-degenerate case, $f_s \ll 1$, emission processes will be dominantly accepted while absorption processes will be mostly rejected. This means that the kinetic behavior is determined by emission processes. On the other side for the degenerate case, when $f_s \sim 1$, it follows from the same relations that emission processes will be mostly rejected while the probability of the acceptance of absorption processes increases. Finally, it should be noted that for elastic processes, $S(\mathbf{k}, \mathbf{k}') = S(\mathbf{k}', \mathbf{k})$, the rejection condition (4.76) takes the following form:

$$r < \frac{1}{2} \quad (4.79)$$

This means that one half of the elastic scattering events will not be accepted in the rejection scheme given above.

4.4.3 Monte Carlo Algorithm for the Impulse Response

Using (4.56) and the combined rejection technique developed for the secondary trajectories based on the inequalities (4.77) to (4.79), the new small-signal Monte Carlo algorithm including the Pauli exclusion principle can be formulated as follows:

1. Simulate the nonlinear Boltzmann equation until f_s has converged.
2. Follow a main trajectory for one free flight. Store the before-scattering state in \mathbf{k}_b , and realize a scattering event from \mathbf{k}_b to \mathbf{k}_a .
3. Start a trajectory $\mathbf{K}^+(t)$ from \mathbf{k}_b and another trajectory $\mathbf{K}^-(t)$ from \mathbf{k}_a .
4. Follow both trajectories for time T using the rejection scheme based on the acceptance conditions (4.77) to (4.79). At equidistant times t_i add $A(\mathbf{K}^+(t_i))$ to a histogram α_i^+ and $A(\mathbf{K}^-(t_i))$ to a histogram α_i^- .
5. Continue with the second step until N \mathbf{k} -points have been generated.
6. Calculate the time discrete impulse response as $\langle A \rangle_{im}(t_i) = (E_{im}(\lambda)/NE_s)(\alpha_i^+ - \alpha_i^-)$.

This algorithm is schematically illustrated in Fig. 4.7 and its flow chart is shown in Fig. 4.8. It should be noted that in a highly degenerate electron gas the main trajectory contains many self-scattering events. As in this case $\mathbf{k}_a = \mathbf{k}_b$, the corresponding two secondary trajectories will give the same contribution, that is $\alpha_i^+ = \alpha_i^-$. This does not change the impulse response. Thus in order to save the computation time it is reasonable not to start trajectories $\mathbf{K}^+(t)$ and $\mathbf{K}^-(t)$ after a self-scattering event has occurred. If a self-scattering event has taken place during the evolution of the main trajectory, the main trajectory is continued until a physical scattering event has happened. Only at this moment the secondary trajectories $\mathbf{K}^+(t)$ and $\mathbf{K}^-(t)$ are started.

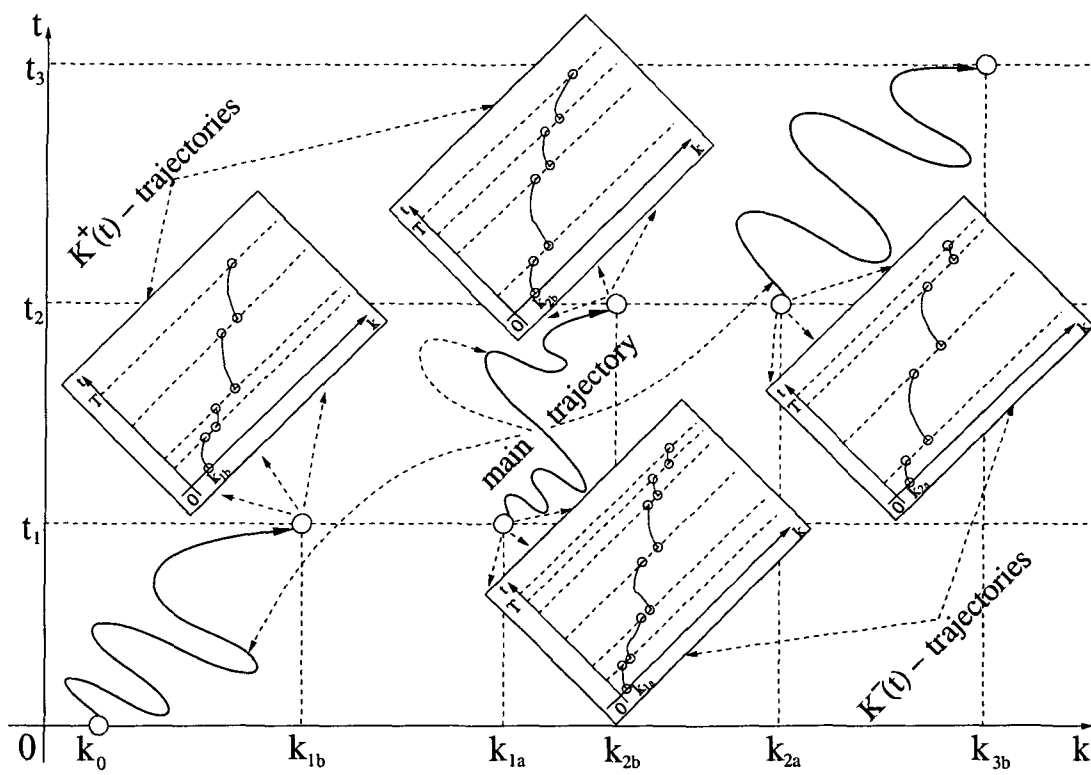


Figure 4.7: Schematic representation of the small-signal algorithm.

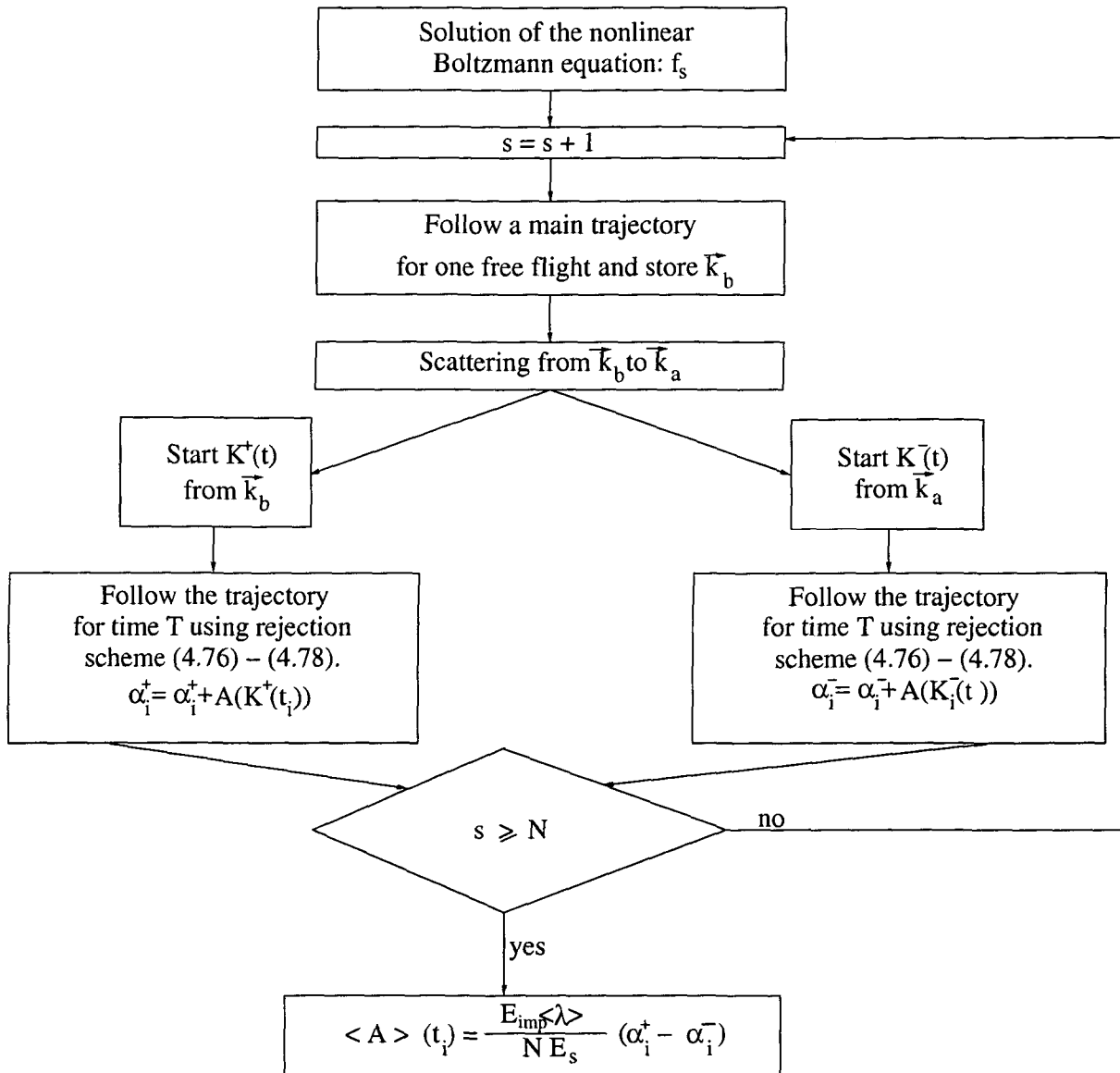


Figure 4.8: Flow chart of the small-signal algorithm.

Chapter 5

Modeling of Strained $\text{Si}_{1-x}\text{Ge}_x$ on $\text{Si}_{1-y}\text{Ge}_y$ Substrates

In this chapter the results of Monte Carlo simulations of electron transport in strained SiGe layers are presented. First the low field electron mobility is investigated as a function of the Ge composition both in the active layer and the substrate for the undoped case. Then strained doped layers are studied. Additionally the influence of the substrate orientation is demonstrated. Finally, a small signal analysis is performed for both non-degenerate and degenerate strained layers. The zero field and small signal Monte Carlo methods developed in the previous chapter are employed to calculate the low field mobility tensor and the small signal response functions at high electric fields, respectively. All results are presented for room temperature.

5.1 Low Field Electron Mobility in Undoped Layers

In undoped layers scattering on ionized impurities and plasmon scattering can be neglected and thus these scattering mechanisms are not included in the scattering operator in this section.

5.1.1 Si layers on $\text{Si}_{1-y}\text{Ge}_y$ substrates

First electron transport in a pure Si strained layer is considered. In this case alloy scattering has no influence.

5.1.1.1 Ge Composition Dependence of Perpendicular and In-plane Components

Fig. 5.1 shows μ_{\perp} , the electron mobility perpendicular to the interface for several substrate orientations, while Fig. 5.2 μ_{\parallel} , the mobility parallel to the interface.

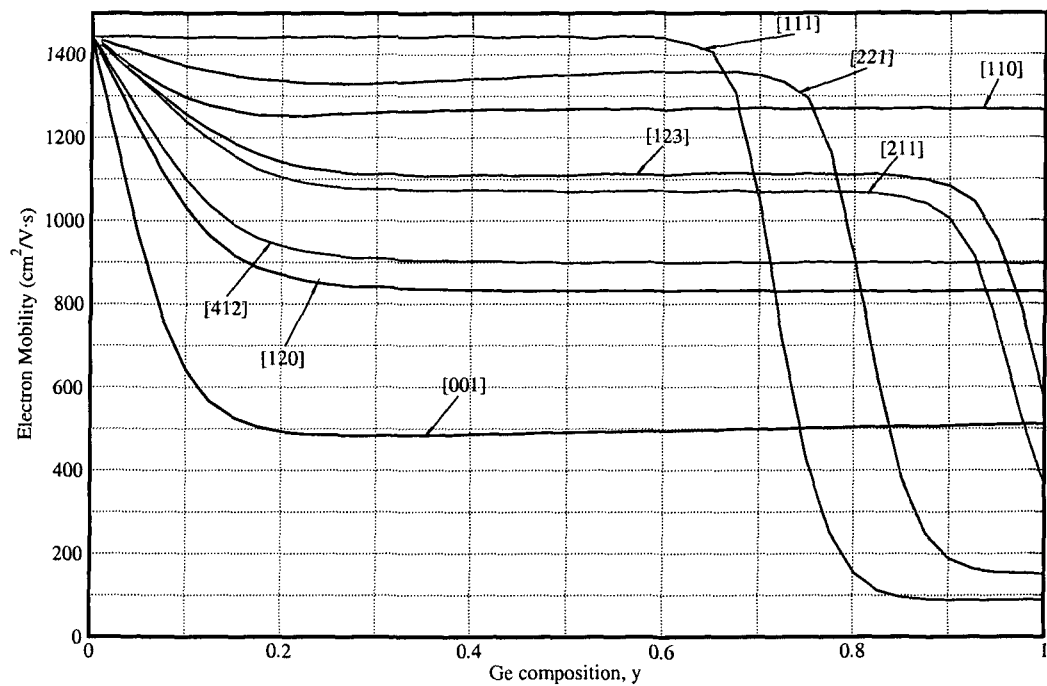


Figure 5.1: The perpendicular component of the low field electron mobility μ_{\perp} .

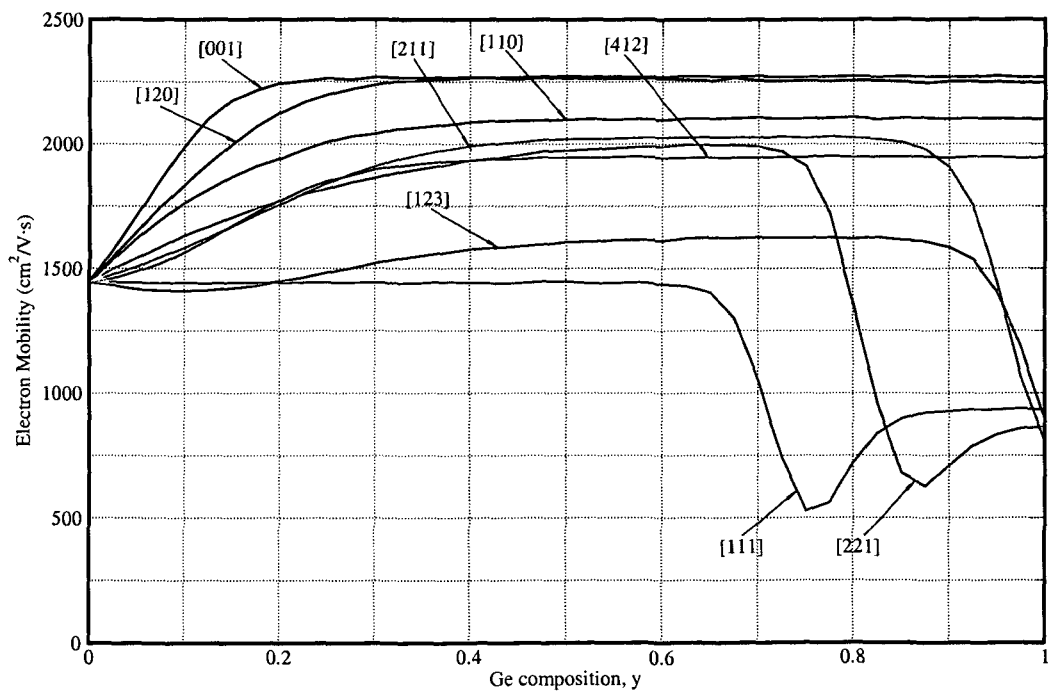


Figure 5.2: The in-plane component of the low field electron mobility μ_{\parallel} .

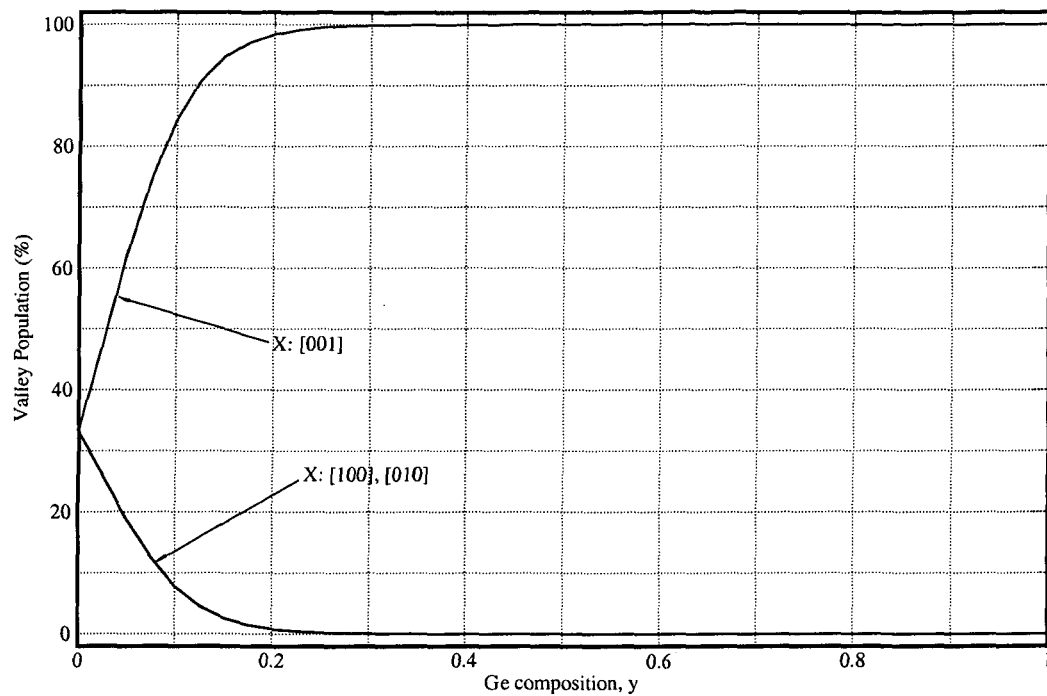


Figure 5.3: The valley population for the substrate orientation [001].

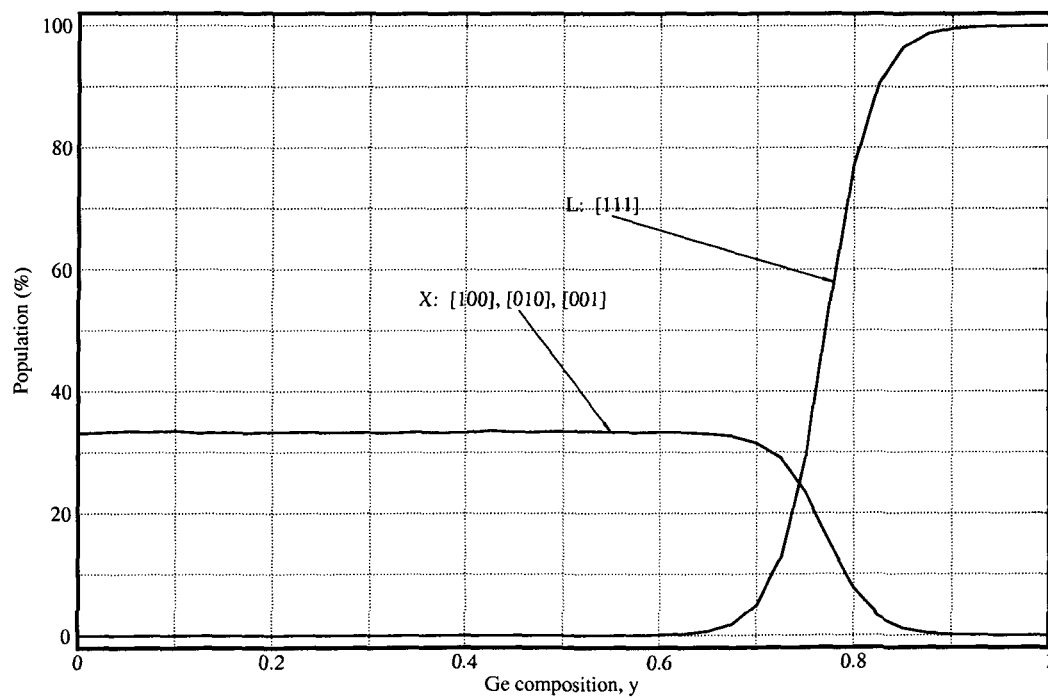


Figure 5.4: The valley population for the substrate orientation [111].

Fig. 5.3 and Fig. 5.4 show the population of the X and L valleys for different orientations. As can be seen from Fig. 5.3, the X valleys with orientations $[100]$ and $[010]$ are not split in accordance with (3.59). The L valleys remain unpopulated in this case as they are much higher than the X valleys. The decrease of μ_{\perp} and increase of μ_{\parallel} is explained by the population of the X valleys with orientation $[001]$ which contribute through m_t^X to the in-plane and m_l^X to the perpendicular transport.

Fig. 5.4 provides an explanation of the mobility components for the substrate orientation $[111]$. The X valleys are not split in accordance with (3.60). When the Ge composition in the substrate increases, the splitting of the L valleys becomes important. The valleys with orientations $[\bar{1}\bar{1}1]$, $[\bar{1}\bar{1}\bar{1}]$ and $[1\bar{1}\bar{1}]$ go up and remain empty while the L valley oriented along $[111]$ goes strongly down as stated by (3.63). This valley is dominant at high Ge mole fractions. Now the in-plane and perpendicular transport is determined by m_t^L and m_l^L , respectively. The increase of μ_{\parallel} at high compositions y is related to the decrease of the $X \rightarrow L$ intervalley transitions. μ_{\perp} does not increase due to the higher value of m_l^L . The range of Ge compositions where the $X \rightarrow L$ transitions are most effective can be seen in Fig. 5.5, showing the band edges versus the substrate composition y .

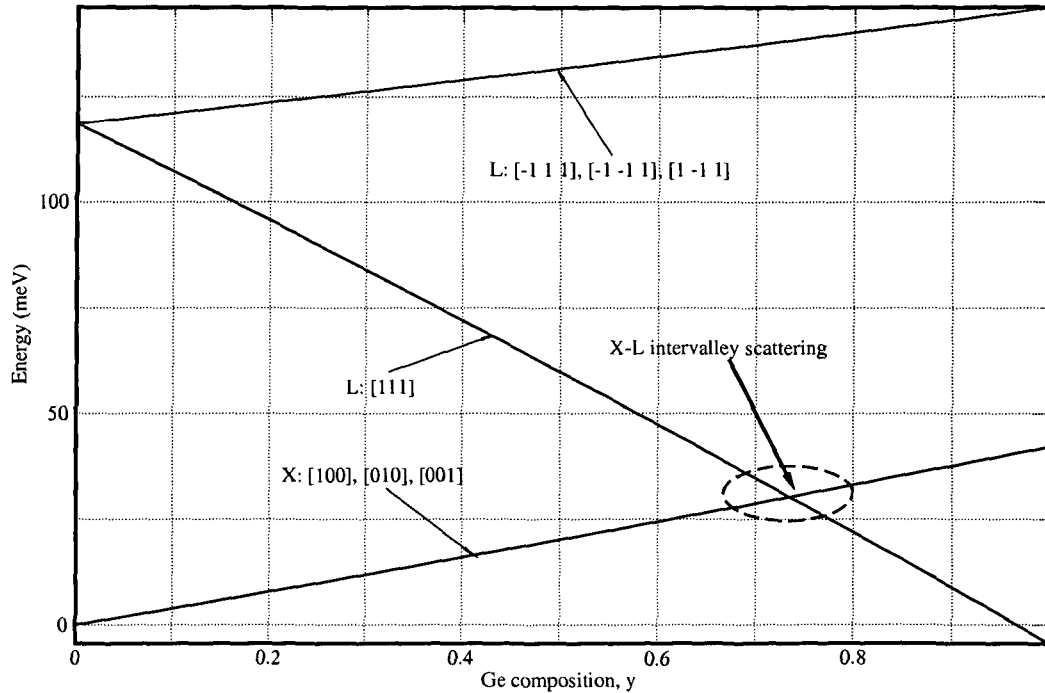


Figure 5.5: The band edges in strained Si grown on the substrate with the orientation $[111]$.

5.1.1.2 Substrate Orientation Dependence

Here the electron mobility as a function of the substrate orientation is presented for two Ge compositions of the substrate. The second Euler angle β is chosen as a parameter while the first one α varies between 0 and $\pi/2$. The third Euler angle is equal to 0 as discussed previously.

Fig. 5.6 illustrates the behavior of the perpendicular component μ_{\perp} of the electron mobility, while Fig. 5.7 shows the same dependence for μ_{\parallel} . The two components μ_{\perp} and μ_{\parallel} for $\beta = 40^\circ$ reach their maximum values at $\alpha = \pi/4$ because at this value of α the population of the X valley with orientation $[001]$ is the highest and due to the orientation the influence of the longitudinal masses m_l^X of the X valleys oriented along $[100]$ and $[010]$ is minimal. However, the influence of the X valleys of these orientations is significant at $\alpha = 0^\circ$ and $\alpha = 90^\circ$ where the two components have their minima.

The analogous results for μ_{\perp} and μ_{\parallel} for a substrate composition of $y = 0.9$ are depicted in Fig. 5.8 and Fig. 5.9. The main difference from the case of $\text{Si}_{0.5}\text{Ge}_{0.5}$ substrate is that here the L valley comes into play which causes an additional intervalley scattering process between X and L valleys.

The repopulation processes are most clearly seen in Fig. 5.10 and Fig. 5.11, which display the populations of different orientations of both the X and L valleys. As can be seen from Fig. 5.10, the X valleys with the orientation $[001]$ are the most populated ones while all the L valleys remain empty. In the case of substrates with higher Ge mole fraction (see Fig. 5.11) the L valley oriented along $[111]$ becomes important.

The next three figures Fig. 5.12, Fig. 5.13, and Fig. 5.14 show the dependence of the in-plane component of the electron mobility μ_{\parallel} on the in-plane angle, that is the third Euler angle γ , in polar coordinates for three substrate orientations. The mobility on these figures is obviously anisotropic. This means that the in-plane transport turns out to be dependent on the orientation of devices grown on the substrate.

Thus in order to reach their optimal characteristics devices, or more specifically, their active strained regions (base, channel, or other parts) can be properly oriented on the surface of the substrate. Where it is necessary this can be used to increase output currents. Additionally, this effect can also be used to reduce leakages by orienting some parts of the device so as to reduce the mobility along the possible leakage directions.

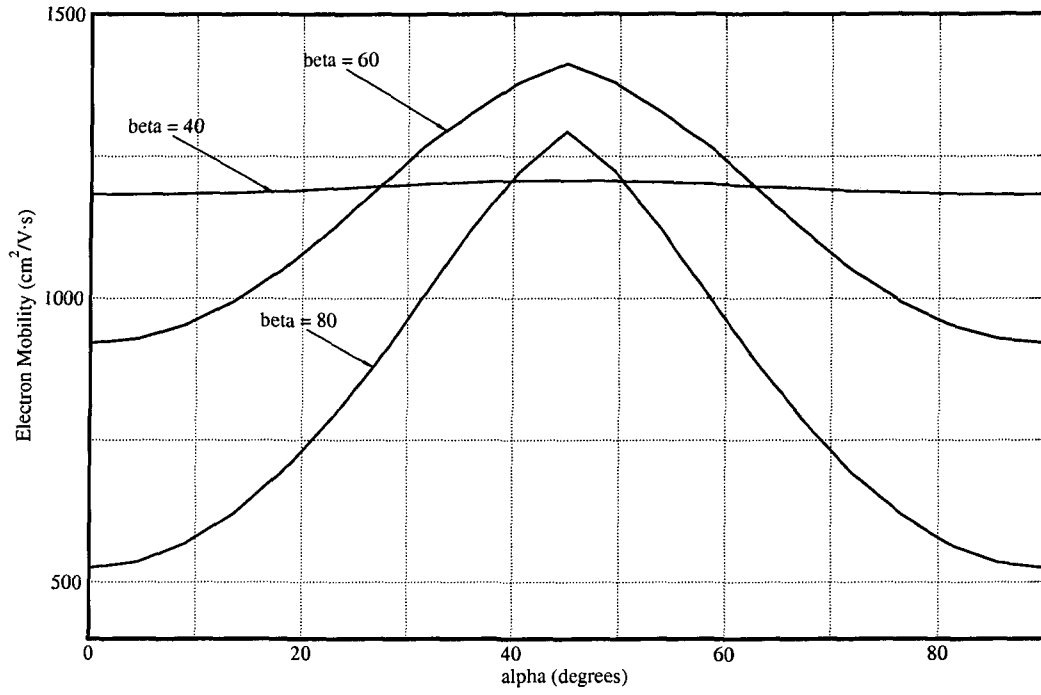


Figure 5.6: μ_{\perp} as a function of α for $\beta = 40^\circ$, 60° , and 80° in $\text{Si}/\text{Si}_{0.5}\text{Ge}_{0.5}$.

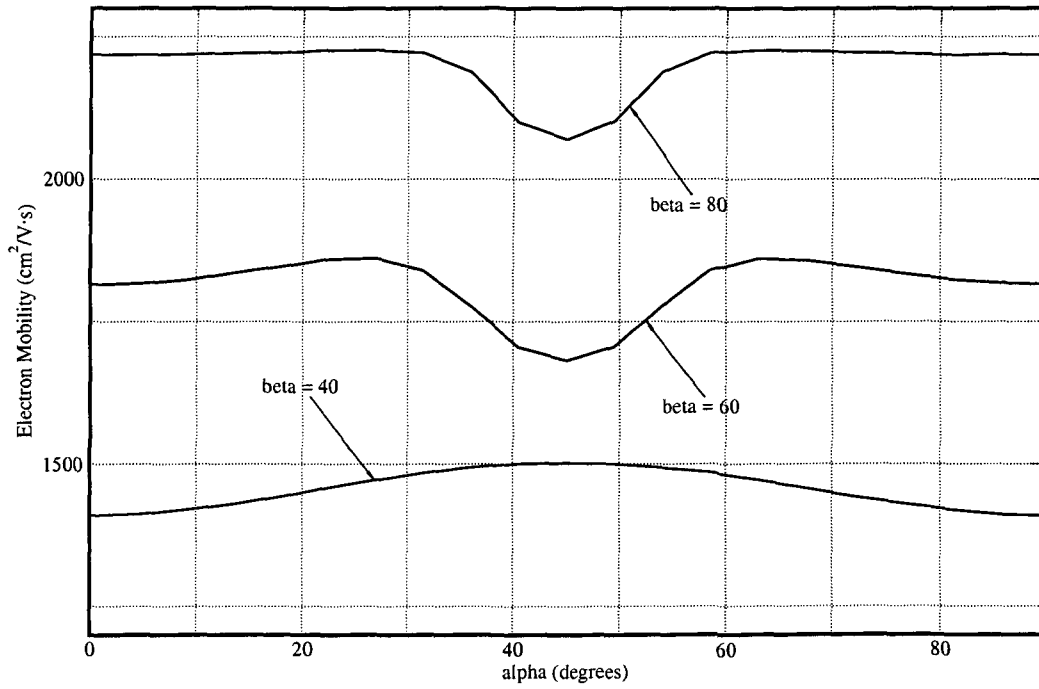


Figure 5.7: μ_{\parallel} as a function of α for $\beta = 40^\circ$, 60° , and 80° in $\text{Si}/\text{Si}_{0.5}\text{Ge}_{0.5}$.

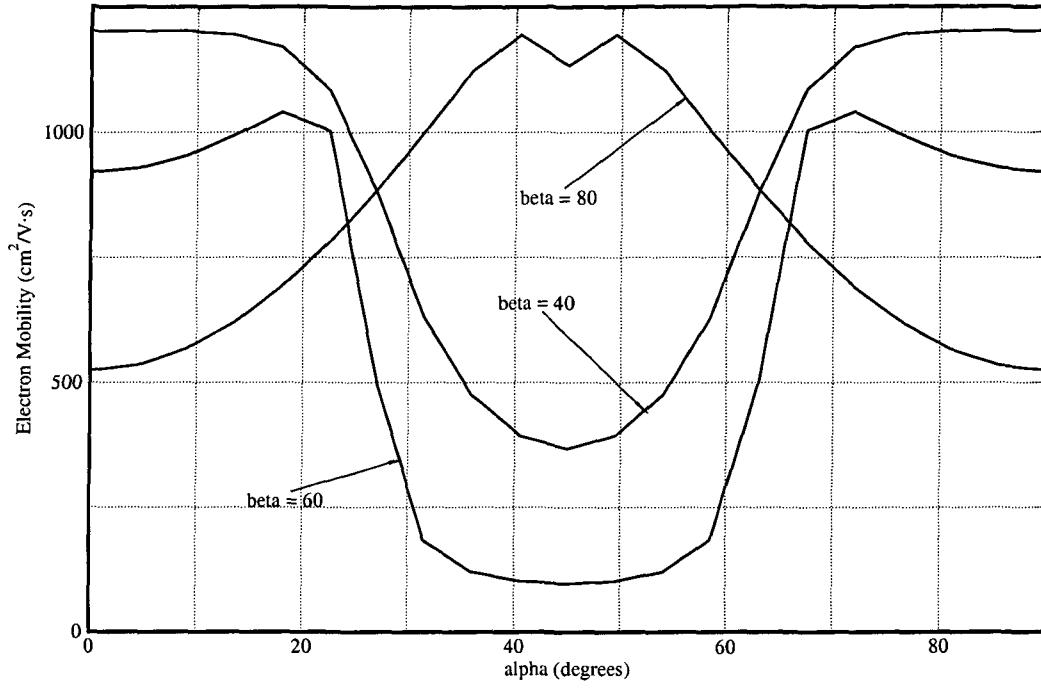


Figure 5.8: μ_{\perp} as a function of α for $\beta = 40^\circ$, 60° , and 80° in $\text{Si}/\text{Si}_{0.1}\text{Ge}_{0.9}$.

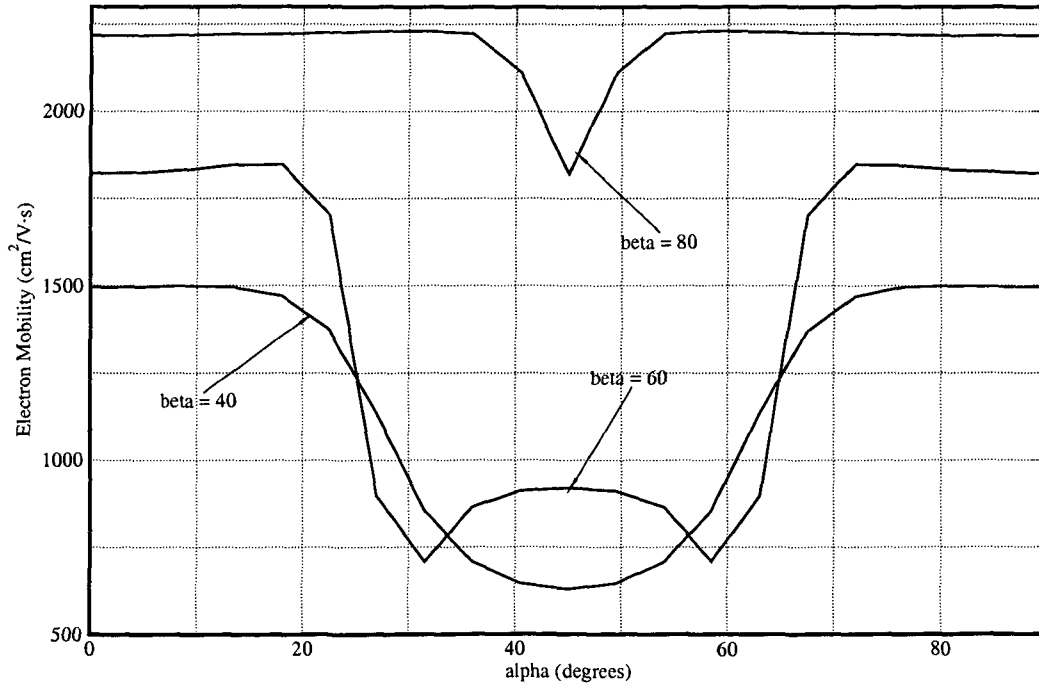


Figure 5.9: μ_{\parallel} as a function of α for $\beta = 40^\circ$, 60° , and 80° in $\text{Si}/\text{Si}_{0.1}\text{Ge}_{0.9}$.

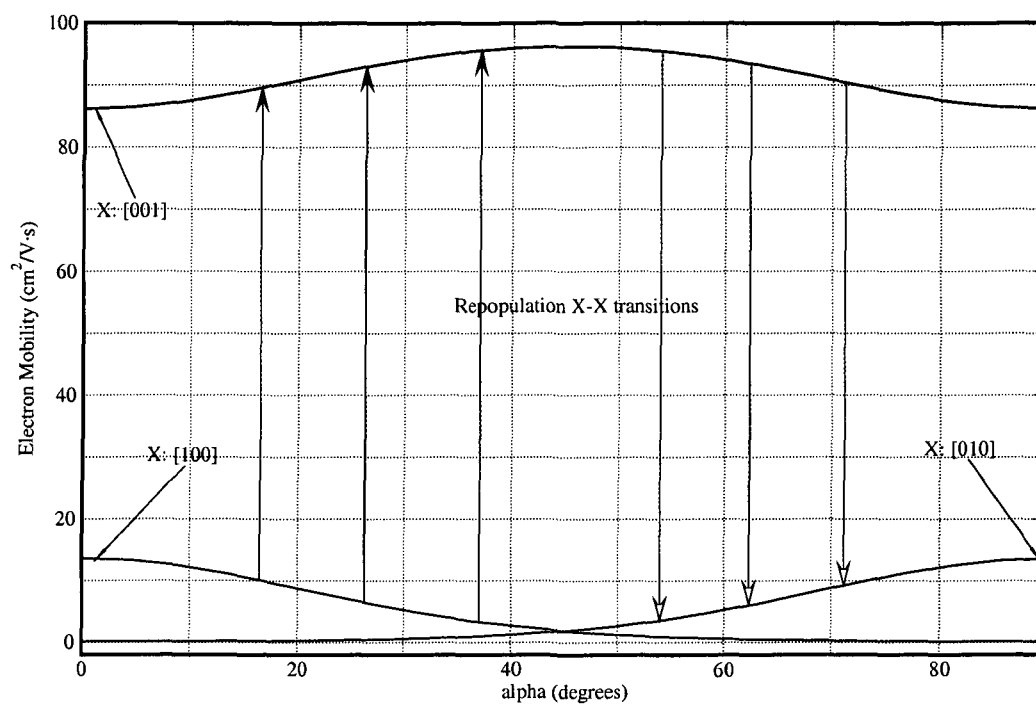


Figure 5.10: The valley populations as functions of α for $\beta = 40^\circ$ in $\text{Si}/\text{Si}_{0.5}\text{Ge}_{0.5}$.

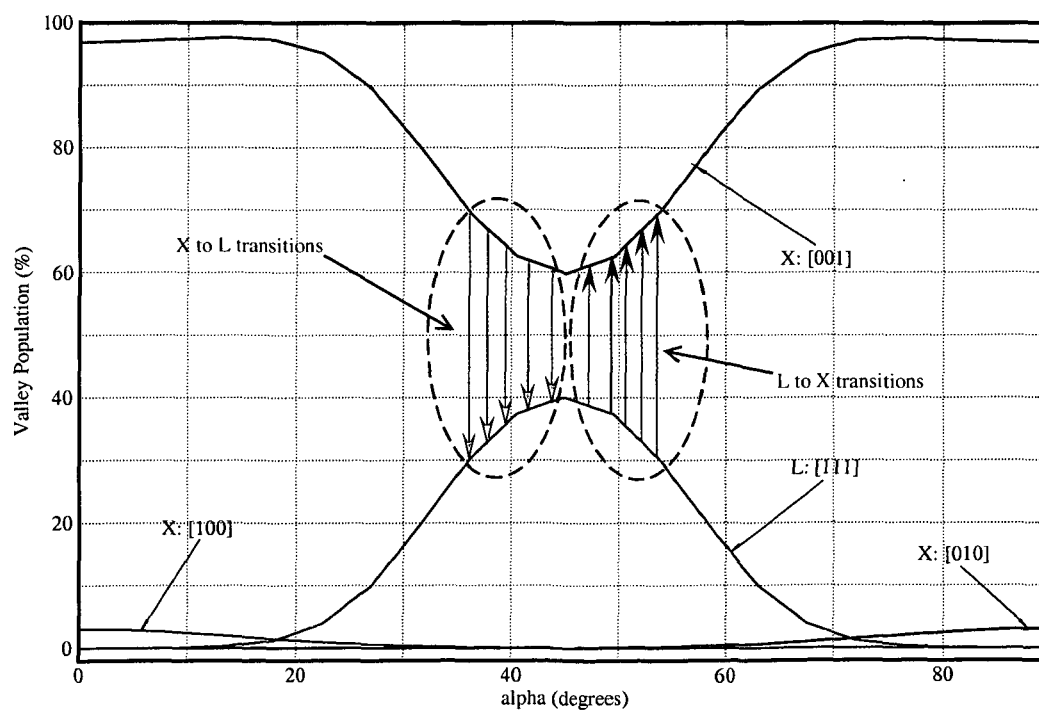


Figure 5.11: The valley populations as functions of α for $\beta = 40^\circ$ in $\text{Si}/\text{Si}_{0.1}\text{Ge}_{0.9}$.

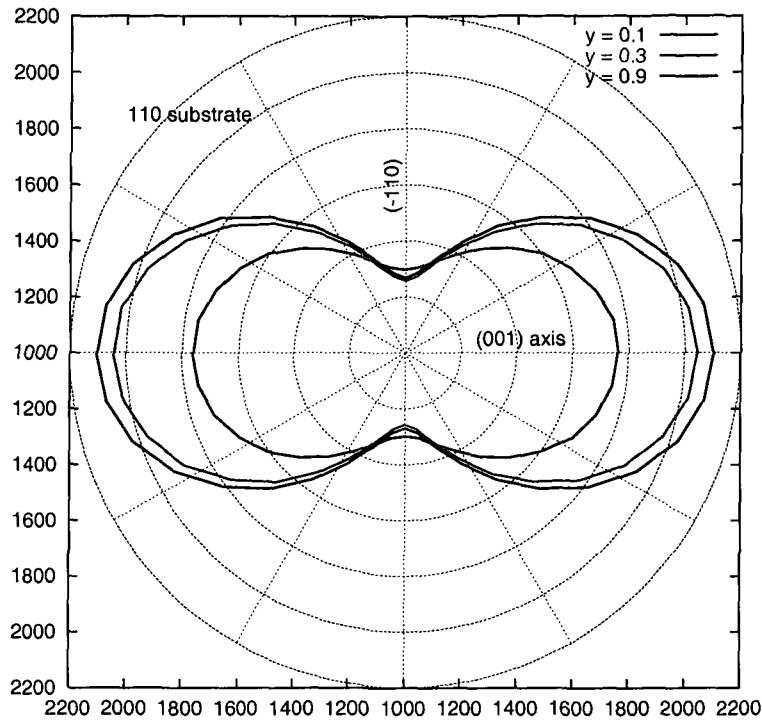


Figure 5.12: The in-plane electron mobility $\mu_{||}$ ($\text{cm}^2/\text{V}\cdot\text{s}$) as a function of γ in Si grown on $[110]$ $\text{Si}_{1-y}\text{Ge}_y$.

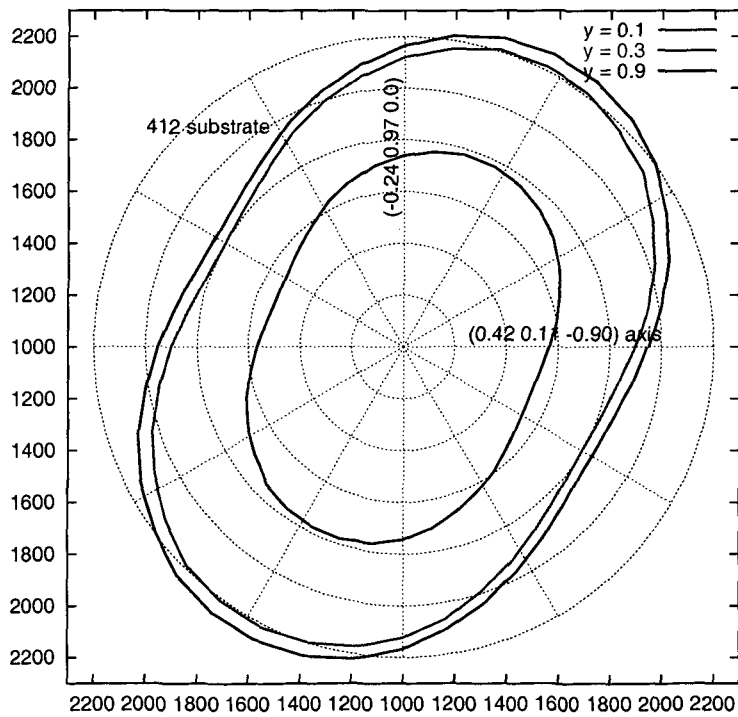


Figure 5.13: The in-plane electron mobility $\mu_{||}$ ($\text{cm}^2/\text{V}\cdot\text{s}$) as a function of γ in Si grown on $[412]$ $\text{Si}_{1-y}\text{Ge}_y$.

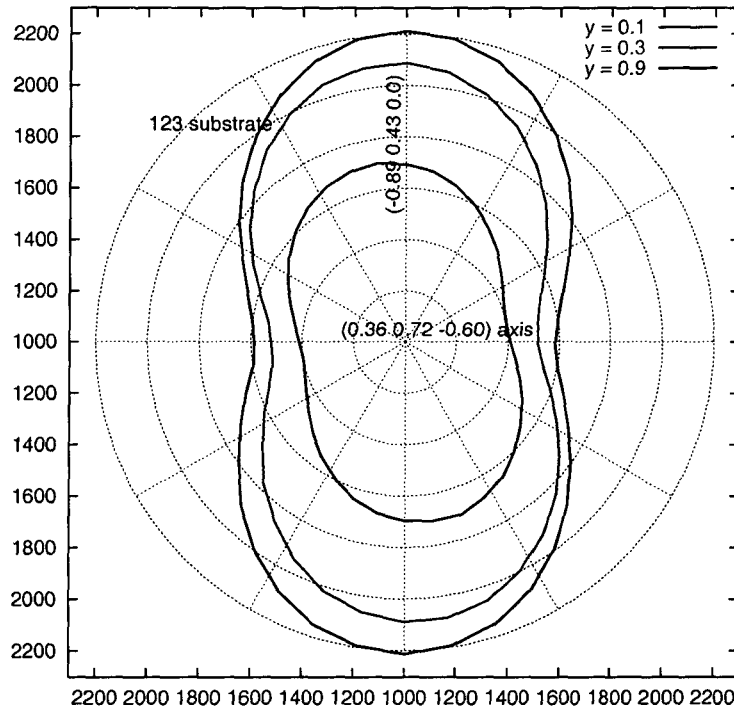


Figure 5.14: The in-plane electron mobility $\mu_{||}$ ($\text{cm}^2/\text{V}\cdot\text{s}$) as a function of γ in Si grown on [123] $\text{Si}_{1-y}\text{Ge}_y$.

5.1.2 $\text{Si}_{1-x}\text{Ge}_x$ layers on $\text{Si}_{1-y}\text{Ge}_y$ substrates

In this subsection the Monte Carlo simulation results for the low field electron mobility in $\text{Si}_{1-x}\text{Ge}_x$ undoped active layers are given. The essential difference in comparison with Si active layers is that in this case alloy scattering strongly influences the transport properties of the active layers. Alloy scattering is described by expression (2.138). As a function of the Ge composition x in the active layer it has a maximum at $x = 0.5$. Therefore it is expected that electron mobility in this case has its minimum at the same point. However, it is shown below that this is not always the case. The reason for this is both the change of the effective masses and various repopulation effects between valleys both of the same and different types. These effects can be strong enough to suppress the decrease of the electron mobility due to alloy scattering.

The results for the perpendicular μ_{\perp} and in-plane μ_{\parallel} components of the electron low field mobility are presented as functions of the layer composition x for several substrates parameterized by their Ge compositions y as well as their orientations in terms of the Miller indices. Again the Miller indices specify only two Euler angles α and β while the third Euler angle γ is kept constant equal to zero.

Fig. 5.15 compares Monte Carlo simulation results and experimental data for a $\text{Si}_{1-x}\text{Ge}_x$ active layer grown on a relaxed Si substrate oriented along [001]. As it is expected the curves have the minima at $x = 0.5$. The electron mobility in the strained case has Si like character over the whole range of Ge mole fractions. In the case of the perpendicular component μ_{\perp} the mobility in the strained layer is higher than that in the unstrained case up to $x = 0.8$. It follows from the fact that the two X valleys along [001] move up and have only little contribution to the mobility. Thus only four in-plane valleys with transverse effective masses determine the mobility. This gives an increase in comparison with unstrained SiGe. At very high Ge mole fractions the mobility in the unstrained case increases rapidly while for the strained SiGe it has lower values. This is related to the increase of biaxial compressive strain which at high x makes the four in-plane valleys move strongly down setting them equal or even lower than the L valleys. In the case of the in-plane component μ_{\parallel} the mobility in the strained layer is lower compared to that in unstrained SiGe. This is explained by the fact that unlike in the relaxed material, where four transverse effective masses determine the electron mobility, only two transverse effective masses are left in strained SiGe which leads to a decrease of the in-plane component.

Fig. 5.16 to Fig. 5.19 display μ_{\perp} and μ_{\parallel} in $\text{Si}_{1-x}\text{Ge}_x$ grown on $\text{Si}_{0.7}\text{Ge}_{0.3}$ and $\text{Si}_{0.1}\text{Ge}_{0.9}$ for several substrate orientations.

Fig. 5.20 explains the behavior of the mobility components in the case of $\text{Si}_{0.1}\text{Ge}_{0.9}$ substrates oriented along [221]. It shows the populations of the X and L valleys with different orientations and the repopulation between them. The L valley oriented along [111] is the most populated one up to $x \approx 0.8$. Thus the contribution of the longitudinal effective masses of the L valley plays the main role up to this value of the Ge composition. This reduces the mobility components μ_{\perp} and μ_{\parallel} . The increase of the in-plane component μ_{\parallel} is related to the effective mass interpolation. When the Ge mole fraction is greater than $x = 0.8$, the repopulation between different L valleys comes into play. First, electrons scatter from the valley located along [111] to the valleys located along $[\bar{1}11]$, $[1\bar{1}1]$ and $[\bar{1}\bar{1}1]$ and then from [111] and $[\bar{1}\bar{1}1]$ to $[\bar{1}11]$, $[1\bar{1}1]$. In this way the influence of the longitudinal masses decreases while the transverse masses contribute stronger, leading to the mobility increase.

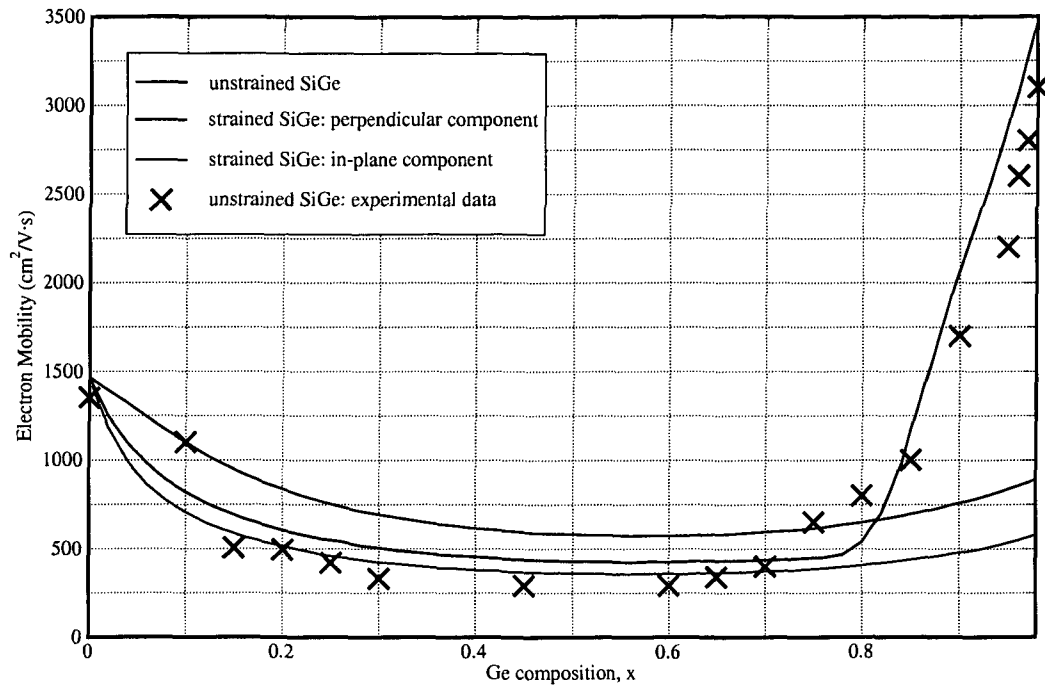


Figure 5.15: The electron mobility μ_{\perp} and μ_{\parallel} in relaxed and strained $\text{Si}_{1-x}\text{Ge}_x$ on the Si substrate with the orientation [001].

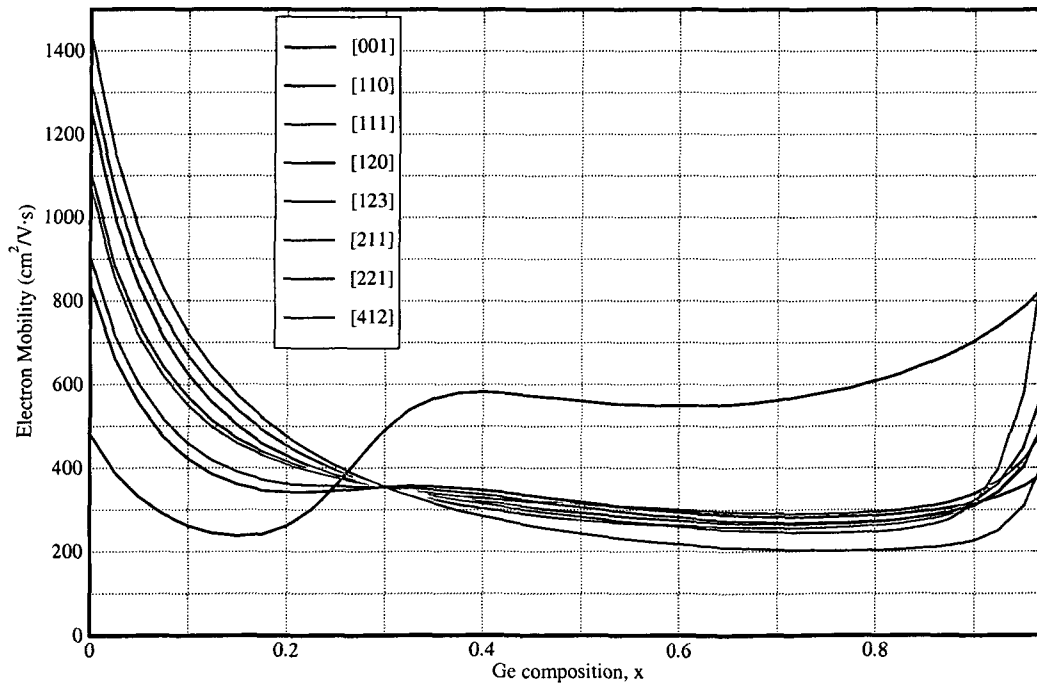


Figure 5.16: μ_{\perp} in $\text{Si}_{1-x}\text{Ge}_x$ on $\text{Si}_{0.7}\text{Ge}_{0.3}$ for several substrate orientations.

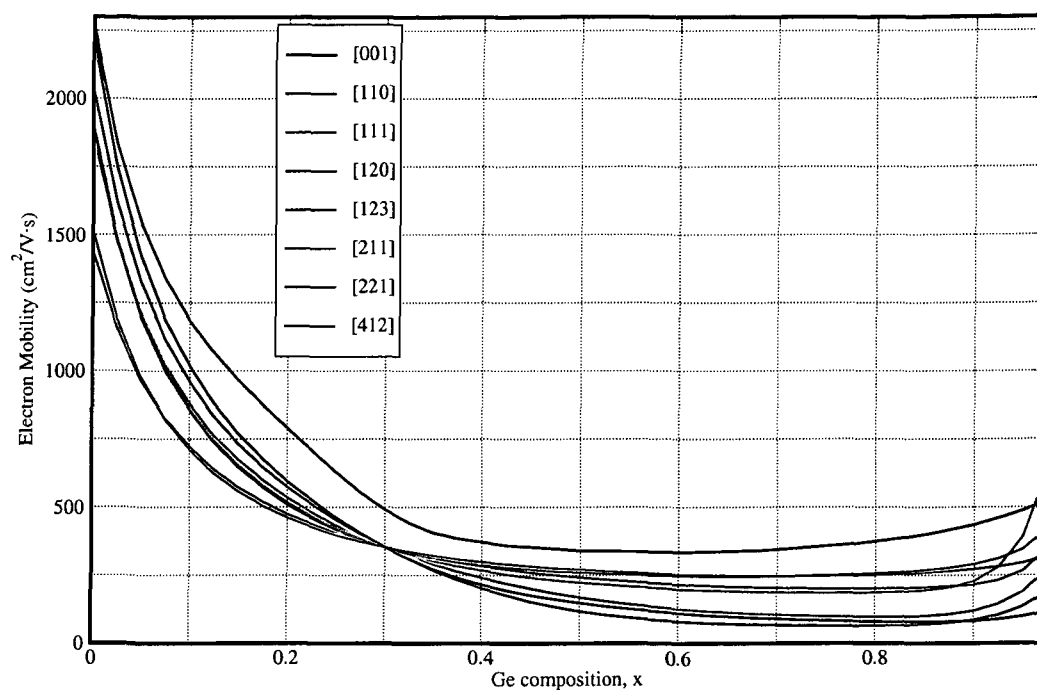


Figure 5.17: $\mu_{||}$ in $\text{Si}_{1-x}\text{Ge}_x$ on $\text{Si}_{0.7}\text{Ge}_{0.3}$ for several substrate orientations.

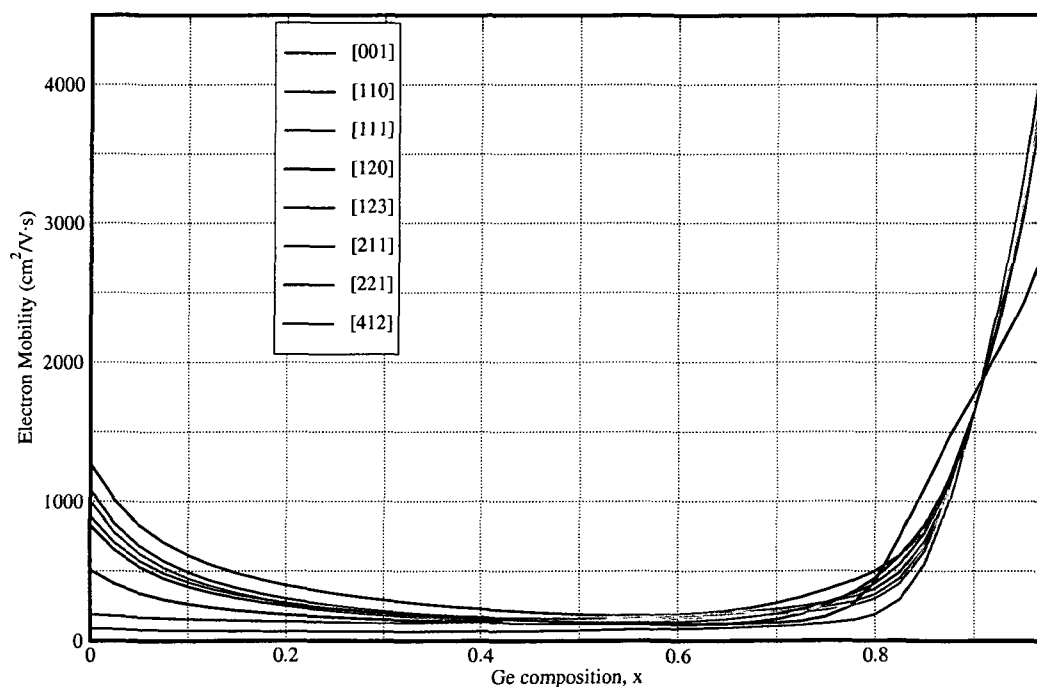


Figure 5.18: μ_{\perp} in $\text{Si}_{1-x}\text{Ge}_x$ on $\text{Si}_{0.1}\text{Ge}_{0.9}$ for several substrate orientations.

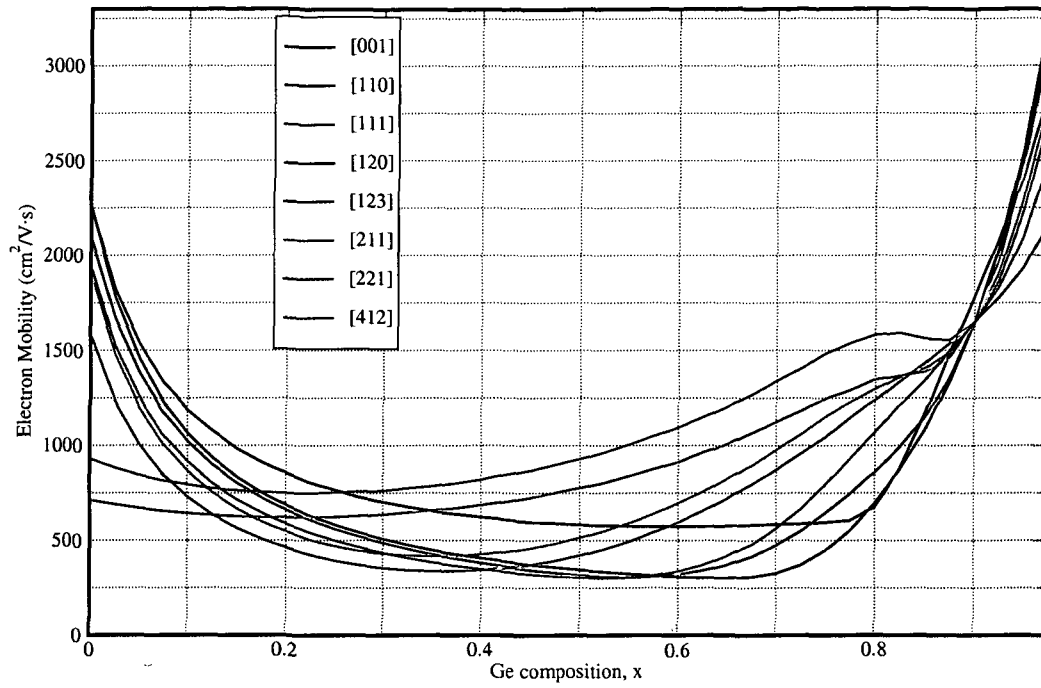


Figure 5.19: $\mu_{||}$ in $\text{Si}_{1-x}\text{Ge}_x$ on $\text{Si}_{0.1}\text{Ge}_{0.9}$ for several substrate orientations.

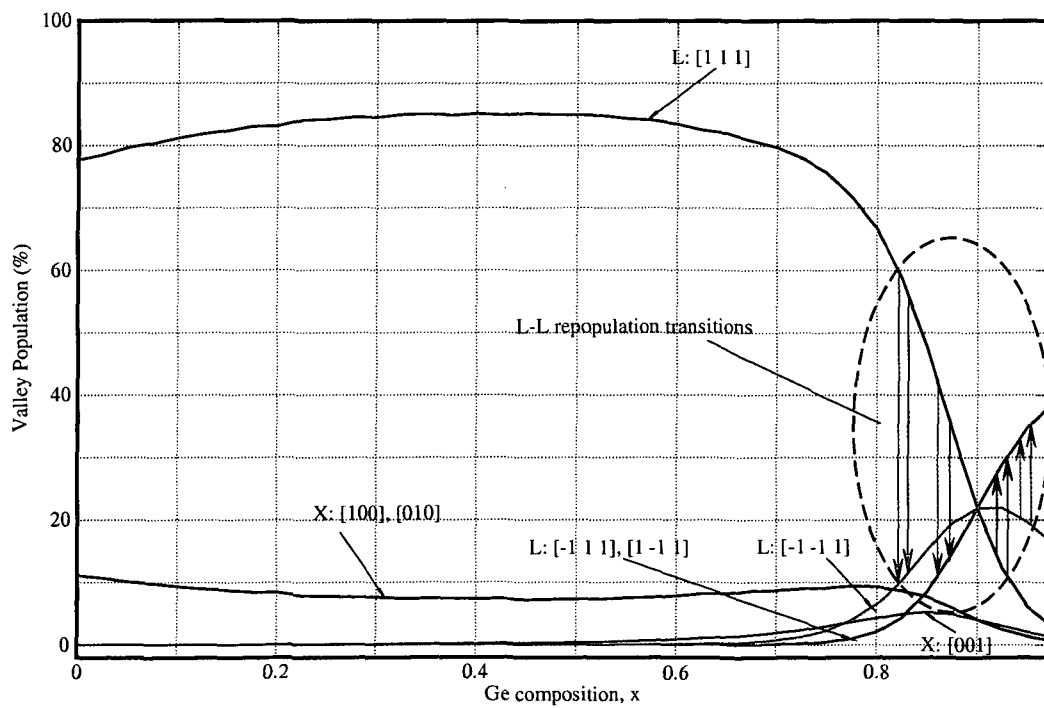


Figure 5.20: The valley populations as functions of the active layer composition for the $\text{Si}_{0.1}\text{Ge}_{0.9}$ substrate with the orientation [221].

5.2 Low Field Electron Mobility in Doped Layers

In this section the results of Monte Carlo simulation of the electron low field mobility in doped strained SiGe layers are presented. Two scattering mechanisms appear additionally to the phonon and alloy scattering, namely plasmon and ionized impurity scattering. The influence of the strain on the screening parameters and its interplay with the Pauli exclusion principle are discussed.

Fig. 5.21 shows the Monte Carlo simulation results for the majority electron mobility in relaxed [001] Si in comparison with experimental data.

Fig. 5.22 and Fig. 5.23 demonstrate the doping dependence of μ_{\perp} and μ_{\parallel} in the Si active layer grown on relaxed $\text{Si}_{0.7}\text{Ge}_{0.3}$. In Fig. 5.23 the curve for the perpendicular component μ_{\perp} exhibits an increase for the substrate oriented along [001] when the doping level becomes high enough. The same increase can be seen in Fig. 5.24, which displays the doping dependence of the perpendicular component μ_{\perp} in strained Si on a relaxed $\text{Si}_{0.1}\text{Ge}_{0.9}$ substrate of orientation [111]. At the same time the in-plane component does not increase as shown in Fig. 5.25. This effect can be explained by the influence of the quantum mechanical Pauli exclusion principle which starts playing an important role at high electron densities.

At low doping level, the L valley oriented along [111] is the lowest one. It is fully populated (see Fig. 5.26) and μ_{\perp} is determined by m_t^L , while μ_{\parallel} is determined by m_t^L . As the donor concentration increases, lower energy levels are forbidden to scatter in by the Pauli exclusion principle and thus electrons scatter to higher energy levels. At doping level about 10^{19}cm^{-3} electrons occupy energies high enough to be able to scatter to the unsplit X valleys which lie higher than the L ones due to strain. The intervalley $L - X$ scattering becomes possible and gets stronger as the donor concentration increases. Finally, most of the electrons are equally distributed between the X valleys. The influence of m_t^L on μ_{\perp} is significantly reduced and which turns out to be enough to suppress increasing ionized impurity scattering. However, the X valleys are oriented in such a way that the influence of m_t^X and m_t^X on μ_{\parallel} is not strong enough to suppress the impurity scattering, and as a result μ_{\parallel} does not show an increase.

Fig. 5.27 and Fig. 5.28 show the Ge composition dependence of μ_{\perp} and μ_{\parallel} in strained $\text{Si}_{1-x}\text{Ge}_x$ layers grown on Si [001] substrates. The increase of the perpendicular component at high doping levels and low composition x can be explained in the following manner. In the undoped material there are two factors which depend on the Ge mole fraction: the splitting of the X valleys and alloy scattering. The first factor increases the perpendicular component of the electron mobility and the second one decreases it. In doped SiGe at high doping levels, ionized impurity scattering dominates the alloy scattering and thus suppresses the second factor leaving the first one that leads to the increase. The in-plane component does not have this increase because both the energy splitting and alloy scattering decrease μ_{\parallel} . Thus after removing the second factor there still exists the second one which decreases the parallel component.

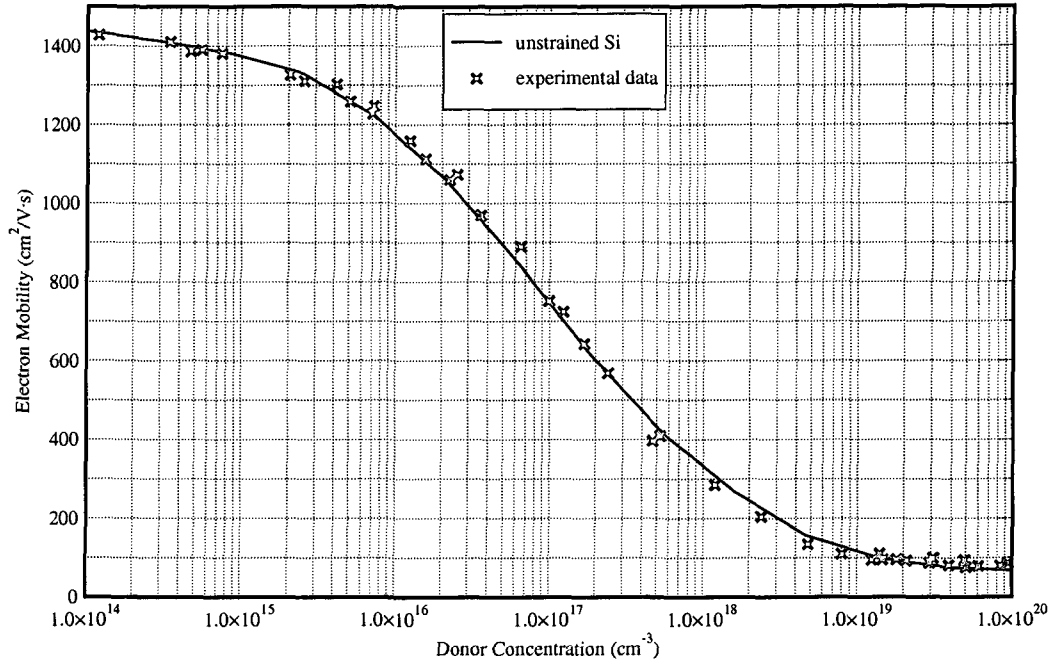


Figure 5.21: The majority electron mobility in relaxed Si.

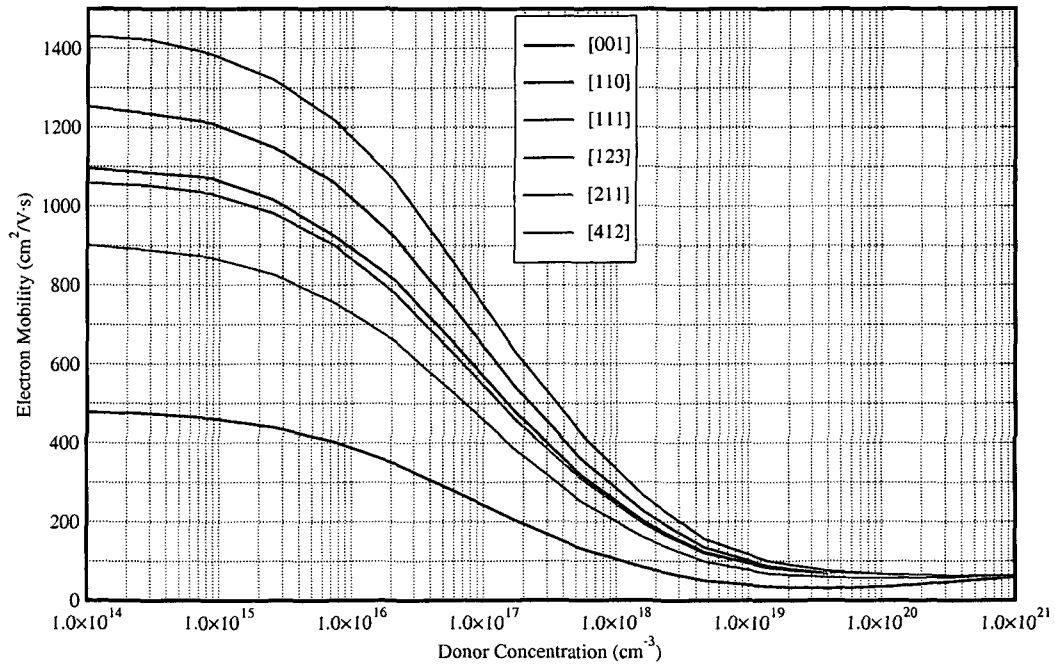


Figure 5.22: The doping dependence of μ_{\perp} in Si on $\text{Si}_{0.7}\text{Ge}_{0.3}$.

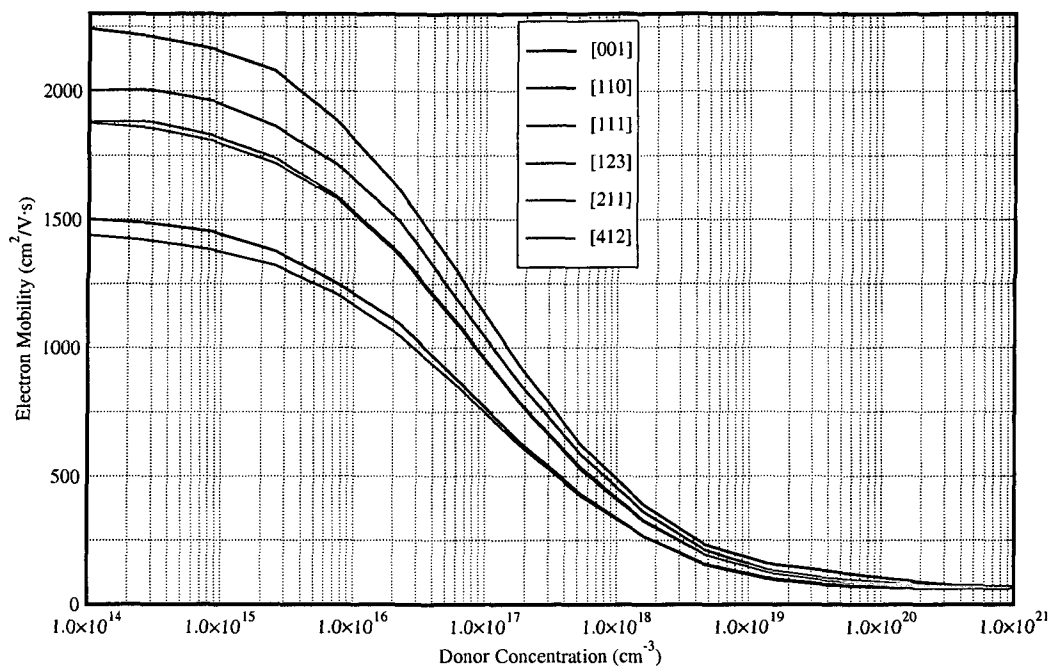


Figure 5.23: The doping dependence of $\mu_{||}$ in Si on $\text{Si}_{0.7}\text{Ge}_{0.3}$.

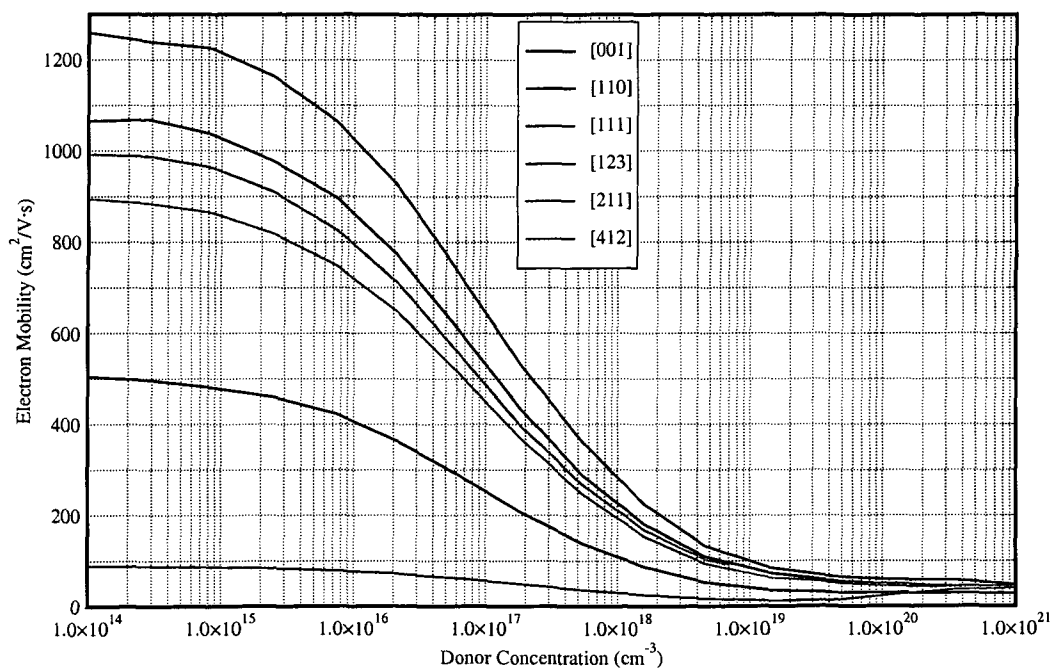


Figure 5.24: The doping dependence of μ_{\perp} in Si on $\text{Si}_{0.1}\text{Ge}_{0.9}$.

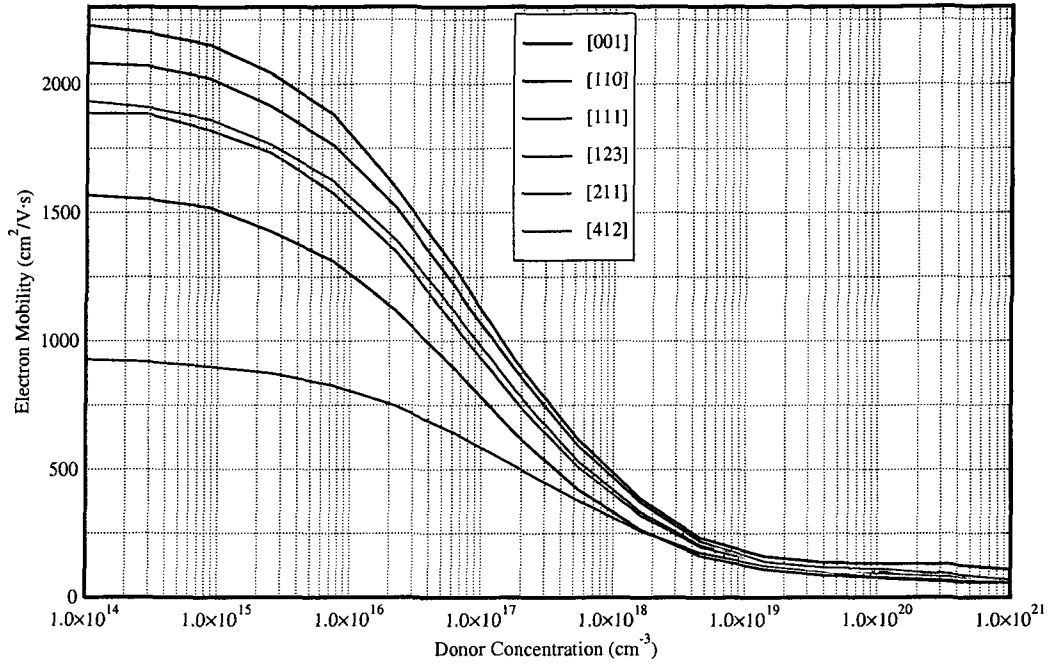


Figure 5.25: The doping dependence of $\mu_{||}$ in Si on $\text{Si}_{0.1}\text{Ge}_{0.9}$.

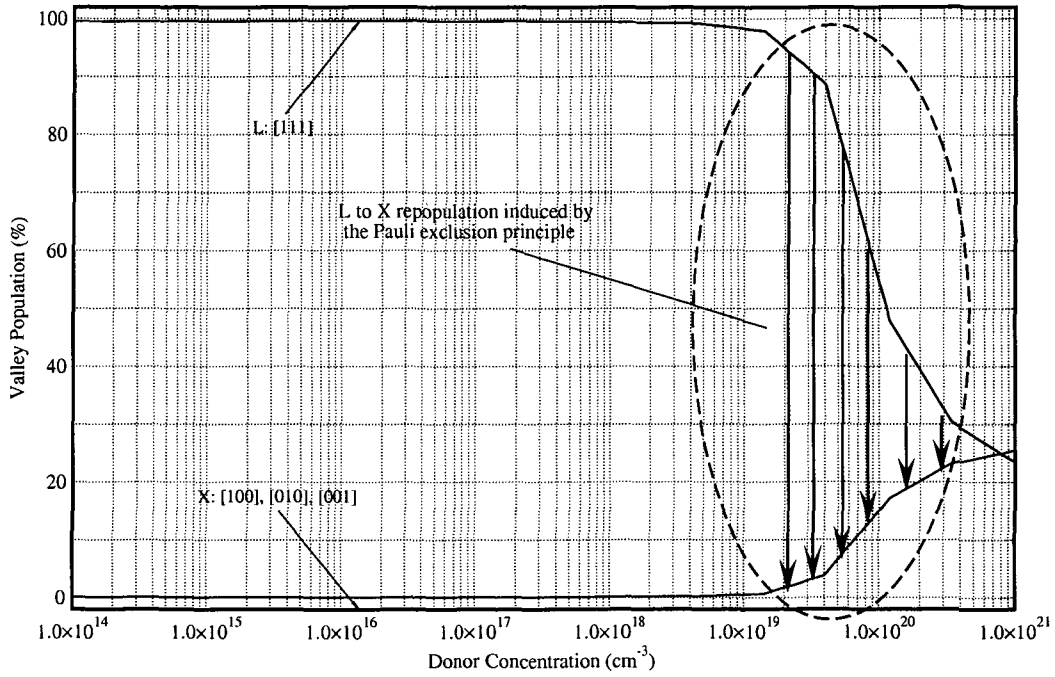


Figure 5.26: The valley population in strained Si grown on the $\text{Si}_{0.1}\text{Ge}_{0.9}$ substrate oriented along [111].

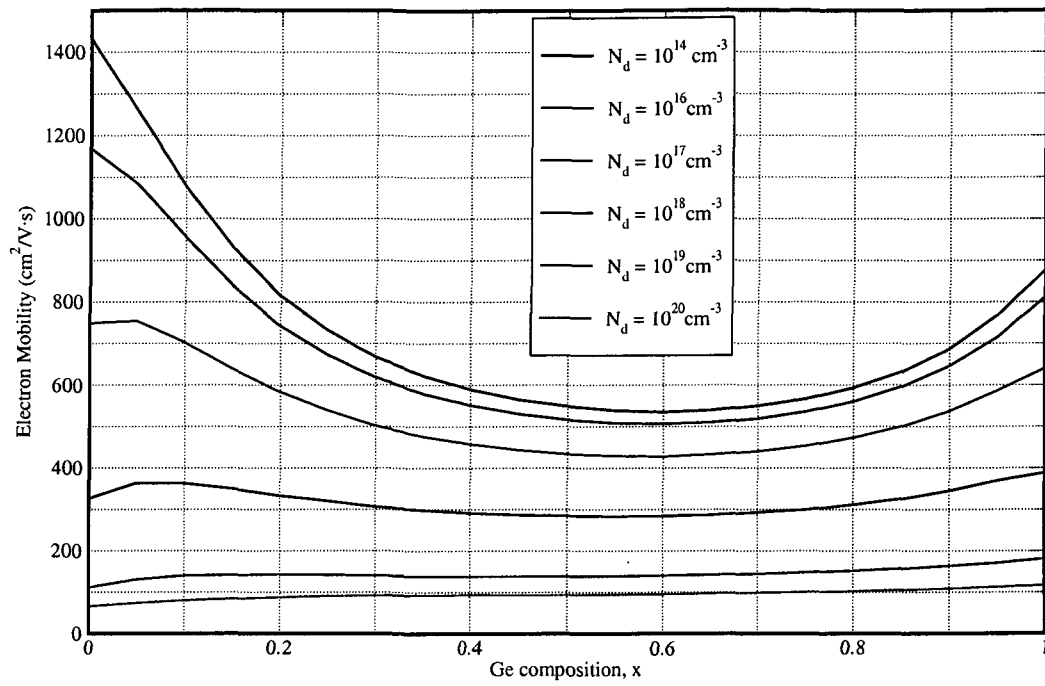


Figure 5.27: The composition dependence of μ_{\perp} in $\text{Si}_{1-x}\text{Ge}_x$ on [001] Si at several doping levels.

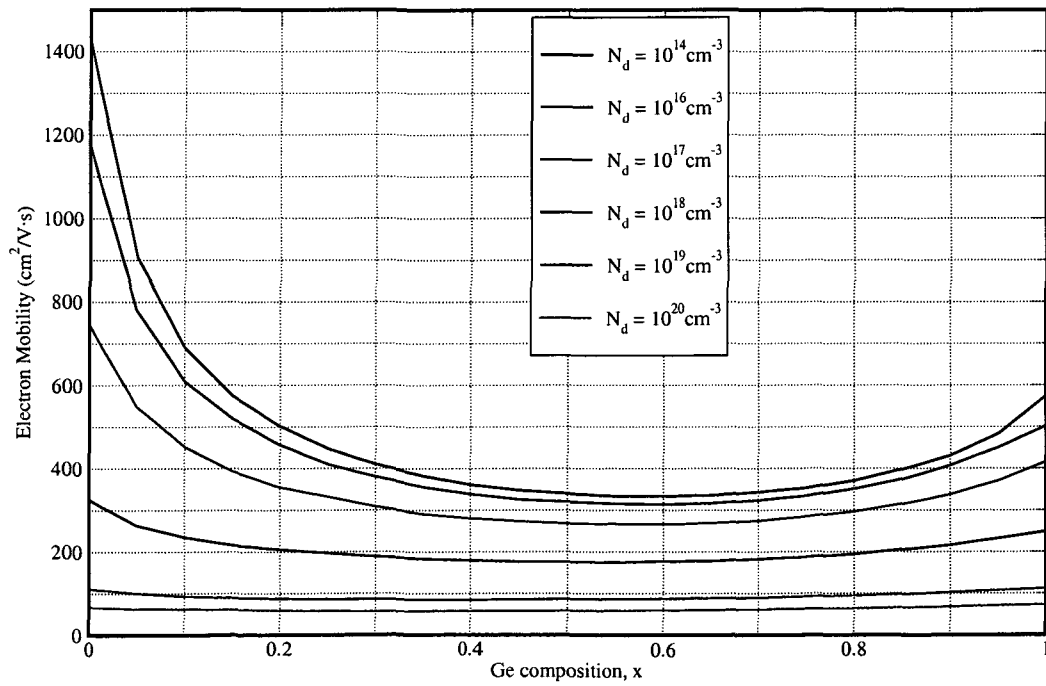


Figure 5.28: The composition dependence of $\mu_{||}$ in $\text{Si}_{1-x}\text{Ge}_x$ on [001] Si at several doping levels.

5.3 Small Signal Response

In this section results of the small signal analysis are presented. A comparison is made between non-degenerate and degenerate electron gases. Finally, small signal analysis of strained Si is performed.

Fig. 5.29 shows the differential velocity in relaxed Si for both the non-degenerate and degenerate cases. The differential velocity obtained from the non-degenerate algorithm displays a weak oscillatory character, while the differential velocity from the degenerate algorithm does not show any oscillations. This can be explained by analyzing the energy distribution functions of the two ensembles introduced in Chapter 4. The small difference of the distribution functions of the two ensembles in the non-degenerate algorithm (see Fig. 5.30) is responsible for the weak oscillation, while for the degenerate algorithm the ensembles have nearly the same distributions at the very beginning as depicted in Fig. 5.31. In addition, in the degenerate case the distribution functions significantly shift to higher energies as the lower energy levels have already been occupied and scattering to these states is quantum mechanically forbidden.

Fig. 5.32 show the differential velocity in the strained Si active layer grown on the relaxed [001] $\text{Si}_{0.7}\text{Ge}_{0.3}$ substrate in comparison with the relaxed Si.

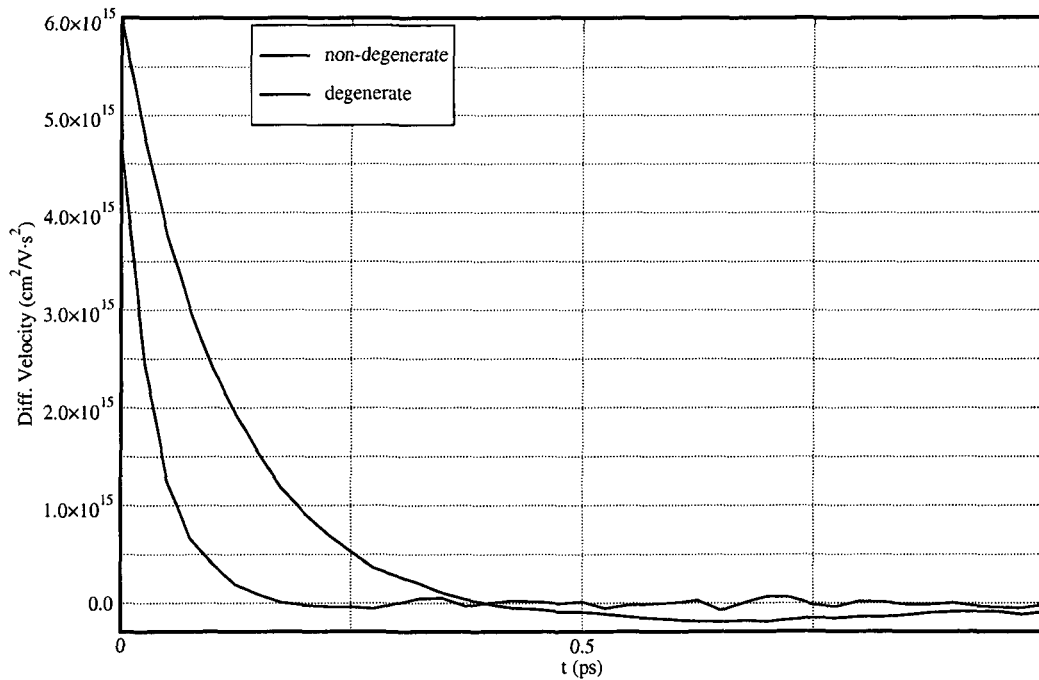


Figure 5.29: The differential velocity in non-degenerate and degenerate ($n=10^{21} \text{ cm}^{-3}$) relaxed Si for a stationary electric field $E_s = 5 \text{ kV/cm}$.

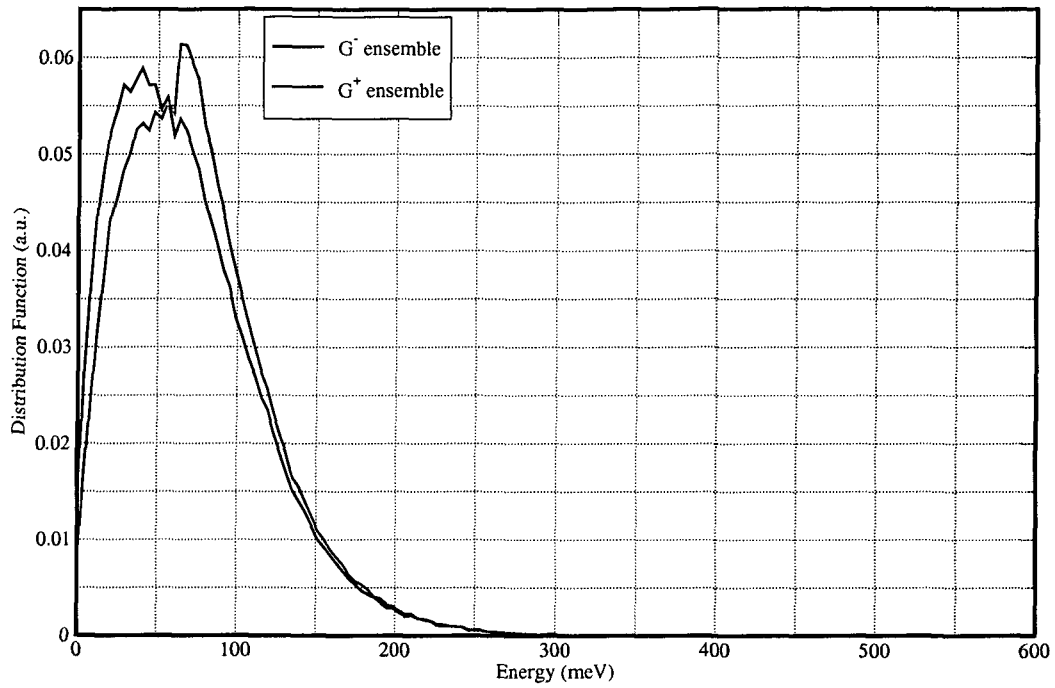


Figure 5.30: Energy distribution functions for the two carrier ensembles in non-degenerate relaxed Si.

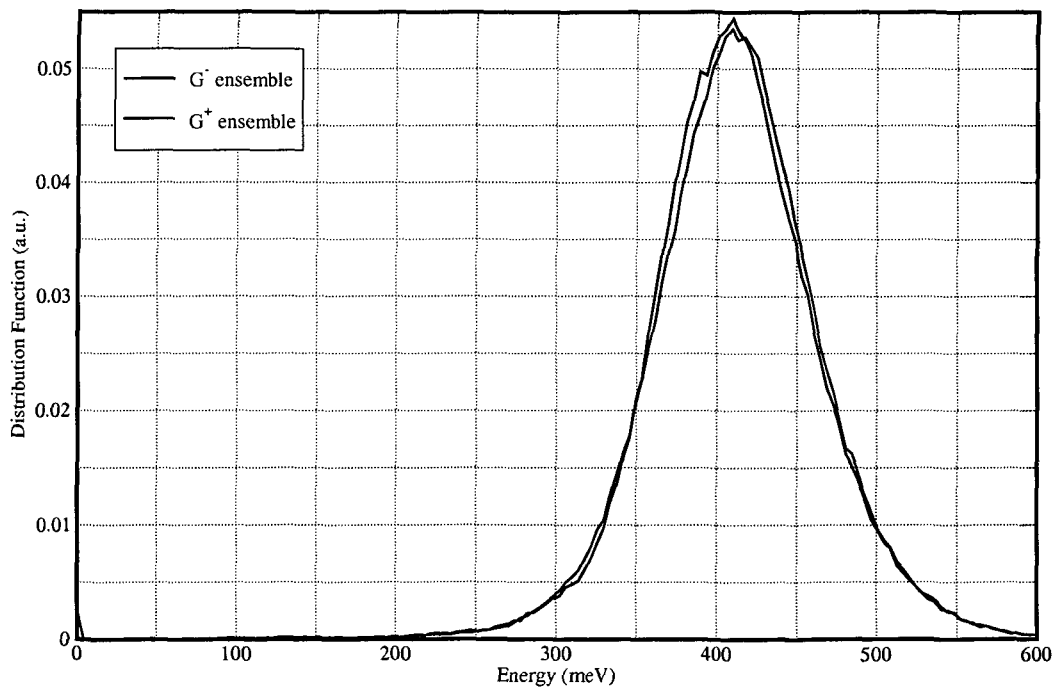


Figure 5.31: Energy distribution functions for the two carrier ensembles in degenerate relaxed Si.

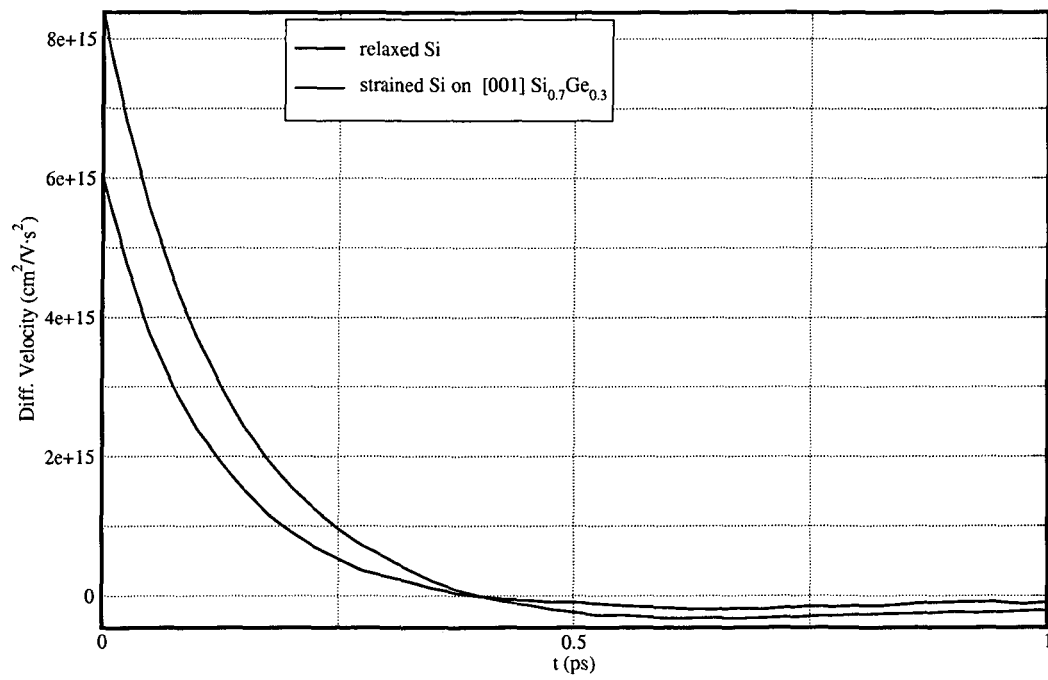


Figure 5.32: The differential velocity in non-degenerate relaxed and strained Si for $E_s = 5\text{kV/cm}$.

Chapter 6

Summary

The influence of strain on the electron transport in strained bulk $\text{Si}_{1-x}\text{Ge}_x$ grown on relaxed $\text{Si}_{1-y}\text{Ge}_y$ substrates with an arbitrary orientation has been studied. The description of the electron transport has been based on the semiclassical model described in Chapter 2. This model includes both the quantum and classical nature of electrons in solids. It uses classical trajectories and treats scattering processes quantum mechanically. Additionally, the quantum mechanical Pauli exclusion principle is taken into account within this transport model. The solids are considered as quantum mechanical objects described through their band structure and quantization of ion vibrations by quasi-particle description. The same quasi-particle concept is used for the electronic system itself at high densities through the plasmon picture. The most general description of semiclassical kinetics is covered by the Boltzmann transport equation with a scattering term including all specific scattering mechanisms. Acoustic phonons, intervalley phonon scattering, plasmon scattering, alloy scattering and ionized impurity scattering have been included in this study of transport in SiGe. To account for the Pauli exclusion principle the scattering term has also been modified leading to a nonlinear form of the Boltzmann equation.

Strain effects have been considered in Chapter 3. The linear theory of deformation-potentials have been applied to the conduction band of SiGe. Within this theory the shape of the bands is kept unchanged while the shift of different valleys leads to a splitting of the equivalent conduction band minima. The influence of the substrate orientation on this splitting has been taken into account. This results in non-zero non-diagonal elements of the strain tensor, which leads to various possible splittings. Finally, the scattering processes have been modified to account for the change of the band structure. The phonon scattering rate has been changed by modifying its prefactor due to the change of the number of final equivalent minima. In addition the energy argument of the delta-function changes due to the splitting. The influence on the ionized impurity scattering has been taken into account through the screening parameters. The Fermi energy is found from the solution of a nonlinear equation. The screening length and the dielectric function are obtained by a proper modification of the expressions known from the unstrained case.

SUMMARY

The Monte Carlo approach has been chosen to solve the nonlinear Boltzmann kinetic equation. To study the low field electron mobility tensor in strained semiconductors and in particular in strained SiGe a zero field Monte Carlo algorithm has been developed in Chapter 4. The algorithm allows the whole mobility tensor to be obtained from one simulation, which is an advantage over standard low field Monte Carlo approaches. It has been found that at high electron densities the inelastic scattering processes reverse. This has been explained as a quantum mechanical effect caused by the Pauli exclusion principle. Finally, the algorithm has been extended to a small signal algorithm for semiconductors in the high field regime. A rejection technique has been proposed to solve the first order perturbation equation. This method is able to deal with an arbitrary shape of the static distribution function and is not limited to the equilibrium distribution as is the case for the zero field algorithm.

The results of Monte Carlo simulation of strained SiGe layers have been discussed in Chapter 5. Both undoped and doped layers have been considered. The influence of repopulation effects in undoped layers caused by energy splitting has been studied. The interplay between the Pauli exclusion principle and strain effects has been observed in doped strained layers. Finally, small signal analyses have been performed for relaxed and strained Si layers.

Appendix A

Second Quantization

For systems composed of many identical particles it is useful to define operators which create or annihilate a particle in a specified state. Operators of physical interest may be expressed in terms of these creation and annihilation operators. They are said to be expressed in second quantized form.

A.1 Many-Body Operators

An operator \hat{U} is a one-body operator if the action of \hat{U} on a state $|\alpha_1 \dots \alpha_N\rangle$ of N particles¹ is the sum of the action of \hat{U} on each particle:

$$\hat{U}|\alpha_1 \dots \alpha_N\rangle = \sum_{i=1}^N \hat{U}_i |\alpha_1 \dots \alpha_N\rangle, \quad (\text{A.1})$$

where the operator \hat{U}_i operates only on the i -th particle.

An operator \hat{U} is a two-body operator if the action of \hat{U} on a state $|\alpha_1 \dots \alpha_N\rangle$ of N particles is the sum of the action of \hat{U} on all distinct pairs of particles:

$$\hat{U}|\alpha_1 \dots \alpha_N\rangle = \frac{1}{2} \sum_{1 \leq i \neq j \leq N} \hat{U}_{ij} |\alpha_1 \dots \alpha_N\rangle, \quad (\text{A.2})$$

where \hat{U}_{ij} operates only on particles i and j .

In general an n -body operator \hat{U} is defined as an operator which acts on a state $|\alpha_1, \dots, \alpha_N\rangle$ in the following way:

$$\hat{U}|\alpha_1 \dots \alpha_N\rangle = \frac{1}{n!} \sum_{1 \leq i_1 \neq i_2 \neq \dots \neq i_n \leq N} \hat{U}_{i_1 i_2 \dots i_n} |\alpha_1 \dots \alpha_N\rangle, \quad (\text{A.3})$$

¹The symbol $|\dots\rangle$ stands for the tensor product of the single-particle states.

where $\hat{U}_{i_1 i_2 \dots i_n}$ acts on the subset of n -particles i_1, i_2, \dots, i_n .

A.2 Creation and Annihilation Operators

For each single-particle state $|\lambda\rangle$ of the single-particle Hilbert space \mathcal{H} a Boson or Fermion creation operator a_λ^+ is defined by its action on any symmetrized or antisymmetrized state $|\lambda_1 \dots \lambda_N\rangle$ of the Hilbert space of N Bosons, \mathcal{B}_N , or N Fermions, \mathcal{F}_N , as follows:

$$a_\lambda^+ |\lambda_1 \dots \lambda_N\rangle = |\lambda \lambda_1 \dots \lambda_N\rangle \quad (\text{A.4})$$

The creation operators a_λ^+ do not operate within one space \mathcal{B}_n or \mathcal{F}_n , but rather operate from any space \mathcal{B}_n or \mathcal{F}_n to \mathcal{B}_{n+1} or \mathcal{F}_{n+1} . It is useful to define the Fock space as the direct sum of the Boson or Fermion spaces

$$\begin{aligned} \mathcal{B} &= \oplus_{n=0}^{\infty} \mathcal{B}_n, \\ \mathcal{F} &= \oplus_{n=0}^{\infty} \mathcal{F}_n, \end{aligned} \quad (\text{A.5})$$

where by definition:

$$\begin{aligned} \mathcal{B}_0 &= \mathcal{F}_0 = |0\rangle, \\ \mathcal{B}_1 &= \mathcal{F}_1 = \mathcal{H}. \end{aligned} \quad (\text{A.6})$$

It can be easily shown that for Bosons the creation operators commute:

$$a_\lambda^+ a_\mu^+ - a_\mu^+ a_\lambda^+ = 0, \quad (\text{A.7})$$

whereas they anticommute for Fermions:

$$a_\lambda^+ a_\mu^+ + a_\mu^+ a_\lambda^+ = 0. \quad (\text{A.8})$$

The annihilation operators a_λ are defined as the adjoints of the creation operators a_λ^+ . The commutation and anticommutation relations of annihilation operators follow from (A.7) and (A.8), respectively. They commute for Bosons:

$$a_\lambda a_\mu - a_\mu a_\lambda = 0, \quad (\text{A.9})$$

whereas they anticommute for Fermions:

$$a_\lambda a_\mu + a_\mu a_\lambda = 0. \quad (\text{A.10})$$

The action of the annihilation operator on a many particle state is given for Bosons as

$$a_\lambda |\alpha_1 \dots \alpha_n\rangle = \sum_{i=1}^n \delta_{\lambda \alpha_i} |\alpha_1 \dots \hat{\alpha}_i \dots \alpha_n\rangle, \quad (\text{A.11})$$

while for Fermions it reads:

$$a_\lambda |\alpha_1 \dots \alpha_n\rangle = \sum_{i=1}^n (-1)^{i-1} \delta_{\lambda \alpha_i} |\alpha_1 \dots \hat{\alpha}_i \dots \alpha_n\rangle. \quad (\text{A.12})$$

Here $\hat{\alpha}_i$ shows that the state α_i has been removed from the mani-particle state $|\alpha_1 \dots \hat{\alpha}_i \dots \alpha_n\rangle$.

The commutation rules for the creation and annihilation operators are:

$$\begin{aligned} a_\lambda a_\mu^+ - a_\mu^+ a_\lambda &= \delta_{\lambda\mu} \text{ (Bosons)} \\ a_\lambda a_\mu^+ + a_\mu^+ a_\lambda &= \delta_{\lambda\mu} \text{ (Fermions)}. \end{aligned} \quad (\text{A.13})$$

If the orthonormal basis $\{\alpha\}$ transforms into another basis $\{\tilde{\alpha}\}$, the creation and annihilation operators transform as follows:

$$\begin{aligned} a_{\tilde{\alpha}}^+ &= \sum_{\alpha} \langle \alpha | \tilde{\alpha} \rangle a_{\alpha}^+, \\ a_{\tilde{\alpha}} &= \sum_{\alpha} \langle \tilde{\alpha} | \alpha \rangle a_{\alpha}. \end{aligned} \quad (\text{A.14})$$

Of particular importance is the coordinate basis $\{|\mathbf{x}\rangle\}$. In this case the creation and annihilation operators are traditionally denoted by $\hat{\psi}^+(\mathbf{x})$ and $\hat{\psi}(\mathbf{x})$ and are called field operators. From (A.14) it follows:

$$\begin{aligned} \hat{\psi}^+(\mathbf{x}) &= \sum_{\alpha} \phi_{\alpha}^*(\mathbf{x}) a_{\alpha}^+, \\ \hat{\psi}(\mathbf{x}) &= \sum_{\alpha} \phi_{\alpha}(\mathbf{x}) a_{\alpha}, \end{aligned} \quad (\text{A.15})$$

where $\phi_{\alpha}(\mathbf{x})$ is the coordinate representation wave function of the state $|\alpha\rangle$.

It can be shown that n -body operators (A.3) can be expressed through the creation and annihilation operators in a simple form:

$$\hat{U} = \frac{1}{n!} \sum_{\lambda_1 \dots \lambda_n} \sum_{\mu_1 \dots \mu_n} (\lambda_1 \dots \lambda_n | U | \mu_1 \dots \mu_n) a_{\lambda_1}^+ \dots a_{\lambda_n}^+ a_{\mu_n} \dots a_{\mu_1}. \quad (\text{A.16})$$

For example using the coordinate representation, the kinetic energy operator \hat{T}

$$\hat{T} = \sum_i \frac{\hat{\mathbf{p}}_i^2}{2m} \quad (\text{A.17})$$

may be rewritten in second quantized form as:

$$\hat{T} = -\frac{\hbar^2}{2m} \int d^3x \hat{\psi}^+(\mathbf{x}) \nabla^2 \hat{\psi}(\mathbf{x}). \quad (\text{A.18})$$

Appendix B

Random Phase Approximation and Plasmons

Random phase approximation (RPA) is obtained by summing all chain Feynman diagrams. The sequence of chain diagrams can be summed by writing an integral equation which iterates the addition of a single link. The single link is shown in Fig. B.1. The corresponding response

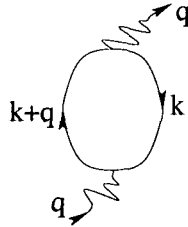


Figure B.1: Feynman diagram for a single link.

function for a non-interacting system is thus given as [84]:

$$D_0(\mathbf{q}, \omega) = 2 \sum_v \int \frac{d^3k}{(2\pi)^2} \left[\frac{(1 - n_v(\mathbf{k} + \mathbf{q}))n_v(\mathbf{k})}{\omega + \epsilon_v(\mathbf{k}) - \epsilon_v(\mathbf{k} + \mathbf{q}) + i\eta} - \frac{n_v(\mathbf{k} + \mathbf{q})(1 - n_v(\mathbf{k}))}{\omega + \epsilon_v(\mathbf{k}) - \epsilon_v(\mathbf{k} + \mathbf{q}) - i\eta} \right], \quad (\text{B.1})$$

where $n_v(\mathbf{k}) = \theta(k_f^v - |\mathbf{k}|)$. For small \mathbf{q} one obtains from (B.1):

$$\text{Re}\{D_0(\mathbf{q}, \omega)\} = \sum_v \frac{(k_f^v)^3}{3\pi^2(m_d^*)_v} \frac{\mathbf{q}^2}{\omega^2}. \quad (\text{B.2})$$

Summation over all direct RPA chain diagrams gives for the particle-hole Green's function:

$$G^{RPA}(\mathbf{k}_1 + \mathbf{q}, \mathbf{k}_1 | \mathbf{k}_2 + \mathbf{q}, \mathbf{k}_2; \omega) = G_0^{ph}(\mathbf{k}_1; \mathbf{q}, \omega) \left[\delta_{\mathbf{k}_1 \mathbf{k}_2} + \frac{\tilde{v}(|\mathbf{q}|) G_0^{ph}(\mathbf{k}_2; \mathbf{q}, \omega)}{1 - \tilde{v}(|\mathbf{q}|) D_0(\mathbf{q}, \omega)} \right], \quad (\text{B.3})$$

where $\tilde{v}(|\mathbf{q}|)$ is the direct matrix element which only depends on the momentum transfer $|\mathbf{q}|$.

Since the poles of the Green's function give the excited states of the system, in RPA the excited states occur at ω such that:

$$\tilde{v}(|\mathbf{q}|)D_0(\mathbf{q}, \omega) = 1. \quad (\text{B.4})$$

In the case of electron gas for the Coulomb potential the direct matrix element becomes:

$$\tilde{v}(|\mathbf{q}|) = \frac{e^2}{\varepsilon \mathbf{q}^2}. \quad (\text{B.5})$$

This equation together with (B.2) gives the expression for the plasmon frequency (2.133).

BIBLIOGRAPHY

- [1] M. Glicksman, "Magnetoresistance of Germanium-Silicon Alloys," *Physical Review*, vol. 100, pp. 1146 – 1147, 1955.
- [2] E. Kasper, H. J. Herzog, and H. Kibbel, "A One-Dimensional SiGe Superlattice Grown by UHV Epitaxy," *Appl.Phys.*, vol. 8, pp. 199 – 201, 1975.
- [3] G. C. Osbourn, "Strained-Layer Superlattices from Lattice Mismatched Materials," *J.Appl.Phys.*, vol. 53, pp. 1586 – 1589, 1982.
- [4] H. Daembkes, H. J. Herzog, H. Jorke, H. Kibbel, and E. Kasper, "The n-Channel SiGe/Si Modulation-Doped Field Effect Transistor," *IEEE Trans.Electron Devices*, vol. 33, pp. 633 – 638, 1986.
- [5] T. Tatsumi, H. Hirayama, and N. Aizaki, "Si/Ge_{0.3}Si_{0.7}/Si Heterojunction Bipolar Transistor Made with Si Molecular Beam Epitaxy," *Appl.Phys.Lett.*, vol. 52, pp. 895 – 897, 1988.
- [6] H. Temkin, J. C. Bean, A. Antreasyan, and R. Leibenguth, "Ge_xSi_{1-x} Strained-Layer Heterostructure Bipolar Transistors," *Appl.Phys.Lett.*, vol. 52, pp. 1089 – 1091, 1988.
- [7] G. L. Patton, S. S. Iyer, S. L. Delage, S. Tiwari, and J. M. C. Stork, "Silicon-Germanium Base Heterojunction Bipolar Transistors by Molecular Beam Epitaxy," *IEEE Electron Device Lett.*, vol. 9, pp. 165–167, 1988.
- [8] D.-X. Xu, G.-D. Shen, M. Willander, W.-X. Ni, and G. V. Hansson, "n-Si/p-Si_{1-x}Ge_x/n-Si Double-Heterojunction Bipolar Transistors," *Appl.Phys.Lett.*, vol. 52, pp. 2239 – 2241, 1988.
- [9] J. Olajos, J. Engvall, and H. G. Grimmeiss, "Band Gap of Strain-Symmetrized, Short-Period Si/Ge Superlattices," *Physical Review B*, vol. 46, pp. 12857 – 12860, 1992.
- [10] U. Menczigar, G. Abstreiter, J. Olajos, H. Grimmeiss, H. Kibbel, H. Presting, and E. Kasper, "Enhanced Band-Gap Luminescence in Strain-Symmetrized (Si)_m/(Ge)_n Superlattices," *Physical Review B*, vol. 47, pp. 4099 – 4102, 1993.

PUBLICATIONS

- [11] J. Engvall, J. Olajos, H. G. Grimmeiss, H. Presting, H. Kibbel, and E. Kasper, "Electroluminescence at Room Temperature of a Si_nGe_m Strained-Layer Superlattice," *Appl. Phys. Lett.*, vol. 53, pp. 491 – 493, 1993.
- [12] R. A. Soref, L. Friedman, and G. Sun, "Silicon Intersubband Lasers," *Superlattices & Microstructures*, vol. 23, pp. 427 – 439, 1998.
- [13] R. Vrijen, E. Yablonovitch, H. W. J. K. Wang, A. Balandin, and V. Roychowdhury, "Electron-Spin-Resonance Transistors for Quantum Computing in Silicon-Germanium Heterostructures," *Physical Review A*, vol. 62, pp. 012306-1 – 012306-10, 2000.
- [14] L. Brillouin, *Wave Propagation in Periodic Structures*. Dover, New York, 1953.
- [15] J. Zak, "Dynamics of Electrons in Solids in External Fields," *Physical Review*, vol. 168, pp. 686 – 695, 1968.
- [16] M. Cardona and F. H. Pollak, "Energy-Band Structure of Germanium and Silicon: The $\mathbf{k} \cdot \mathbf{p}$ Method," *Physical Review*, vol. 142, pp. 530 – 543, 1966.
- [17] T. B. Bahder, "Eight-Band $\mathbf{k} \cdot \mathbf{p}$ Model of Strained Zinc-Blende Crystals," *Physical Review B*, vol. 41, pp. 11992 – 12001, 1990.
- [18] C. Jacoboni and L. Reggiani, "The Monte Carlo Method for the Solution of Charge Transport in Semiconductors with Applications to Covalent Materials," *Reviews of Modern Physics*, vol. 55, pp. 645 – 705, 1983.
- [19] C. Jacoboni and P. Lugli, *The Monte Carlo Method for Semiconductor Device Simulation*. Springer-Verlag, Wien, New York, 1989.
- [20] C. V. Fischetti, "Monte Carlo Simulation of Transport in Technologically Significant Semiconductors of the Diamond and Zinc-Blende Structure - Part I: Homogeneous Transport," *IEEE Trans. Electron Devices*, vol. 38, pp. 634 – 649, 1991.
- [21] C. Herring and E. Vogt, "Transport and Deformation-Potential Theory for Many-Valley Semiconductors with Anisotropic Scattering," *Physical Review*, vol. 101, pp. 944 – 661, 1955.
- [22] W. Kohn and J. M. Luttinger, "Quantum Theory of Electrical Transport Phenomena," *Physical Review*, vol. 108, pp. 590 – 611, 1957.
- [23] J. M. Luttinger and W. Kohn, "Quantum Theory of Electrical Transport Phenomena. II," *Physical Review*, vol. 109, pp. 1892 – 1909, 1958.
- [24] L. D. Landau and E. M. Lifshitz, *Statistical Physics*. Butterworth-Heinemann, Oxford, Boston, 1999.
- [25] C. Kittel, *Quantum Theory of Solids*. Wiley, New York, 1963.
- [26] W. Pötz and P. Kocevar, "Electronic Power Transfer in Pulsed Laser Excitation of Polar Semiconductors," *Physical Review B*, vol. 28, pp. 7040 – 7047, 1983.

PUBLICATIONS

- [27] P. Bordone, C. Jacoboni, P. Lugli, and L. Reggiani, "Effect of a Perturbed Acoustic-Phonon Distribution on Hot-Electron Transport: A Monte Carlo Analysis," *J. Appl. Phys.*, vol. 61, pp. 1460 – 1468, 1987.
- [28] P. Lugli, C. Jacoboni, L. Reggiani, and P. Kocevar, "Monte Carlo Algorithm for Hot Phonons in Polar Semiconductors," *Appl. Phys. Lett.*, vol. 50, pp. 1251 – 1253, 1987.
- [29] L. Reggiani and C. Calandra, "Bloch States Mixing in Si Conduction Band," *Phys. Lett. A*, vol. 43, pp. 339 – 340, 1973.
- [30] W. A. Harrison, "Scattering of Electrons by Lattice Vibrations in Nonpolar Crystals," *Physical Review*, vol. 104, pp. 1281 – 1290, 1956.
- [31] D. Bohm and D. Pines, "A Collective Description of Electron Interactions: I. Magnetic Interactions," *Physical Review*, vol. 82, pp. 625 – 634, 1951.
- [32] D. Pines and D. Bohm, "A Collective Description of Electron Interactions: II. Collective vs Individual Particle Aspects of the Interactions," *Physical Review*, vol. 85, pp. 338 – 353, 1952.
- [33] D. Bohm and D. Pines, "A Collective Description of Electron Interactions: III. Coulomb Interactions in a Degenerate Electron Gas," *Physical Review*, vol. 92, pp. 609 – 625, 1953.
- [34] D. Pines, "Collective Energy Losses in Solids," *Reviews of Modern Physics*, vol. 28, pp. 184 – 198, 1956.
- [35] O. Madelung, *Introduction to Solid State Physics*. Springer, Berlin-Heidelberg-New York, 1978.
- [36] B. B. Varga, "Coupling of Plasmons to Polar Phonons in Degenerate Semiconductors," *Physical Review*, vol. 137, pp. A1896 – A1902, 1965.
- [37] A. Mooradian and G. B. Wright, "Observation of the Interaction of Plasmons with Longitudinal Optical Phonons in GaAs," *Physical Review Letters*, vol. 16, pp. 999 – 1001, 1966.
- [38] M. E. Kim, A. Das, and S. D. Senturia, "Electron Scattering Interaction with Coupled Plasmon-Polar-Phonon Modes in Degenerate Semiconductors," *Physical Review B*, vol. 18, pp. 6890 – 6899, 1978.
- [39] M. V. Fischetti, "Effect of the Electron-Plasmon Interaction on the Electron Mobility in Si," *Physical Review B*, vol. 44, pp. 5527 – 5534, 1991.
- [40] J. W. Harrison and J. R. Hauser, "Alloy Scattering in Ternary III-V Compounds," *Physical Review B*, vol. 13, pp. 5347 – 5350, 1976.
- [41] P. A. Flinn, "Electronic Theory of Local Order," *Physical Review B*, vol. 104, pp. 350 – 356, 1956.
- [42] H. Brooks, "Scattering by Ionized Impurities in Semiconductors," *Physical Review*, vol. 83, pp. 879 – 879, 1951.

PUBLICATIONS

- [43] E. Conwell and V. F. Weisskopf, "Theory of Impurity Scattering in Semiconductors," *Physical Review*, vol. 77, pp. 388 – 390, 1950.
- [44] H. Kosina and G. Kaiblinger-Grujin, "Ionized-Impurity Scattering of Majority Electrons in Silicon," *Solid-State Electron.*, vol. 42, pp. 331 – 337, 1998.
- [45] G. Kaiblinger-Grujin, H. Kosina, and S. Selberherr, "Influence of the Doping Element on the Electron Mobility in n-Silicon," *J.Appl.Phys.*, vol. 83, pp. 3096 – 3101, 1998.
- [46] P. Csavinsky, "Variational Principles for Solving Nonlinear Poisson Equations for the Potential of Impurity Ions in Semiconductors," *Physical Review B*, vol. 14, pp. 4483 – 4487, 1976.
- [47] K. R. Brownstein, "Addendum to "Variational Principle for Poisson's Equation for an Impurity Ion in a Medium with Spatially Variable Dielectric Constant"," *Physical Review B*, vol. 22, pp. 2131 – 2131, 1980.
- [48] J. R. Meyer, "Numerical Solution to the Nonlinear Poisson's Equation Including a Spatially Variable Dielectric Constant," *Physical Review B*, vol. 20, pp. 1762 – 1765, 1979.
- [49] L. D. Landau and E. M. Lifshitz, *Electrodynamics of Continuous Media*. Elsevier Science Ltd, 1985.
- [50] D. Ferry, *Semiconductors*. Macmillan, 1991.
- [51] J. Meyer and F. Bartoli, "Phase-Schift Calculation of Ionized Impurity Scattering in Semiconductors," *Physical Review B*, vol. 23, pp. 5413 – 5427, 1981.
- [52] B. Ridley, "Reconciliation of the Conwell-Weisskopf and Brooks-Herring Formulae for Charged-Impurity Scattering in Semiconductors: Third Body Interference," *J.Phys.C:Solid State Phys.*, vol. 10, pp. 1589 – 1593, 1977.
- [53] F. Nabarro, *Theory of Crystal Dislocations*. London: Clarendon, 1967.
- [54] J. W. Matthews and A. E. Blakeslee, "Defects in Epitaxial Multilayers - I: Misfit Dislocations," *J.Cryst.Growth*, vol. 27, pp. 118 – 125, 1974.
- [55] R. People and J. C. Bean, "Calculation of Crytical Layer Thickness Versus Lattice Mismatch for $\text{Ge}_x\text{Si}_{1-x}/\text{Si}$ Strained-Layer Heterostructures," *Appl.Phys.Lett.*, vol. 47, pp. 322 – 324, 1985.
- [56] G. C. Osbourn, "Strained-Layer Superlattices: A Brief Review," *IEEE J.Quantum Electronics*, vol. 22, pp. 1677 – 1681, 1986.
- [57] U. Koenig, *n-Type and p-Type Hetero Field Effect Transistors with Si and SiGe or Ge Channels*, vol. 24 of *Electronic Materials Information Service*, ch. 7, pp. 319–330. INSPEC, 2000.
- [58] J. Bardeen and W. Shockley, "Deformation Potentials and Mobilities in Non-Polar Crystals," *Physical Review*, vol. 80, pp. 72 – 80, 1950.
- [59] B. K. Ridley, *Quantum Processes in Semiconductors*. Oxford University Press, New York, 1993.

PUBLICATIONS

- [60] I. Balslev, "Influence of Uniaxial Stress on the Indirect Absorption Edge in Silicon and Germanium," *Physical Review*, vol. 143, pp. 636 – 647, 1966.
- [61] M. M. Rieger and P. Vogl, "Electronic-Band Parameters in Strained $\text{Si}_{1-x}\text{Ge}_x$ Alloys on $\text{Si}_{1-y}\text{Ge}_y$ Substrates," *Physical Review B*, vol. 48, pp. 14276 – 14287, 1993.
- [62] G. L. Bir and G. E. Pikus, *Symmetry and Strain-Induced Effects in Semiconductors*. John Wiley, New York, 1974.
- [63] E. M. Conwell, *High Field Transport in Semiconductors. Solid State Physics. Suppl. 9*, Academic Press, New York, 1967.
- [64] N. Goldsman, L. Henrickson, and J. Frey, "A Physics-Based Analytical/Numerical Solution to the Boltzmann Transport Equation for Use in Device Simulation," *Solid-State Electron.*, vol. 34, pp. 389 – 396, 1991.
- [65] H. Lin and N. Goldsman, "An Efficient Solution of the Boltzmann Transport Equation which Includes the Pauli Exclusion Principle," *Solid-State Electron.*, vol. 34, pp. 1035 – 1048, 1991.
- [66] J. Yamashita and K. Inoue, "Hot Electron in n-type Germanium," *J. Phys. Chem. Solids*, vol. 12, pp. 1 – 21, 1959.
- [67] H. G. Reik and H. Risken, "Drift Velocity and Anisotropy of Hot Electrons in n Germanium," *Physical Review*, vol. 126, pp. 1737 – 1746, 1962.
- [68] H. D. Rees, "Calculation of Distribution Functions by Exploiting the Stability of the Steady State," *J. Phys. Chem. Solids*, vol. 30, pp. 643 – 655, 1969.
- [69] C. Hammar, "Iterative Method for Calculating Hot Carrier Distributions in Semiconductors," *J. Phys. C: Solid State Phys.*, vol. 6, pp. 70 – 78, 1973.
- [70] J. P. Nougier and M. Rolland, "Mobility, Noise Temperature, and Diffusivity of Hot Holes in Germanium," *Physical Review B*, vol. 8, pp. 5728 – 5737, 1973.
- [71] H. Kosina, M. Nedjalkov, and S. Selberherr, "Theory of the Monte Carlo Method for Semiconductor Device Simulation," *IEEE Trans. Electron Devices*, vol. 47, pp. 1898 – 1908, 2000.
- [72] F. W. Byron and R. W. Fuller, *Mathematics of Classical and Quantum Physics*. Dover, New York, 1992.
- [73] H. Kosina, M. Nedjalkov, and S. Selberherr, "Monte Carlo Analysis of the Small-Signal Response of Charge Carriers," in *Proc. of the 3rd Intl. Conf. on Large-Scale Scientific Computations*, (Sozopol), pp. 175 – 182, 2001.
- [74] H. Kosina, M. Nedjalkov, and S. Selberherr, "A Monte Carlo Method for Small Signal Analysis of the Boltzmann equation," *Appl. Phys.*, vol. 87, pp. 4308 – 4314, 2000.
- [75] S. Smirnov, H. Kosina, M. Nedjalkov, and S. Selberherr, "A Zero Field Monte Carlo Algorithm Accounting for the Pauli Exclusion Principle," in *Proc. of the 4th Intl. Conf. on Large-Scale Scientific Computations*, (Sozopol), p. in print, 2003.

PUBLICATIONS

- [76] L. D. Landau and E. M. Lifshitz, *Quantum Mechanics: Non-Relativistic Theory*. Butterworth-Heinemann, 1981.
- [77] P. Price, "On the Calculation of Differential Mobility," *Appl. Phys.*, vol. 54, pp. 3616 – 3617, 1983.
- [78] E. Starikov, P. Shiktorov, V. Gruzinskis, L. Varani, J. C. Vaissiere, J. P. Nougier, and L. Reggiani, "Monte Carlo Calculation of Noise and Small-Signal Impedance Spectra in Submicrometer GaAs n^+nn^+ Diodes," *Appl. Phys.*, vol. 79, pp. 242 – 252, 1996.
- [79] M. Nedjalkov, H. Kosina, and S. Selberherr, "Monte-Carlo Method for Direct Computation of the Small Signal Kinetic Coefficients," in *Proceedings SISPAD 99 Conf.*, (Kyoto, Japan), pp. 155 – 158, 1999.
- [80] V. Gruzinskis, E. Starikov, and P. Shiktorov, "Conservation Equations for Hot Carriers - I. Transport Models," *Solid-State Electron.*, vol. 36, pp. 1055 – 1066, 1993.
- [81] L. Reggiani, E. Starikov, P. Shiktorov, V. Gruzinskis, and L. Varani, "Modelling of Small-Signal Response and Electronic Noise in Semiconductor High-Field Transport," *Semicond.Sci.Technol.*, vol. 12, pp. 141 – 156, 1997.
- [82] S. Bosi and C. Jacoboni, "Monte Carlo High-Field Transport in Degenerate GaAs," *J.Phys.C:Solid State Phys.*, vol. 9, pp. 315 – 319, 1976.
- [83] P. Lugli and D. K. Ferry, "Degeneracy in the Ensemble Monte Carlo Method for High-Field Transport in Semiconductors," *IEEE Trans.Electron Devices*, vol. 32, pp. 2431 – 2437, 1985.
- [84] G. D. Mahan, *Many-Particle Physics*. Plenum, New York, 1990.

OWN PUBLICATIONS

- [1] S. Smirnov, H. Kosina, and S. Selberherr, "Monte Carlo Modeling of the Electron Mobility in Strained $\text{Si}_{1-x}\text{Ge}_x$ Layers on Arbitrarily Oriented $\text{Si}_{1-y}\text{Ge}_y$ Substrates," *Solid-State Electron.*, vol. 48, no. 4, 2004 (in print, invited).
- [2] S. Smirnov, H. Kosina, M. Nedjalkov, and S. Selberherr, "Monte Carlo Method for Modeling of Small Signal Response Including the Pauli Exclusion Principle," *J. Appl. Phys.*, vol. 94, no. 9, pp. 5791–5799, 2003.
- [3] S. Smirnov, H. Kosina, M. Nedjalkov, and S. Selberherr, *A Zero Field Monte Carlo Algorithm Accounting for the Pauli Exclusion Principle*. Lecture Notes in Computer Science, Springer, 2003 (in print).
- [4] S. Smirnov, H. Kosina, and S. Selberherr, "Substrate Orientation-Dependence of Electron Mobility in Strained SiGe Layers," in *Proc. Int. Conf. Simulation of Semiconductor Processes and Devices*, (Boston, USA), pp. 55–58, 2003.
- [5] S. Smirnov, H. Kosina, M. Nedjalkov, and S. Selberherr, "A Zero Field Monte Carlo Algorithm Accounting for the Pauli Exclusion Principle," in *Proc. Intl. Conf. on Large-Scale Scientific Computations*, (Sozopol, Bulgaria), pp. 40–41, 2003.
- [6] S. Smirnov, H. Kosina, and S. Selberherr, "Investigation of the Electron Mobility in Strained $\text{Si}_{1-x}\text{Ge}_x$ at High Ge Composition," *IEICE Trans. Electron.*, vol. 86, no. 3, pp. 350 – 356, 2003.
- [7] V. Palankovski, G. Röhrer, T. Grasser, S. Smirnov, H. Kosina, and S. Selberherr, "Rigorous Modeling Approach to Numerical Simulation of SiGe-HBTs," in *Proc. Intl. SiGe Technology and Device Meeting*, (Nagoya, Japan), pp. 97–98, 2003.
- [8] S. Smirnov, H. Kosina, and S. Selberherr, "Investigation of the Electron Mobility in Strained $\text{Si}_{1-x}\text{Ge}_x$ at High Ge Composition," in *Proc. Int. Conf. Simulation of Semiconductor Processes and Devices*, (Kobe, Japan), pp. 29–32, 2002.

OWN PUBLICATIONS

	Author	Co-Author	Total
Journals	3	0	3
Conferences	3	1	4
Contribution to Books	1	0	1
Total	7	1	8

Table 1: Publication Statistics

Curriculum Vitae



March 6th, 1976

Born in Skhodnya, Moscow Region, Russia.

September 1983

Start of school education.

September 1991 – May 1993

School of physics and mathematics at Moscow State Institute of Electronic Technology (Technical University) (MIET (TU)).

September 1993

Enrolled as a student of MIET (TU) at the faculty of physics and technology.

June 1997

Received B.S. degree (with honors) from MIET (TU) in electronics and microelectronics.

June 1999

Received M.S. degree (with honors) from MIET (TU) in electronics and microelectronics.

October 1999 - December 2001

Research fellow at MIET (TU): numerical simulation of semiconductor devices.

January 2002

Entered doctoral program at the Institute for Microelectronics, Vienna, under the supervision of Prof. Dr. Hans Kosina and Prof. Dr. Siegfried Selberherr. Subject of the PhD study: "Physical Modeling of Electron Transport in Strained Silicon and Silicon-Germanium". The research project has been carried out in cooperation with Intel Corporation and Semiconductor Research Corporation (SRC).